On the Investigation of Coating Characteristics Within the Experimental Domain Imposed by Inner-Diameter HVOF Process

by

Cassandra PRUDNIKOV

THESIS PRESENTED AT THE ÉCOLE DE TECHNOLOGIE SUPÉRIEURE
IN PARTIAL FULFILLMENT FOR A MASTER'S DEGREE WITH THESIS
IN MECHANICAL ENGINEERING
M.A.Sc

MONTREAL, DECEMBER 14, 2023

ÉCOLE DE TECHNOLOGIE SUPÉRIEURE
UNIVERSITÉ DU QUÉBEC

BOARD OF EXAMINERS

THIS THESIS HAS BEEN EVALUATED

BY THE FOLLOWING BOARD OF EXAMINERS :

Mr Lucas A. Hof, Thesis Supervisor
Department of Mechanical Engineering, École de technologie supérieure

Mr Philippe Bocher, Thesis Cosupervisor
Department of Mechanical Engineering, École de technologie supérieure

Mr Ricardo J. Zednik, President of the Board of Examiners
Department of Mechanical Engineering, École de technologie supérieure

Mr Vincent Demers, Member of the jury
Department of Mechanical Engineering, École de technologie supérieure

THIS THESIS WAS PRENSENTED AND DEFENDED

IN THE PRESENCE OF A BOARD OF EXAMINERS AND PUBLIC

NOVEMBER 22, 2023

AT ÉCOLE DE TECHNOLOGIE SUPÉRIEURE

ACKNOWLEDGMENTS

This project is the result of a collaboration between three parties: Surftec, the École de Technologie Supérieure (ÉTS) and the National Research Council of Canada (NRC).

I would like to express my sincere gratitude to my supervisors, M. Philippe Bocher and M. Lucas Hof, who patiently guided me through my work, gave me relevant feedback on my reports and helped me achieve my goals throughout these two years of research.

I am grateful to M. Jörg Oberste-Berghaus, senior research officer at the NRC, who gave me the opportunity to work in collaboration with the NRC and also provided the precious samples who allowed us to carry out several characterization tests.

I would also like to thank the researchers at ÉTS, especially M. Mohsen Mokhtabad-Amrei and M. Yasser Zedan, and the employees of the NRC, especially M. David De Lagrave, who helped me with the experimental part of my project and trained me on different equipment.

I am grateful for my family and friends who accompanied me during the entire process. Without their love and support, this journey would have been a lot harder.

Finally, I would like to thank all of the participants in my study for their time and willingness to share their knowledge. This work would have not been possible without their contribution.

Investigation des caractéristiques des revêtements dans le domaine expérimental imposé par le processus de HVOF intra-diamétral

Cassandra PRUDNIKOV

RÉSUMÉ

Souvent utilisés dans de nombreuses industries, les revêtements de chrome dur présentent de bonnes propriétés. En revanche, le processus de chromage dur est extrêmement toxique. C'est pourquoi la projection High Velocity Oxy Fuel (HVOF) remplace progressivement le chromage dur dans de nombreuses industries. Cependant, la projection HVOF n'est pas adaptée aux géométries complexes et aux diamètres internes inférieurs à six pouces en raison de la taille de l'appareil de projection. L'objectif de ce projet est d'établir des liens processus-propriétés entre les paramètres de projection inhérents au ID-HVOF (inner diameter high velocity oxyfuel) et les caractéristiques du revêtement WCCoCr qui en résulte.

Pour ce projet, deux nuances de poudre WCCoCr ont été utilisées. Pour mettre en évidence d'éventuelles différences, les tests de caractérisation des poudres comprennent une analyse de composition des phases par diffraction des rayons X (XRD), une analyse morphologique et une étude de la granulométrie. Il a été constaté que la distribution de la taille des particules a un effet sur les phénomènes de décarburation à l'intérieur du revêtement.

L'objectif est d'établir des relations entre la température la plus élevée atteinte au cours du processus de dépôt et les propriétés de l'échantillon. Les tests de caractérisation des revêtements comprenaient une analyse de la morphologie, une quantification de la porosité, une analyse de la composition chimique par diffraction des rayons X (XRD), des mesures de microdureté et une série de tests d'abrasion. Une première série d'échantillons plats en acier 4340 AISI revêtus de WCCoCr ont été produits. En imposant une distance de projection plus courte que celle préconisée par le HVOF standard, il a été possible de simuler les conditions ID-HVOF. Après rectification de la zone de décarburation sur les substrats en acier 4340 AISI, une deuxième série de revêtements WCCoCr a été produite. La troisième série de revêtements WCCoCr a été déposée sur des substrats en acier doux, afin d'étendre les tests de caractérisation menés sur la série 2. Pour la quatrième série de revêtements WCCoCr, deux types de coupons en acier 4340 AISI ont été utilisés. Les deux types de substrats ont reçu deux traitements de surface différents. Cette fois-ci, l'objectif était de comparer l'effet du traitement de surface du substrat sur la performance globale des échantillons.

L'influence de la température maximale sur les propriétés du revêtement a été étudiée. Il a été constaté que les paramètres de projection ont un effet sur l’épaisseur déposée par passe. La porosité et l'abrasion ne sont cependant pas affectées par la variation de la température. Une corrélation étroite entre la température, la perte de dureté et la décarburation a pu être établie.

Mots-Clés: High Velocity Oxyfuel, WC-Co-Cr, caractérisation, relation processus-propriétés, sur-revenu

On the Investigation of Coating Characteristics Within the Experimental Domain Imposed by Inner-Diameter HVOF Process

Cassandra PRUDNIKOV

ABSTRACT

Widely used in multiple industries, hard chrome plated coatings are proven to exhibit good properties. Yet, the process of hard chrome plating is extremely toxic. Therefore, High Velocity Oxyfuel (HVOF) spraying is gradually replacing hard chrome plating in many industries. Yet, HVOF is not adapted for complex geometries and inner diameters smaller than six inches due to the size of the spraying apparatus. The aim of this project is to establish process-properties relations between the spraying parameters inherent to ID-HVOF (inner diameter high velocity oxyfuel) and the resulting WCCoCr coating characteristics.

For this project, two WCCoCr powder compositions were used. To highlight any possible differences, powder characterization tests included phase composition analysis by X-Ray Diffraction (XRD), morphology analysis and granulometry. It was found that the particle size distribution has an effect on the decarburization phenomena within the coating during the deposition process.

For each produced set of samples, the goal was to establish relations between the highest temperature reached during the deposition process and the sample's properties. Coating characterization tests included morphology analysis, porosity quantification, phase composition analysis by X-Ray Diffraction (XRD), microhardness measurements and abrasion tests. A first set of flat samples of 4340 AISI steel and a WCCoCr coating were produced. By imposing a shorter spraying distance, it was possible to simulate ID-HVOF conditions. After rectification of the decarburization zone on the 4340 AISI steel substrates, a second set of WCCoCr coatings was produced. The third set of WCCoCr coatings was deposited onto mild steel substrates, in order to extend the characterization tests led on set 2. For the last set of WCCoCr coatings, two types of 4340 AISI steel coupons were employed. Each substrate type received two different surface treatments. For these experiments, the goal was to compare the effect of substrate surface treatment on the overall performance of the samples.

In summary, the influence of the maximum temperature on the coating's properties and behavior was studied. It was found that the spraying parameters affected the deposited thickness per pass. Porosity and abrasion were nonetheless not correlated to temperature variation. In addition, a close correlation between temperature, hardness loss and decarburization was established.

Keywords: High Velocity Oxyfuel, WC-Co-Cr, characterization, process-property relation, over-tempering

TABLE OF CONTENTS

Page

LIST OF TABLES

Page

LIST OF FIGURES

Page

LIST OF ABREVIATIONS, SIGNS AND ACRONYMS

AMS	Aerospace Material Specification
ASTM	American Society for Testing and Materials
AFS	American Foundrymen's Society
ÉTS	École de technologie supérieure
HVOF	High Velocity Oxy Fuel
ID-HVOF	Inner Diameter High Velocity Oxy Fuel
IR	Infrared
XRD	X-Ray Diffraction
EBSD	Electron Back Scattered Diffraction
NRC	National Research Council (of Canada)
OSHA	Occupational Safety and Health Administration
SEM	Scanning Electron Microscope

LIST OF SYMBOLS AND UNITS OF MEASURE

DISTANCE UNITS
m meter
mm millimeter
µm micrometer
nm nanometer
in inch

ATOMIC ELEMENTS
W Tungsten
C Carbon
Cr Chrome
Co Cobalt
Fe Iron
Al Aluminium
Ar Argon
H Hydrogen
O Oxygen
Cu Copper

TEMPERATURE UNITS
°C Celsius degree
K Kelvin
°F Fahrenheit degree

ELECTRICAL UNITS
A ampere
mA milliampere
V volt
kV kilovolt
eV electronvolt

MECHANICAL UNITS
HRC Rockwell hardness
HV Vickers hardness
g gram
kg kilogram
N newton
kN kilonewton
Pa pascal
MPa megapascal
psi pounds per square inch
min minute
s second
° degree
Ra roughness

SPEED
m/s meter per second

DENSITY
g/cm^3 gram by cubic centimeter

VOLUMETRIC FLOW RATE
cm^3/s cubic centimeter by second
slpm standard liter per minute

SYMBOLS
$d_{(h,k,l)}$ interplanar spacing
λ wavelength of X rays
θ diffraction angle
n diffraction order
(h, k, l) atomic plan
k constant variable
I_d decarburization indicator
T temperature

INTRODUCTION

Hard chrome electrodeposition, also called hard chrome plating, is a coating process that has been employed in several industries for years. Although proven to exhibit excellent mechanical properties, hard chrome coatings are yet to be the ideal solution. During hard chrome electrodeposition, specimens are submerged in chromic acid, which contains hexavalent chrome (CrVI). Unfortunately, CrVI is a highly carcinogenic component and contaminated rinse water is complicated to dispose of. For years now, researchers and engineers seek to replace hard chrome electrodeposition with a more environment-friendly process while still ensuring high quality coatings. One of the options has been found among the variety of thermal spray processes: high velocity oxyfuel (HVOF) thermal spray. More specifically, carbide-based coatings seem to yield even better properties than hard chrome coatings. Many studies have compared mechanical properties, adhesion, fatigue, wear and corrosion resistance and have concluded that HVOF coatings often perform better than the hard chrome alternative.

Nowadays, HVOF thermal spray is extensively used in various industries and companies have almost perfected the deposition technique. Despite being a now common process, HVOF is not adapted to complex geometries and narrow spaces due to the size of the apparatus. More specifically, inner surfaces of less than six inches in diameter are not reachable by common HVOF spraying guns. Therefore, industries still rely on hard chrome plating to cover complex surfaces.

Contrary to classic HVOF, inner diammeter HVOF (ID-HVOF) requires the use of smaller equipment such as a miniaturized spraying gun. Smaller apparatus produces a weaker flame, hence a lower flame enthalpy. Also, with the use of smaller equipment comes the use of finer powders and shorter spraying distances, generating new issues that need to be addressed in the context of ID-HVOF.

The main goal is to develop an ID-HVOF process capable of replacing chromium plating in inner diameters of six inches or less of landing gear components. In order to reach the main

goal of the project, three sub-objectives have been defined. The first axis focuses on defining coating characteristics within the experimental domain imposed by ID-HVOF. More specifically, the goal is to establish relations between the process parameters and the coating properties. The second axis will investigate the mechanical behavior and fatigue properties of coated samples. The third axis will develop the digitalisation of ID-HVOF process and the application of machine learning. More specifically, a model translating temperature measurements on outer surfaces of simple geometries to the surfaces complex geometries will be established. The present thesis will focus on the first defined research axis.

The challenges brought up by ID-HVOF will be addressed in partnership with the National Research Council of Canada (NRC), located in Boucherville (QC, Canada) and the Surftec industrial R&D group. The studied samples were provided by the NRC, where an operator chose the HVOF process parameters. Depending on the size of each provided set of samples, a selected amount of tests were possible. Therefore, relations were defined between the process parameters chosen by the NRC group and the results of the characterization tests that were performed on the samples. This project will focus of carbide-based coatings, more specifically WCCoCr coatings. The study will start by characterizing WCCoCr coatings deposited on flat substrates whilst mimicking ID-HVOF conditions by modifying the spraying parameters. The first goal is to establish the correct characterization tests to do on the available samples. Once the properties of the specimens are quantified, the next step will be to find a relation between these properties and the process' parameters. A second and third sets of flat substrates were coated with a WCCoCr powder in order to continue to investigate the process-properties relations. Once the characterization tests on the flat samples completed, a set of flat substrates will be coated by being placed inside of a cylinder made of the same material as the substrate. This way, it will be possible to study the effect of inner diameter conditions on the properties of the coatings.

This thesis is organised in 4 chapters. The first chapter presents a literature review on thermal spraying basics, followed by the specificities of HVOF thermal spraying, the common characterization tests and the degradation modes inherent to HVOF. The second chapter will

detail the experimental protocol of the manufacturing of the samples and of the different characterization tests. The third chapter will address the results of the different characterization tests and the found interpretations. The fourth chapter will introduce the perspectives for the continuation of the project and present a study of the effect of surface treatment of the substrate on its properties. Finally, the most significant findings of this study are discussed in the conclusion section to complete the study.

CHAPTER 1

LITTERATURE REVIEW

1.1 Introduction to thermal spraying

Materials used in the industry interact with their environment through their surface. A coating is deposited onto a substrate's surface to ensure its durability in its environment and good mechanical properties. This review will focus on thermal spray coatings as it is the subject of the rest of the project.

As illustrated on figure 1.1, during thermal spraying, a heat source melts the feedstock material, and a jet is used to impart kinetic energy tothe molten particles. They then impinge the substrate surface and rapidly cool down to form a solid splat, continuously building up the desired thickness (Tejero-Martin et al., 2019*)*.

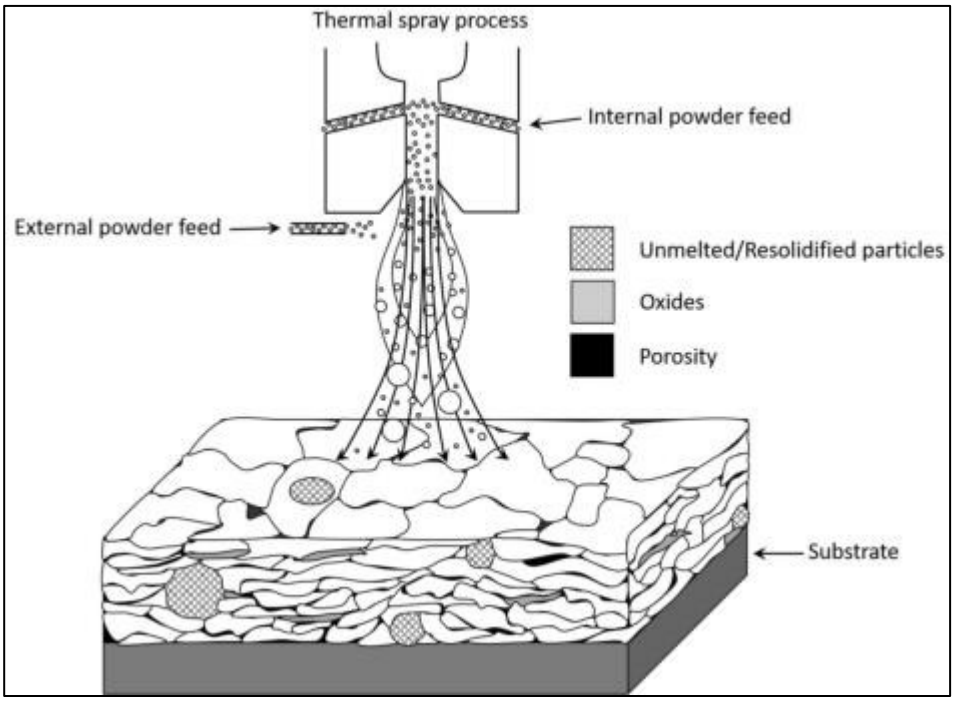

Figure 1.1 Schematic representation of a thermal spraying process with the two main components, a heat source and a jet, and the main features of the produced coating
From Tejero-Martin et al. *(*2019, p.4)

Thermal spraying has become quite popular for several reasons. First, when depositing a coating by thermal spraying, the substrate isn't exposed to overheating. Coatings deposited by thermal spraying can often be easily removed or layered with a new coating without modifying the substrate's characteristics and dimensions. Thermal spraying has also broadened the variety of materials that can be used as a coating.

Thermal spray coatings have been used for advanced gas turbine components such as compressor blades, compressor stator vanes, bearing housings, and labyrinth seals since the early 1960s (Tucker, 2013).

The most common types of thermal spraying are plasma spraying, wire arc spraying and flame spraying. The principle of plasma spraying is the generation of a gas plasma by an inert gas through an electric arc. Feedstock enters the plasma jet and is sprayed onto the substrate. In wire arc spraying, an electric arc appears between two conductive wires. A jet of atomizing gas accelerates the molten wires unto the substrate's surface. Flame spraying relies on the combustion of a combination of gases which heats up and accelerates particles unto the substrate.

This project focuses on a specific type of flame spraying called High Velocity Oxy Fuel (HVOF). Oxygen is the fuel gas in this process. The gas mixture propels the feedstock particles through a small diameter nozzle. The specificity of this process is the high values of in-flight particle parameters such as velocity and temperature.

1.2 HVOF: an alternative to hard chrome electrodeposition

1.2.1 Hard chrome electrodeposition

Electrodeposited hard chrome coating have been used in the industry since the middle of the XXth century. Yet, they contain a highly toxic component called hexavalent chrome (CrVI). This component is dangerous for the environment and for human health. Production and security measures linked to this process are very expensive.

Despite the fact that hard chromium electroplating is used to guarantee combinations of adhesion, hardness, corrosion and wear resistance, the method decreases the fatigue resistance of aeronautical components due to the high tensile residual stresses and microcracks density contained in the coating (Vieira et al., 2015).

The main problematic is to find an alternative to hard chrome electrodeposition. The alternative coatings must present equal or better mechanical properties than hard chrome coatings. Research has led to HVOF deposited coatings. As detailed in the next sub-chapter, HVOF creates high quality coatings with very good mechanical properties. This review will narrow the large variety of coatings that can be deposited by HVOF to carbide based (WCCoCr) ones for they have proven to be most successful.

1.2.2 HVOF process

1.2.2.1 Process presentation

HVOF is powered by a combustion of oxygen with a fuel gas, like hydrogen, or a fuel liquid such as kerosene. The chemical reaction within the high-pressure combustion chamber creates a flame whose temperature can go up to around 3000 °C and exits the chamber througha small diameter nozzle. The combustion jet's speed reaches supersonic velocities as high as 2000 m/s. To create the coating, feedstock powder is fed to the flame and sprayed upon the substrate's surface at very high velocities reaching 800 m/s. Figure 1.2 illustrates the HVOF coating process. HVOF coatings are known to be high quality and present good mechanical properties such as high density, high hardness, low porosity, low residual stress, good wear andcorrosion resistance.

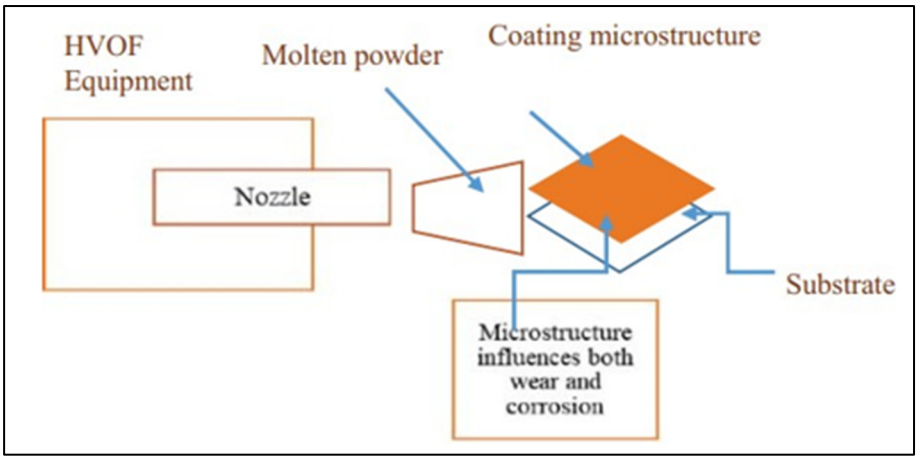

Figure 1.2 Schematic diagram showing HVOF coating features
From Vats et al. (2021, p.3)

1.2.2.2 Projection systems

Each projection system is designed for a specific geometry using a specific fuel gas and feedstock powder. This review will present the systems adapted to tungsten-carbide based (WC… composition) coatings as they will be used further in the project.

As HVOF requires combustion to function, the materials used to build the spraying guns are carefully chosen to prevent oxidation and failure. Most of the systems include an air-or water-cooling system.

ID-Nova

The ID-Nova HVOF torch has been developed by Spraywerx Technologies. It is designed to deposit coatings on inner diameters measuring as small as 114.3 mm thanks to an axial feed of powder. It functions with a spraying distance of 27.5 mm with the standard elbow and 28.2 mm with the high angle elbow. It can operate with either hydrogen, propylene or propane as a fuel gas.

Coatings deposited by the ID-Nova HVOF torch present porosities under 1 % and their hardness can go above 1000 $HV_{0.3}$ (Spraywerx Technologies,2021). Figures 1.3 and 1.4 show the ID-Nova torch in operation, the design of the standard and high angle elbow.

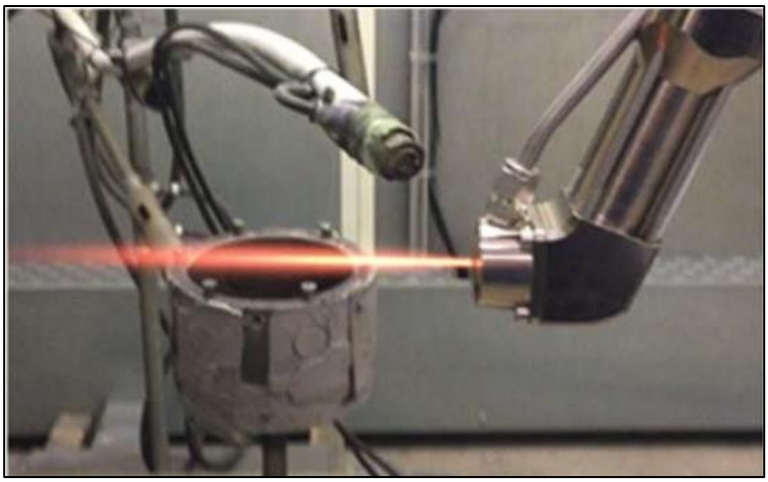

Figure 1.3 ID-Nova HVOF torch in operation
From Spraywerx Technologies (2021, p.1)

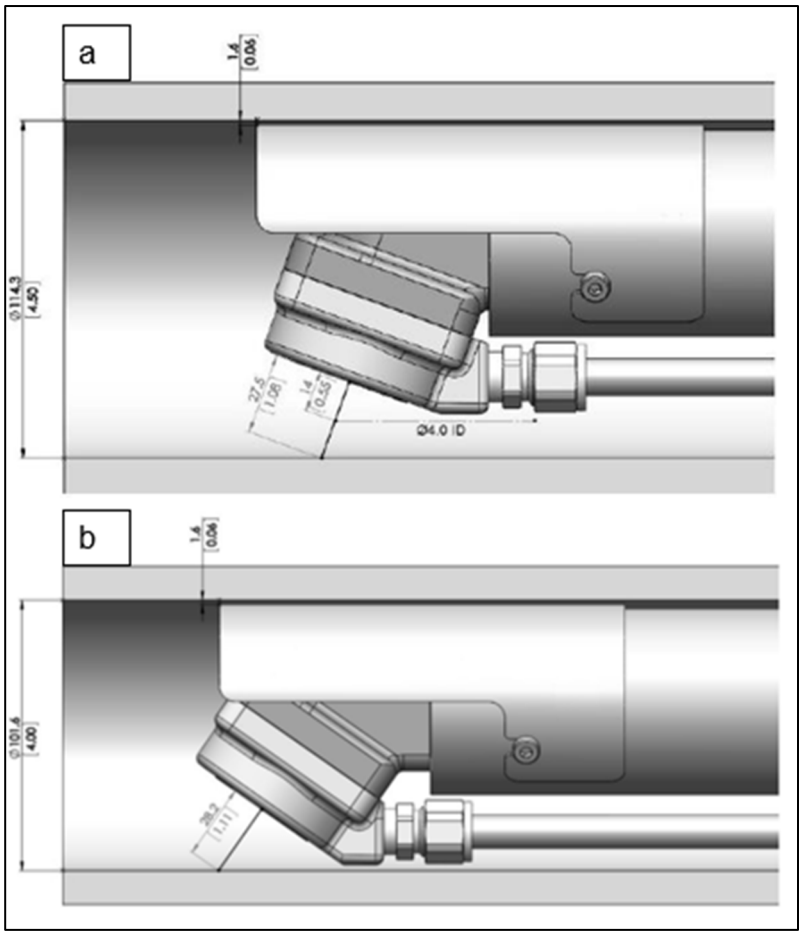

Figure 1.4 ID-Nova HVOF a) Standard elbow b) High angle elbow in 114.3 mm ID
From Spraywerx Technologies (2021, p.1)

Mini-Nova

The Mini-Nova HVOF gun has also been developed by Spraywerx Technologies. It is designed todeposit coatings on even smaller inner diameters reaching 76.2 mm. The design is based on the classic ID-Nova torch. It can operate with either hydrogen or propane as a fuel gas.

Coatings deposited by the Mini-Nova HVOF torch present porosities under 1 % and their hardness can go above 1000 $HV_{0.3}$. The Mini-Nova is more thermally efficient allowing for high power at lower gas flow rates (Spraywerx Technologies, 2021). Figures 1.5 and 1.6 show the Mini-Nova torch in operation, the design of the standard and high angle elbow.

Figure 1.5 Mini-Nova HVOF torch in operation
From Spraywerx Technologies (2021, p.1)

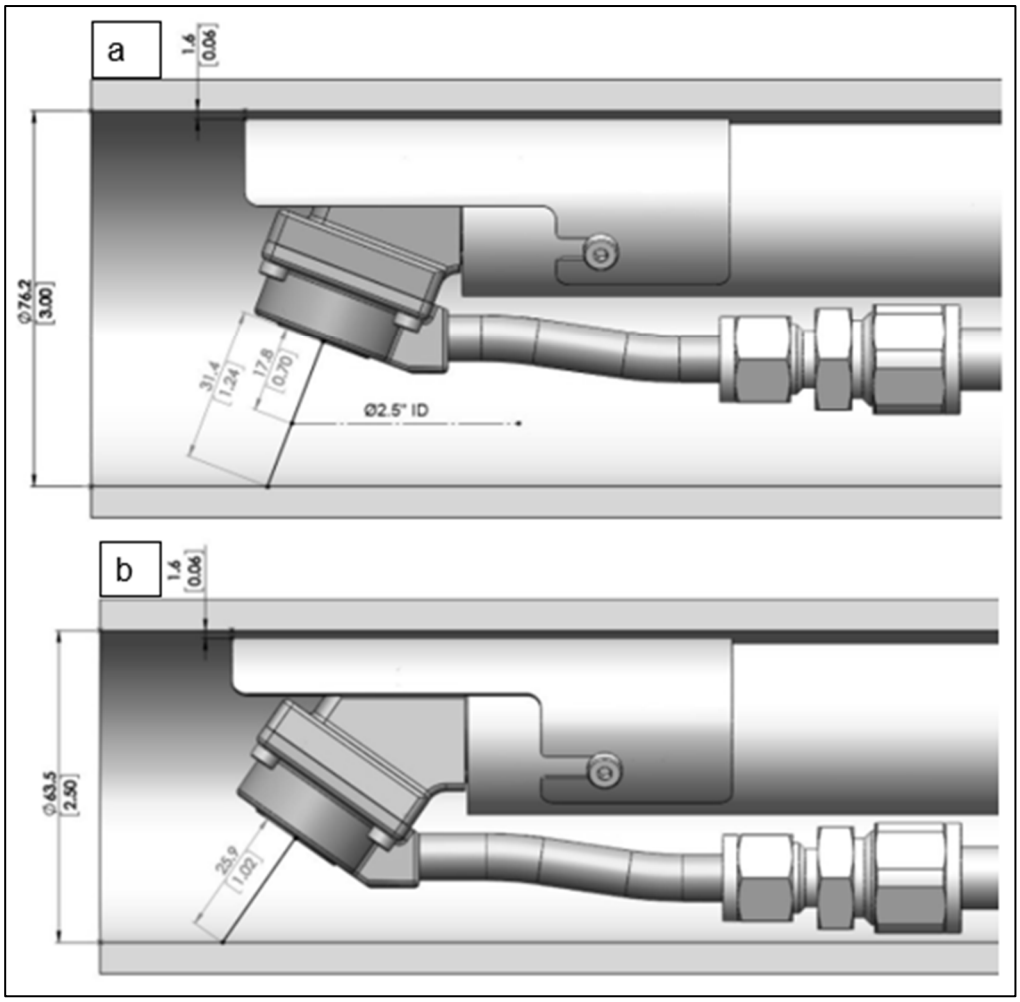

Figure 1.6 Mini-Nova HVOF a) Standard elbow b) High angle elbow in 114.3 mm ID
From Spraywerx Technologies (2021, p.1)

Differences between ID-Nova and Mini-Nova

Table 1.1 reviews the main differences between the ID-Nova and the Mini-Nova torches. When the size of the diameter allows it, the standard elbow is recommended for it has a higher deposition efficiency (Spraywerx Technologies, 2021).

Table 1.1 ID-Nova and Mini-Nova specifications.
From Spraywerx Technologies (2021, p.1)

Specifications	ID-Nova	Mini-Nova
Minimum recommended ID (Standard Elbow)	4.5” (114.3 mm)	3.0” (76.2 mm)
Minimum ID (High Angle Elbow)	4.0” (101.6 mm)	2.5” (63.5 mm)
Rated hydrogen flow	1.165 scfh (550 slpm)	848 scfh (400 slpm)
Rated power	99 kW	72 kW

1.3 Parameters

The coating properties are influenced not only by the properties of the used powders but also significantly by the used spray process and spray parameters. For this reason, the production of HVOF coatings requires the careful control of the process variables together withthe design and geometry of the spray gun (Picas et al., 2013).

1.3.1 Spraying distance

Spraying distance is measured between the substrate’s surface and the point of the gun’s nozzle. For HVOF coatings, spraying distance is usually between 150 mm and 400 mm. The spraying distance affects the in-flight parameters of the particles such as their temperature and velocity. Thus, it indirectly affects the coating’s characteristics (see section 1.5). According to Zhao et al. (2004), “when decreasing the spray distance, the particle velocity and temperature […] increased”.

As shown on figure 1.7, if the distance is too long, particles tend to cool down and they adhere less to the surface. And if the distance is too short, the substrate is exposed to

overheating. It is thus important to figure out the optimal spraying distance and maintain its value to assure a good quality coating (Fang, 2011).

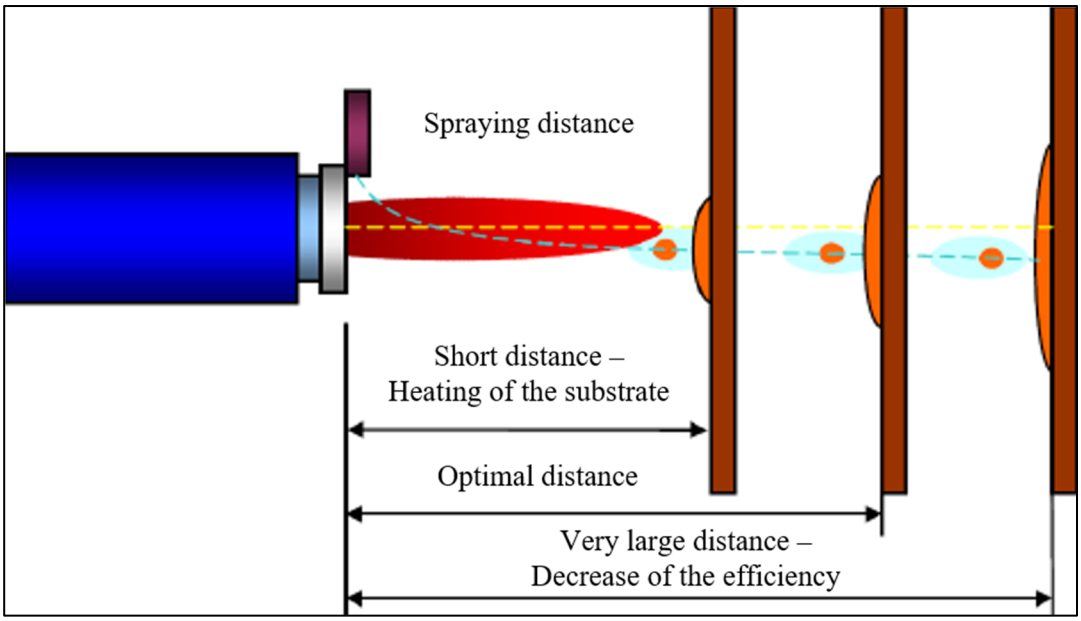

Figure 1.7 Spraying distance
Adapted from Fang (2011, p.12)

1.3.2 Spraying angle

The spraying angle is measured between the flame direction and the substrate's surface that will be coated. The spraying angle has an influence on the spraying efficiency and on the coating's properties such as microstructure, microhardness, residual stress, wear rate and porosity. A 90° angle is usually set for HVOF thermal spray to obtain the best spraying efficiency and therefore is used on simple geometries. According to Houdková et al. (2010),at a 90° angle, the microstructure of the sprayed coating is formed by splats that are elongated parallel to the coating/surface boundary. The same study shows that when decreasing the angle, the coating's porosity increases and its density decreases.

The challenge with HVOF is to coat complex geometries. In this case, the spraying angle can be decreased down to 65° for most cases, and down to 45° in extreme cases (Fang, 2011). According to Vanat et al. (2021), a 60° angle is very well adapted to external and internal corners while increasing porosity and reducing adhesion on inner diameters.

1.3.3 Fuel parameters

HVOF deposited coatings are affected by the nature of the fuel, its flow rate and the oxygen/fuel ratio. Each type of fuel is employed with an appropriate and unique spraying system. Thus, the type of spraying system majorly affects the quality of the coating. As described in the work of Picas et al. (2011), if the system injects the powder through the combustion chamber, the powder's in-flight temperature will be higher compared to a powder injected behind the combustion chamber. Fuel parameters such as the flow rate or the oxygen/fuel ratio can affect the particles' in-flight parameters. On one hand, when increasing the fuel's flow rate, the global flow rate also increases thus accelerating the particles in-flight. Zhao et al. (2004) also observed that the particles' temperature also increased when the total gas flow rate got higher. On the other hand, the oxygen/fuel ratio affects the stoichiometry of the combustion. The stoichiometry affects the flame's temperature. When increasing the ratio until the complete combustion of fuel gas or liquid, the flame's temperature increases as observed in the works of Picas et al. (2011) and Salehi Doolabi et al. (2017). Yet after reaching the flame's highest temperature, the excess of oxygen acts as a cooling gas and the flame's temperature lowers. The oxygen/fuel ratio thus indirectly affects the particles' in-flight temperature as they gain heat from the flame. When increasing the oxygen/fuel ratio, the total gas flow also increases and the particles' gain velocity in-flight. By affecting the particle's in-flight parameters, the oxygen/fuel ratio affects the coating's mechanical properties such as microhardness and adhesion.

1.3.4 Flame parameters

The energy of the flame and its temperature have a big influence on the coating and the substrate. A higher flame temperature produces denser coatings with less un-melted particles. Yet, substrates are often shot peened or undergo a heat treatment before being coated. Thus, each substrate has a critical temperature above which the effects of the shot peeing or the heat treatment are lost. To prevent the substrate from heating above its critical temperature, it can be cooled down by CO_2 or liquid N_2. But this method has proven to be expensive. It is therefore necessary to sometimes reduce the flame's energy, thus reducing its temperature to prevent

overheating. Agüero et al. (2011) attempted to reduce the flame's energy, without changing any other spraying parameters, while keeping the spraying efficiency ang the coating's quality as high as possible. He observed that after decreasing the flame's energy, only the microstructure was affected and the microhardness slightly lowered.

1.3.5 Powder parameters

Each type of powder is designed to a certain use. The coating's characteristics depend on the powder's composition. The grain size has an influence on the coating's density and porosity. For HVOF applications, the size of powder grains is usually between 5 and 60 μm. The initial powder's composition plays a main role in the decarburization process (see section 1.4).

The powder feeding rate is the rate at which the powder passes through the gun nozzle. The powder feeding rate affects the deposition efficiency and uniformity. For lower rate values, the coating's density will not be high enough because the particles' velocity will not be fast enough. Yet for higher rate values, particles will heat too much and create defects in the coating. Powdered feedstock generally is used and sprayed at typical rates of 2.3 to 14 kg/h (5.1 to 31 lb/h) (Tucker, 2013).

1.3.6 In-flight particle parameters

In-flight particle parameters correspond to the temperature and the velocity of the particles when being in projected. Particle velocities are in the range between 400 m/s and 800 m/s. Particle temperatures vary between 1600°C and 2200°C.

In-flight particle parameters can have an influence on the coating's characteristics suchas porosity or microhardness. According to Picas et al. (2011), the amount of porosity and surface roughness tended to decrease with increasing the particle temperature and velocity. Figure 1.8.a shows a high porosity coating associated with a low particle temperature. Figure 1.8.b shows the coating obtained at an intermediate particle temperature. Figure 1.8.c shows a degraded

carbide phase associated to a high particle temperature. When it comes to microhardness, Zhao et al. (2004) observed that it increased with the temperature and velocity of the particles.

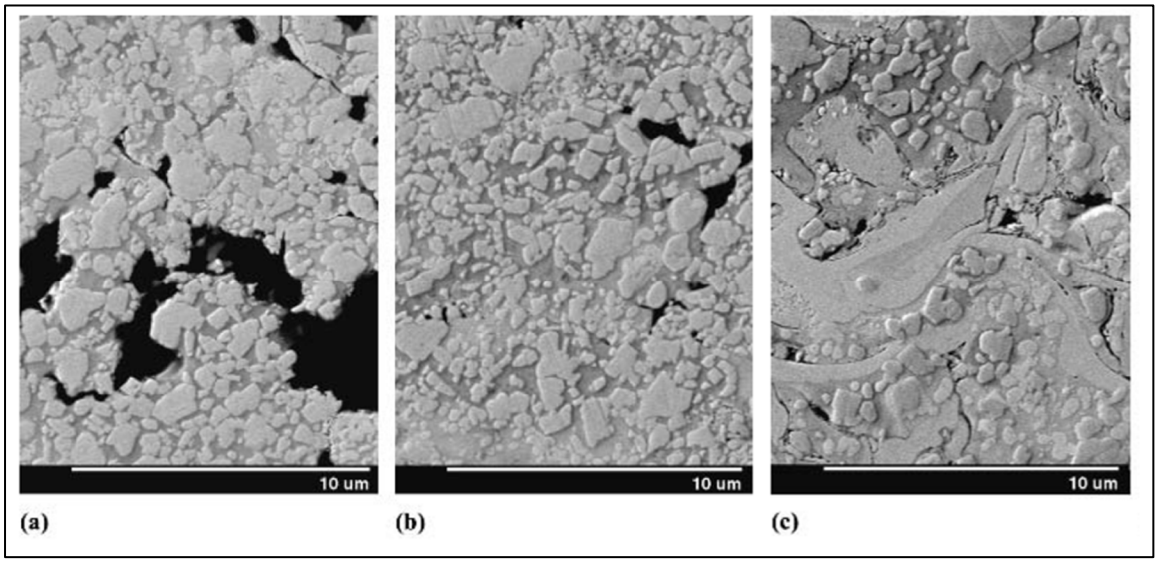

Figure 1.8 Backscattered electron SEM images of carbide-based coatings
Adapted from Marple, Lima (2005, p.9)

1.4 Characterization of WCCoCr powders used for HVOF coatings

As the coating's properties are directly linked to the powder's properties, it is necessary to do some characterization tests on the used powder. The main characterization tests for powders are phase composition analysis, morphology analysis and granulometry.

1.4.1 Phase composition

X-Ray Diffraction (XRD) is the most common method used to identify and quantify the chemical phases of a powder. As illustrated on figure 1.9, X rays scan the surface of the powder sample and interact with the particles. The intensity of the reflected ray depends on the composition of the scanned particle.

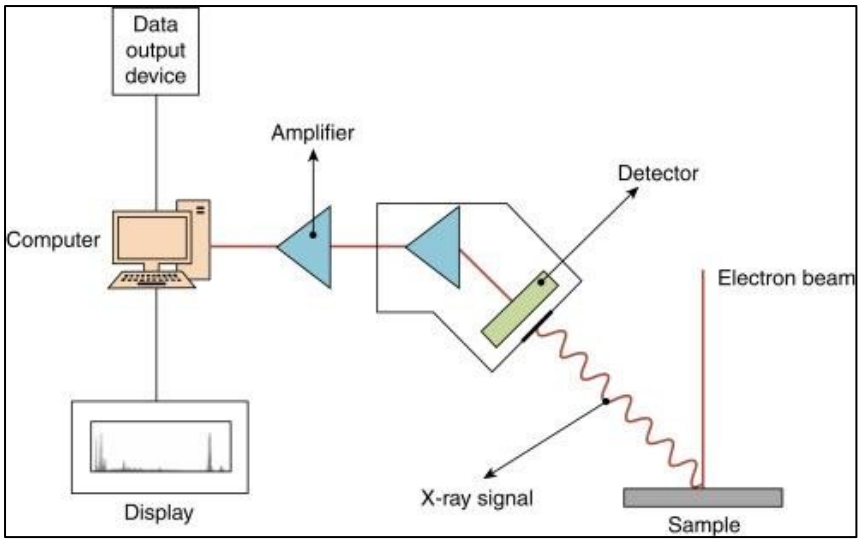

Figure 1.9 Energy dispersive X-ray spectroscopy
From Colpan et al. (2018)

The exact parameters used for WCCoCr powders are detailed in section 2.2. Obtained diffraction patterns, also called spectrums, are compared to reference spectrums published by the Joint Committee on Powder Diffraction Standards (JCPDS). The reference diffraction

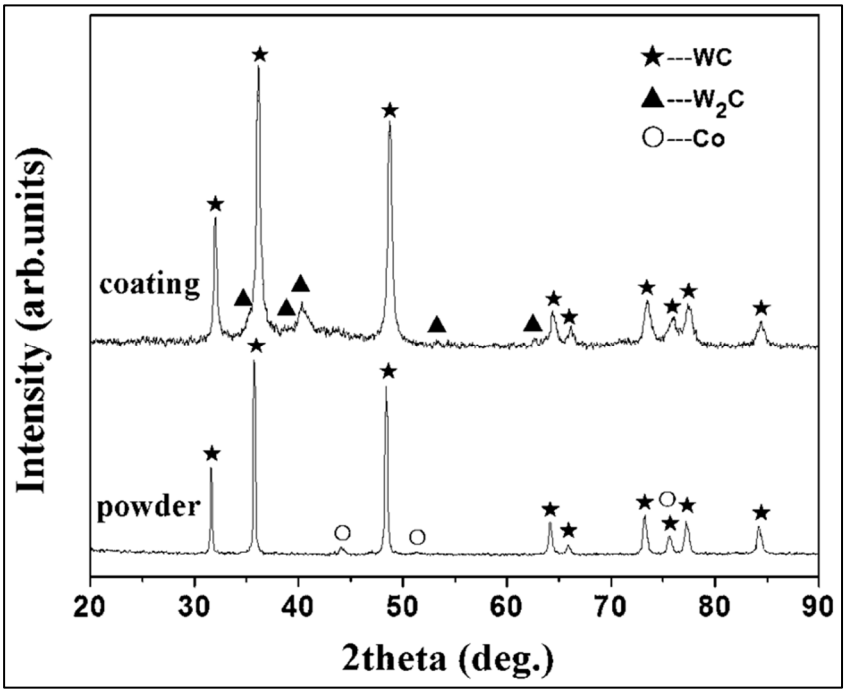

Figure 1.10 X-Ray diffraction patterns of feedstock powder and as sprayed coating
From Hong et al. (2014, p.2)

pattern for WCCoCr powders is displayed on figure 1.10. Usually, the main identified phases are WC, W_2C and a negligeable proportion of a Co based phase.

1.4.2 Morphology analysis

Morphology analysis is the study of the shape of the particles of a selected powder. It is common to use a scanning electron microscope (SEM) to visualize the morphology of the particles. Particle morphology has an influence on the powder's properties, such as its flowability and density. Examples of particle shapes are illustrated on figure 1.11.

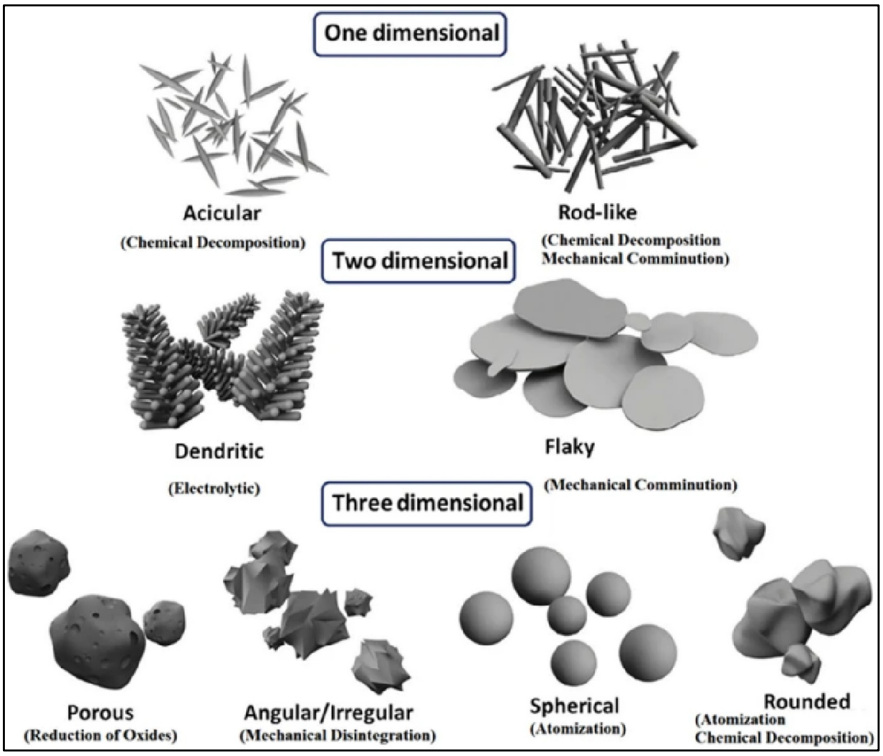

Figure 1.11 Different types of particle shape found in powders
From Bulut et al. (2021, p.2)

1.4.3 Granulometry

Granulometry, also called particle size distribution, is a characterization test that exhibits the particle size and particle size distribution of a selected powder. Granulometry is often done by laser diffraction. According to Bertula (2022), larger particles scatter light at small angles and

high intensity whereas smaller particles scatter light at high angles and low intensity. Laser diffraction is convenient for WCCoCr powders since it can detect particle sizes ranging from 0.02 µm to 2 mm.

1.5 Characterization of WCCoCr coatings deposited by HVOF

Characterization tests allow to assess the quality of a coating and to validate it according to normalized requirement. Each type of powder producing HVOF coatings comes with its own set of requirements. This chapter will present the most common tests used to characterize coatings without enunciating any specific requirements related to a particular type of coating.

1.5.1 Microstructure and phase composition

A coating's microstructure is usually examined with a scanning electron microscope (SEM). The SEM is often coupled with an energy dispersive X-ray spectrometer, which analyses the phase composition. X-ray spectroscopy is a technique that detectsand measures photons, or particles of light, that have wavelengths in the X-ray portion of the electromagnetic spectrum (Ross, 2018). Obtained diffraction patterns, also called spectrums, are compared to reference spectrums published by the Joint Committee on Powder Diffraction Standards (JCPDS). The reference diffraction pattern for WCCoCr coatings is displayed on figure 1.10 (see section 1.4.1).

Image analysis reveals the different phases in the metal but also its porosity, potential defects, and quality of the surface preparation. Figure 1.12 shows the microstructure of a HVOF coating cross section. As we can see on figure 1.12, coatings are not perfect. Defects such as cracks and pores can be present. Image analysis is also used to determine the coating's porosity, as detailed in the next paragraph.

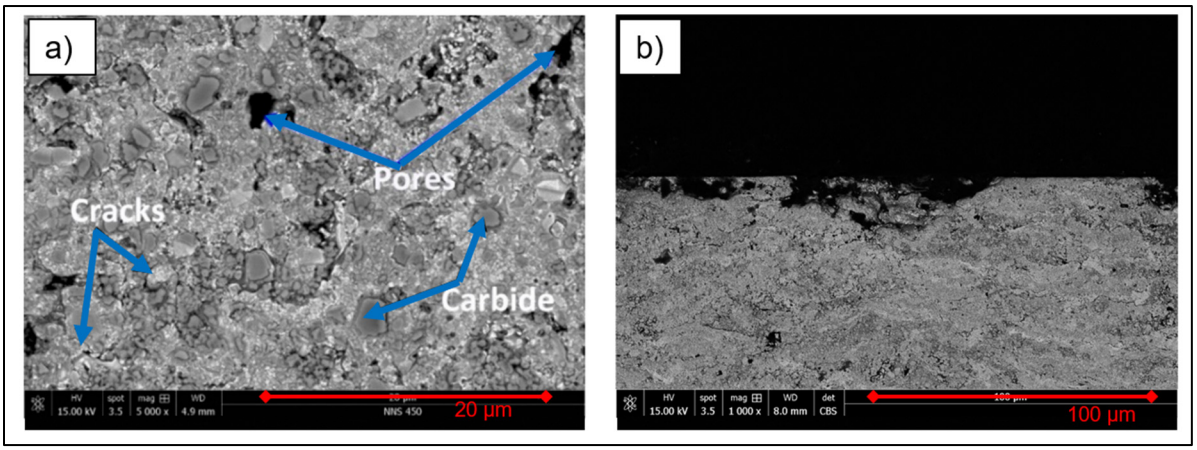

Figure 1.12 Surface and cross-section morphologies of WC–CoCr coating at a) 5000 x magnification and b) 1000 x magnification
Adapted from Xu et al. (2018, p.9)

1.5.2 Porosity

The porosity of a material is the proportion of cavity type discontinuities within a sprayed coating. The porosity can be measured by analyzing the image obtained with an optical microscope. In HVOF thermal spray, the aim is to have the smallest porosity possible. Certain guns can produce coatings with a porosity lower than 1 % (see section 1.2.2.2).

According to (Tucker, 2013), the porosity of thermal spray coatings typically ranges from 5 to 15 % by volume; however, higher-velocity processes may produce coatings with porosity by volume inferior to 2 %.

1.5.3 Microhardness

Microhardness measurements follow the ASTM E384 standard test method for microindentation hardness of materials. For HVOF coatings, a load of 300 gf is commonly used. According to Agüero et al. (2011), WCCoCr coatings deposited by HVOF have hardness values between 1000 and 1200 $HV_{0.3}$. Lower hardness values are due to lower flame energy parameters.

In the work of Picas et al. (2011), hardness values of WCCoCr coatings deposited by HVOF range from 1082 to 1375 $HV_{0.3}$. Higher particle in-flight temperatures can lead to harder coatings.

1.5.4 Adhesion

Adhesion tests for HVOF coatings follow the ASTM C633-01 standard. The test consists of coating one face of a substrate fixture, bonding this coating to the face of a loading fixture, and subjecting this assembly of coating and fixtures to a tensile load normal to the plane of the coating.

During an adhesion test, the operator checks if the coating adheres correctly to the substrate it was deposited. ASTM International published a standard adhesion test coating adapted for HVOF coatings. The test consists of coating one face of a substrate fixture, bonding this coating to the face of a loading fixture, and subjecting this assembly of coating and fixtures to a tensile load normal to the plane of the coating (ASTM C633-01). Other adhesion tests include bend testing, bond strength measurement and pull-off adhesion testing. The bond failure can be either adhesive, in which case the bond has failed at the coating/substrate interface, or cohesive, in which case the bond failure comes from within the coating or the substrate.

1.5.5 Abrasion resistance

A common abrasion test follows the ASTM G65-16 protocol and is called Standard Test Method for Measuring Abrasion Using the Dry Sand/Rubber Wheel. The studied sample is placed against a rubber wheel and sand falls down between the sample and the wheel. A simplified diagram illustrates the setup on figure 1.13.

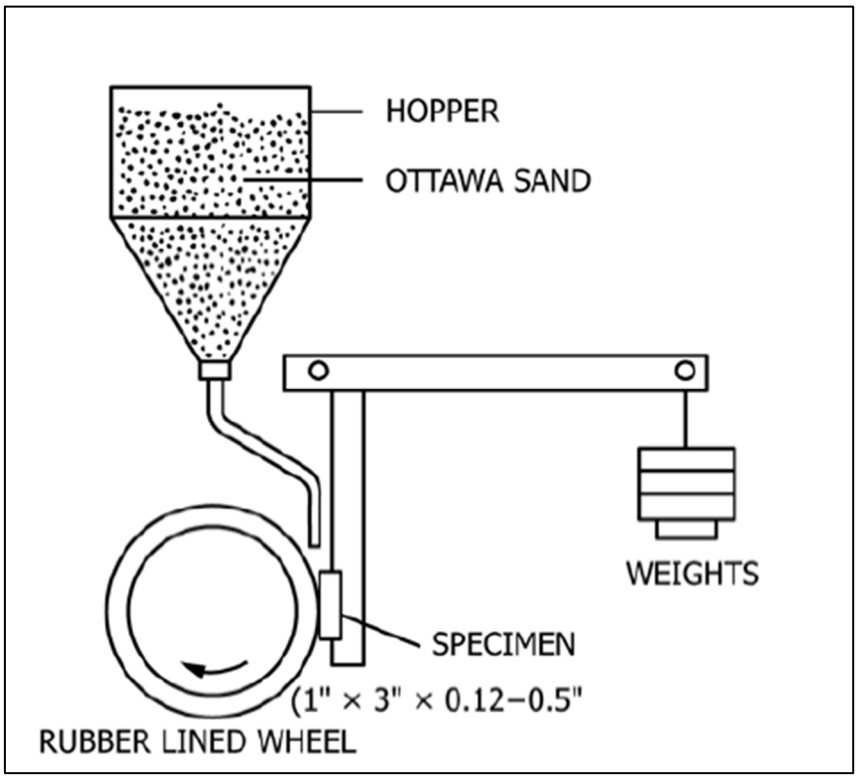

Figure 1.13 Schematic diagram of abrasion test apparatus
From ASTM (2017, p.2)

The main parameters of the test are the force applied against the specimen (N), the number of wheel revolutions and the lineal abrasion (m/ft). Weights are added to the lever arm to ensure that the force is evenly applied. Depending on the abrasive resistance and the thickness of the studied material, one of five existing procedures will be used (figure 1.14). Procedure A is adapted to material with medium to high abrasive resistance. Procedure B is a shorter version of procedure A, adapted to material with low to medium abrasive resistance. Procedure C is used preferably for thin coatings. Procedure D is tailored for materials with low abrasive resistance hence the lower applied force. Procedure E is a shorter version of procedure B.

Specified Procedure	Force Against Specimen,[B] N (lb)	Wheel Revolutions	Lineal Abrasion[A] m	(ft)
A	130 (30)	6000	4309	(14 138)
B	130 (30)	2000	1436	(4 711)
C	130 (30)	100	71.8	(236)
D	45 (10.1)	6000	4309	(14 138)
E	130 (30)	1000	718	(2 360)

[A] See 8.4.
N = Newton (SI metric term for force)
1 lbf = 4.44822 N
1 Kgf = 9.806650 N
[B] Force tolerance is ±3 %.

Figure 1.14 Abrasion test parameters
From ASTM (2017, p.5)

After the abrasion test is done, volume loss (mm^3) is measured with a profilometer. Weight loss is measured by comparing the weight of the sample before the test to its weight after. Higher abrasive resistance will match lower volume loss.

1.5.6 Fatigue resistance

When evaluating fatigue resistance, only axial fatigue is measured. To determine the fatigue strength, it is recommended to follow the ASTM E466 procedure. This standard practiceis an axial fatigue test by applying a controlled, periodic, and constant amplitude load on the material. Standard shaped samples are used during this test as seen on figure 1.15.

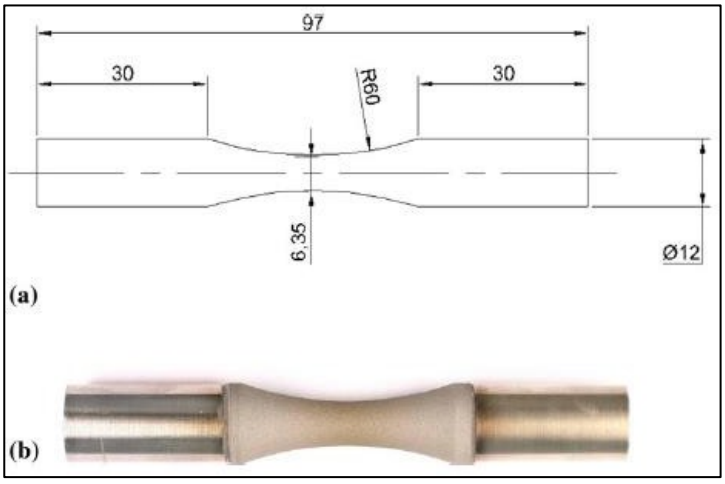

Figure 1.15 Fatigue specimens. Dimensions in mm.
(a) Drawing and (b) as WCCoCr sprayed
From Agüero et al. (2011, p.5)

1.6 Degradation modes inherent to HVOF deposition

1.6.1 Microcracks

Microcracks often propagate along defects, such as semi-molten particles or oxides. Figure 1.16 shows the crack initiation and propagation mechanism. Differences are observed during the propagation stage.

According to Garcia-Rodriguez et al. (2019), the crack's mode of propagation depends on three values: the substrate's strength, the coating's strength, and the adhesion strength at the coating/substrate interface. Depending on the value of each of these strengths, the crack will not propagate the same way.

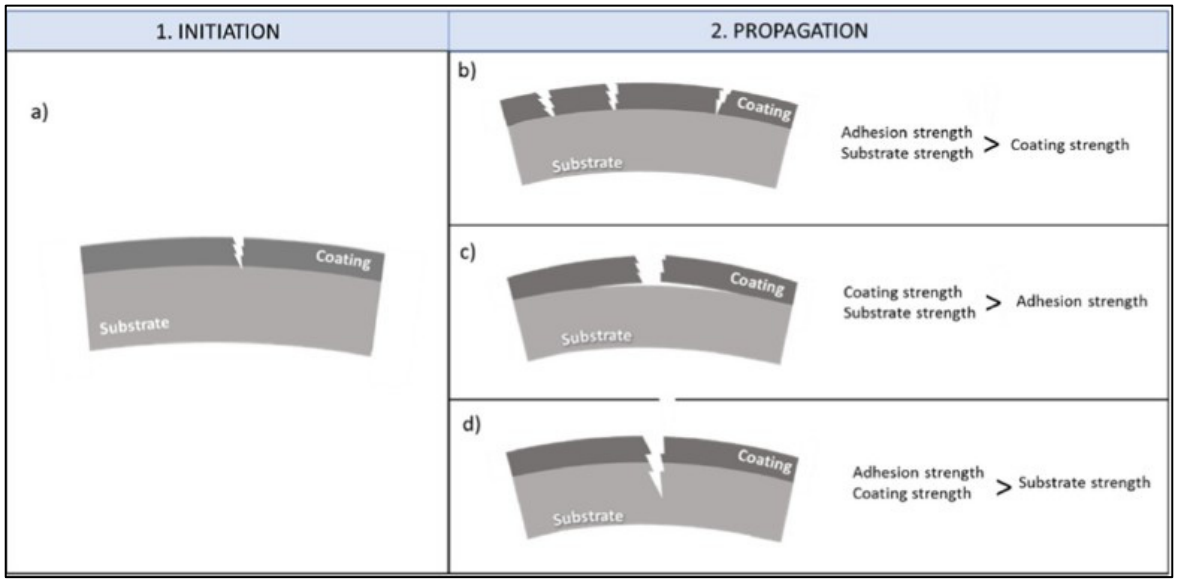

Figure 1.16 Crack initiation, propagation, and criteria
From Garcia-Rodriguez et al. (2019, p.10)

1.6.2 Oxidation

Thermal spray process inevitably brings about oxidation of sprayed particles by heating in air and remains pores near the coatings surface (Kawakita, Kuroda, 2004). HVOF coatings are less oxidized are denser compared to other types of flame spraying, such as plasma spraying.

As the flame used in HVOF contains oxygen, the outer layer of the substrate's surface can become oxidized during the deposition of the coating. When depositing several layers of feedstock powder during the process, oxides layers appear in-between the coating's layers.

Kawakita and Kuroda (2004) studied a mechanism by which a high flow rate of nitrogen gas surrounds the spray particles in flight. This mechanism, called gas shroud (GS), not only lowered the coatings porosity under 0.1 vol % but also lowered the oxygen content from 1.0 wt % to 0.2 wt %. The oxidation level of the deposited coating depends on the feedstock powder. According to Vasudev et al. (2019), nickel (Ni-Cr) based powders minimize oxidation evenmore than tungsten (WC-Co) based powders.

Song et al. (2017), compare the effects of short-term (4 hours) and long-term (100 hours) oxidation on the coating's morphology. Further oxidation characterization can beperformed by long-term exposure to air (100h). Figure 1.17 shows the morphology obtained after1 hour and 10. As we can see, the longer the exposure to air, the bigger the oxide flakes. As described in section 1.6.1, oxides form a pathway for crack propagation.Thus, oxides present in the coating make it easier for potential cracks to propagate onto to substrate and later on, into the core of the substrate. The oxidation of material starts from the surface, which propagates towards the bulk material's core and eventually causes the components to fail (Vasudev et al., 2019).

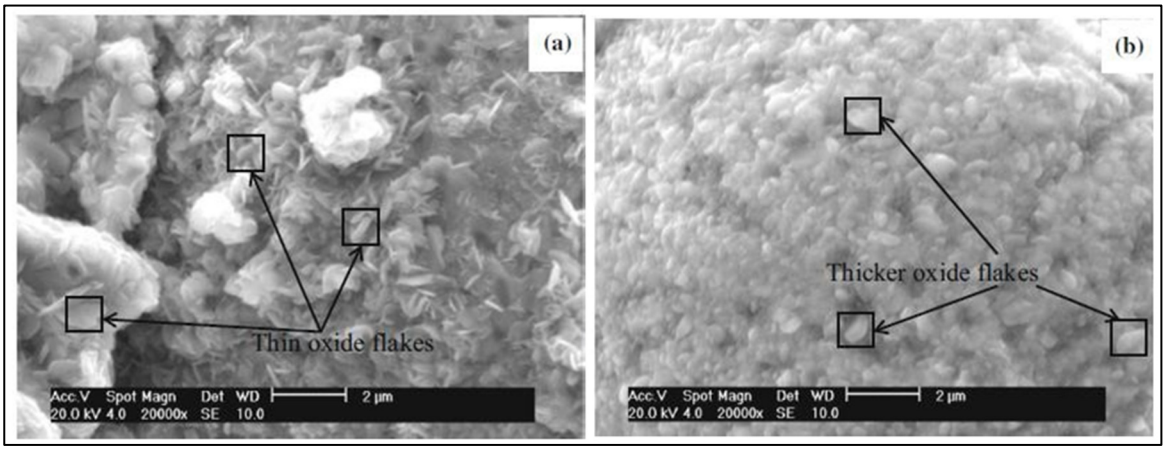

Figure 1.17 Morphology of coating after a) 1 hour exposure b) 10h exposure
Adapted from Song et al. (2017, p.9)

1.6.3 Decarburization

Decarburization is the loss of carbon in a metal. As shown on figure 1.18, decarburization reduces content of WC in coatings, leading to the formation of undesirable phases such as W_2C, W, and amorphous or nanocrystalline CoWC phase (Yuan, 2013). To quantify the degree of decarburization, the proportion of WC found initially in the powder is compared to the amount found in the coating. Decarburization affects the metal's hardness, decreases the material's strength and fatigue resistance.

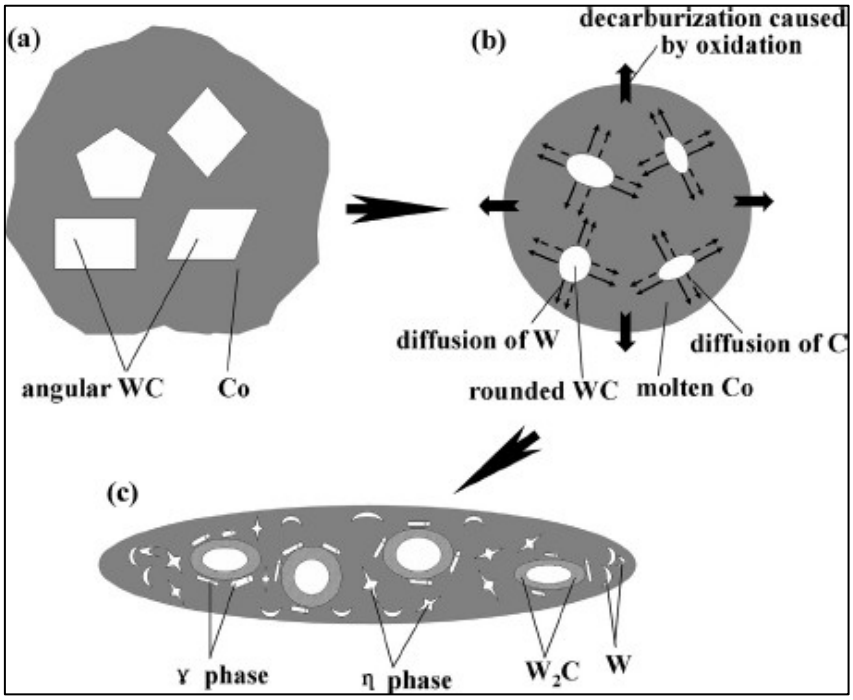

Figure 1.18 Schematic depiction illustrating the decarburization behavior of WCeCo powders, (a) starting WCeCo particle showing irregular WC grains embedded in Co, (b) the particle after in-flight stage showing diffusion-controlled carbon loss, and (c) the splat after the coating formation stage showing distribution of the decarburization-induced phases.
From Yuan et al. (2013, p.6)

Decarburization is affected by the particle characteristics (see section 1.3.5) and the temperature of the heat source which depends on the fuel to oxygen ratio. Agüero et al. (2011), found out that after decreasing the flame energy, thus decreasing the flame temperature, the

deposited coating presented more carbon compared to another coating that used the same powder, but a higher flame energy.

1.6.4 Over-tempering

Over-tempering is a phenomenon that occurs during heat treatments of high strength metals that are quenched and tempered. If a tempered martensite is exposed to a temperature low enough to transform it back into austenite but also high enough to cause further tempering of the martensite, its hardness will drop (Nazemi et al., 2017). Over-tempering creates a heat affected zone (HAZ), found between the surface and the metal's core. The core's properties remain unchanged, and the surface is hardened, as expected, by the heat treatment. Yet, the mechanical properties of the HAZ are altered, especially its hardness, which drops significantly (Barényi et al., 2014). Mechanical properties are affected in the HAZ because of a change in the metal's microstructure. Because of the over-tempering, the cementite precipitates become bigger and hardness decreases.

In the context of HVOF, over-tempering can induce property gradients, such as a hardness gradient below the coating, thus adversely affecting fatigue life. In some cases, the substrate receives a surface treatment prior to the deposition process in order to increase fatigue life. Yet if the sprayed component is heated above 177°C, the effect of the surface treatment may be lost (Agüero et al., 2011). In the context of ID-HVOF thermal spraying, shorter spraying distances can impose a significantly higher heat load on the substrate thus over-tempering the steel even more than in the context of classic HVOF.

CHAPTER 2

EXPERIMENTAL APPROACH

2.1 Objectives and method

Since the domain of ID-HVOF is still at an experimental stage, the goal of this project is to redefine relations between process parameters and coating characteristics based on established relations within the classic HVOF domain. Four sets of samples were provided by the research partner NRC, with spraying parameters established by one of their operators. For each set, depending on the available samples, more or less characterization tests were possible. Interpretations and relations were drawn depending on what tests could have been done.

The first set of samples was done in classic HVOF conditions whilst trying to mimic ID-HVOF conditions by reached temperatures above the standards. A WCCoCr coating was deposited on 4340 AISI steel. The second set was also manufactured in classic HVOF conditions but this time temperatures did not exceed 300°C. The materials were the same as in set 1. Spraying conditions for set 3 were similar to set 2. Yet, the samples of the third set are made of WCCoCr coating deposited on soft steel, since the goal was to optimize spraying parameters and assess their effect on the coating. For set 4, samples were placed inside a spinning cylinder as a way to simulate the deposition process in a complex geometry.

This chapter will describe the methodology applied to manufacture and characterize the diverse sets of samples. For each set of samples, the chapter will overview the base metal characteristics, the powder used for the coating, the spraying conditions, the chosen temperature monitoring method and the characterization tests that had been led. The main restrictions for ID-HVOF WCCoCr coatings are hardness above 950 $HV_{0.3}$ and porosity below 1%. These criteria are based on the requirements of the used torches. Figure 2.1 illustrates the methodology applied to each set of samples that was produced. One set of samples is defined by the substrate's characteristics, the spraying parameters, and the temperature measurement mode. Depending on the available material, some of characterization tests listed in figure 2.1

were done on the studied set. The last step consists in establishing correlations and relations between the different results.

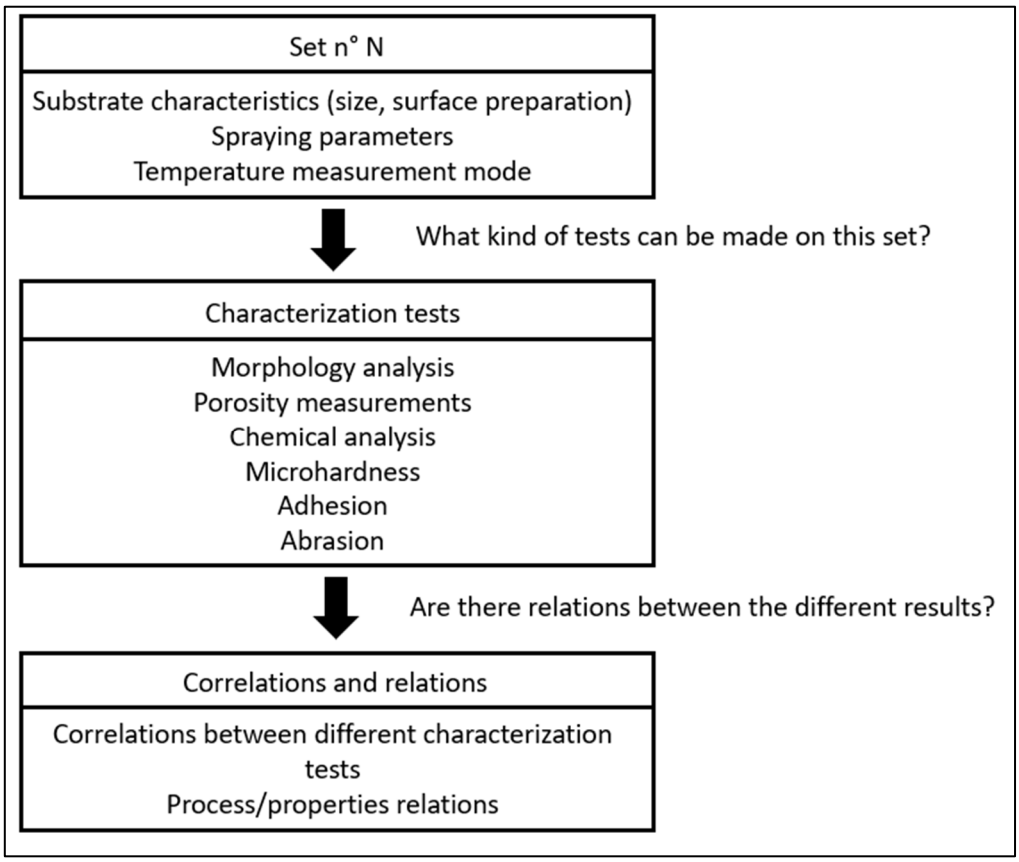

Figure 2.1 Diagram illustrating the steps followed for each set of samples

2.2 Base metal

For sets 1, 2 and 4, the employed substrate was AISI 4340 steel. For set 3, a soft steel was used since the goal for set 3 was to optimize spraying parameters and focus specifically on the coating. AISI 4340 steel is a low alloy, medium carbon steel. Its complete composition is detailed in table 2.1.

Table 2.1 Chemical composition of 4340 AISI Steel. Adapted from (MatWeb, 2023).

Element	Fe	C	Cr	Ni	Mn	Mo	Si	S	P
Composition (%)	95.195 – 96.33	0.370 – 0.430	0.7 – 0.9	1.65 - 2	0.6 – 0.8	0.2 – 0.3	0.15 – 0.3	≤ 0.04	≤ 0.04

In the industry, M300 is most commonly used as a substrate for its high resilience, great fatigue and wear resistance. Yet, it is quite expensive. In order to simulate M300, 4340 AISI steel samples were used at an equivalent hardness as they are similar. To reach the desired hardness of 52 $HRC_{0.3}$ (600 $HV_{0.3}$), (equivalent to a tensile strength of 1792-1930 MPa (260-280 ksi). The 4340 plates received an annealing heat treatment to 845°C for 1 hour, quenched in oil, and then, tempered at 200°C for 1 hour until. Figure 2.2 represents the hardness measured by Vickers indentation on the cross section of a 4340 coupon. Each coupon has an average hardness of 54.5 $HRC_{0.3}$ (600 $HV_{0.3}$). Lastly, the plates were rectified to remove the carbon depleted surface.

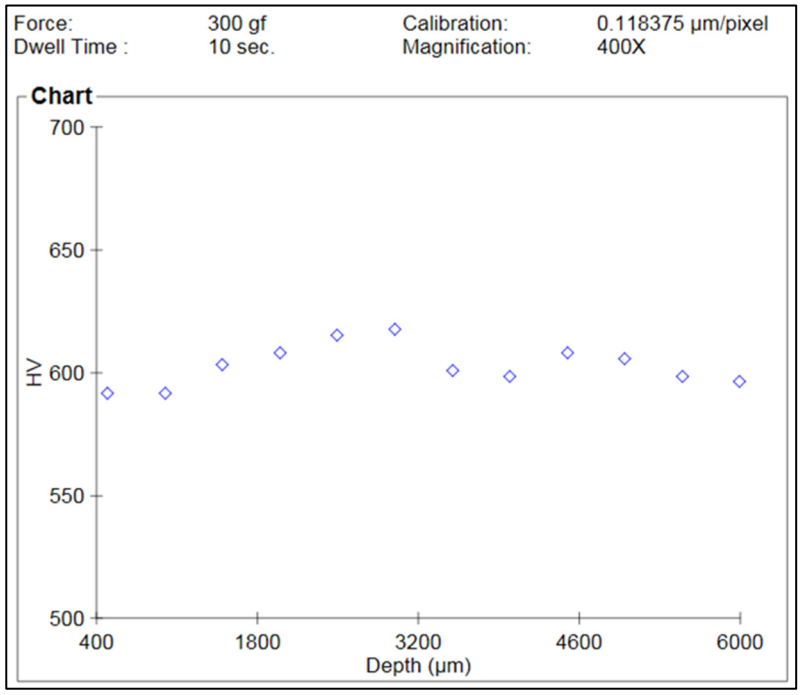

Figure 2.2 Hardness profile of the 4340 substrate

2.3 Overview of the powders used for the WCCoCr coatings

For this project, the NRC provided the powders used for the coatings. Two different powders were used. According to the NRC, powder A is commonly used for HVOF applications and powder B should be more optimal for shorter spraying distances. Both have the same composition: WC-10Co-4Cr. WCCoCr powders resist high velocities and high temperatures thus they are widely used for HVOF applications. These powders are composed of tungsten carbides inserted into a cermet matrix. Both are approved for HVOF coatings by the AMS 2448 standard. Their characteristics are listed in table 2.2. The exact composition of the powder is confidential, therefore they will be named powder A and powder B.

Table 2.2 Characteristics of the used powders

Powder name	Particle diameter (µm)	Composition
A	3.5 – 14.5	WC-10Co-4Cr
B	4.5 – 8.9	WC-10Co-4Cr

2.4 Overview of the manufactured sets of samples

2.4.1 Set 1: Imitation of ID-HVOF conditions on as heat treated material

2.4.1.1 Spraying conditions

For the first set of samples, the goal was to mimic ID-HVOF conditions on a classic HVOF setup. During the ID-HVOF process, smaller equipment is required, hence shortening the spraying distances. Therefore, spraying temperatures are higher compared to classic HVOF. By controlling the path of the spraying gun, it was possible to reach sample temperatures as high as 592°C on a classic HVOF setup. Usually, the sample does not exceed 177°C during classic HVOF. Yet, as explained further in section 3.2.1, by reach extremely high temperatures,

a loss of carbon begins in the coating/surface interface. This phenomenon is called decarburization and has a major influence on the coating's and the substrate's properties.

The dimensions of the 4340 plates are 5.08x5.08x0.625 cm (2x2x0.25 inches). One plate was manufactured for each spraying condition. An example of a 4340 coupon is shown on figure 2.3.

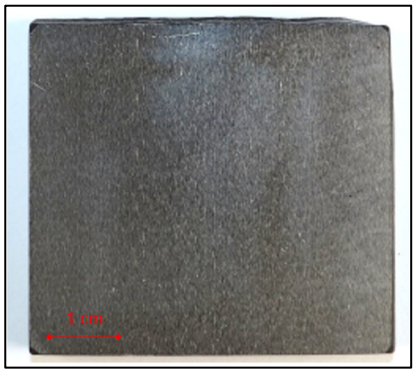

Figure 2.3 Size of 4340 coupon used for set 1

The ID-Nova MK6 torch was used for deposition. The powder used for this set is the coarser one (powder A). Surface temperature variation was controlled by the spraying gun's tangential speed, the pitch (step of the nozzle between each pass), the wait between passes and the type of sample holder (stationary or rotating). The two types of sample holders are shown on figure 2.4 : a stationary holder and a rotating one. Spraying distance was maintained constant at 30 mm. Main spraying parameters are listed in table 2.3. The exhaustive list of spraying parameters is given in appendix II.

Table 2.3 Spraying parameters for the first set of samples

Parameter	**Value**
Gas flows $H_2/O_2/N_2$	440/220/100 slpm
Spraying distance	30 mm
Feedstock WC-10Co – 4Cr	A
Surface tangential speed	1 - 1.5 m/s (stationary holder) 2 - 3 m/s (rotating holder)
Pitch	0.625 – 1.27 mm
Cooling	N_2 jet cooling and/or air jet cooling or none
Rotating holder diameter	17.78 cm (7 inches)
Pause between passes	0 – 15 s

Figure 2.4 Setups of a) stationary sample holder and b) rotating sample holder

2.4.1.2 Temperature measurement mode

In order to measure the surface temperature on set 1, a thermocouple and an IR camera were used. An infra red (IR) camera was used to monitor the temperature at the surface of the sample while being processed. An example of IR camera recordings is displayed on figure 2.5a. The IR camera video recording shows the monitoring of the temperature of 5 points placed across the surface of the sample. For each sample, the variation between the 5 points did not exceed 30°C. Figure 2.5.b displays the analog data recorded by the IR camera. An emissivity of ε = 0.6 was assigned to the sample The radiation emitted by the surface was disrupted by the radiation of the flame and the radiation of the reflected spray jet during the deposition, resulting in some noise. This can be seen when document the thermal history using some regions of the figure 2.5 above the peaks on the analog reading.

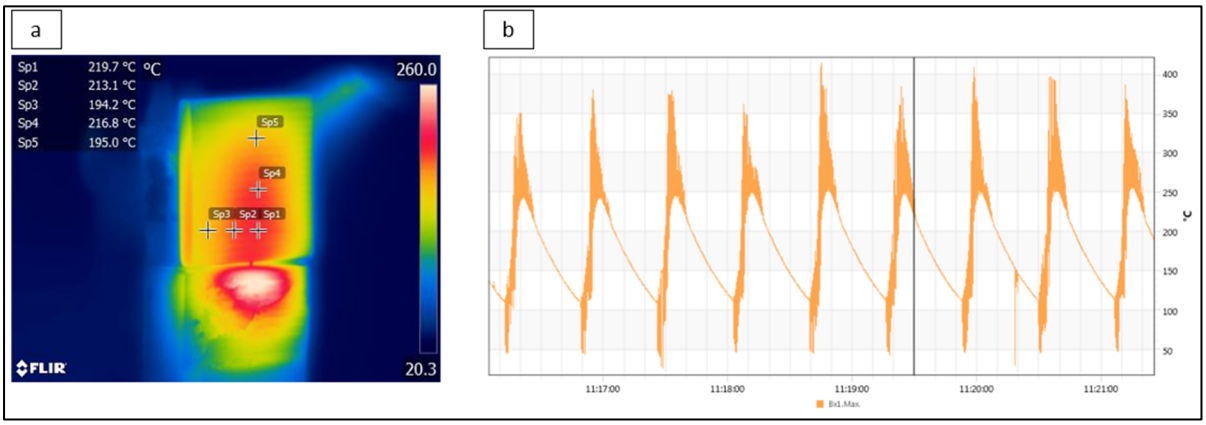

Figure 2.5 Example of IR camera recordings a) IR camera video and b) IR camera analog data

A K-type thermocouple of 0.87 mm diameter has been positioned in a hole 1.6 mm below the surface of the samples. Figure 2.6 displays an example of the analog reading recorded by the thermocouple. The thermocouple readings did not contain any noise. As the thermocouple and the IR camera temperature reading can be matched to approximately 10°C, the temperatures of the thermocouple were considered as the temperatures of the samples.

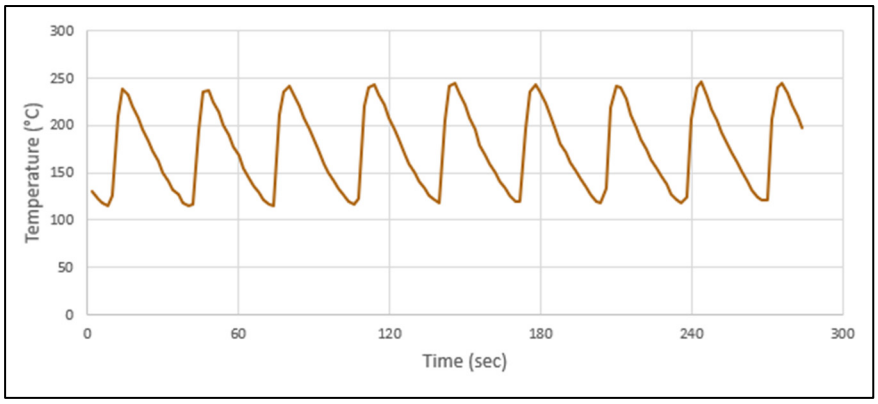

Figure 2.6 Example of thermocouple recording

2.4.1.3 Resulting samples

On the first set of samples, the maximum surface temperature ranges from 90°C to 592°C. Table 2.4 lists the resulting samples with the maximum surface temperature recorded by the thermocouple. The respective coating thickness varied significantly from one sample to the other.

Table 2.4 First set of samples with respective thermocouple recordings of temperature and main variable parameters

Sample number	Max temperature (°C)	Type of holder	Tangential speed (m/s)	Pitch (mm)	Wait between passes (s)
2201214	90	Rotating	2	1.27	15
2201215	111	Rotating	3	1.27	15
2201213	246	Stationary	1.5	1.27	15
2201191	246	Stationary	1	1.27	15
2201192	305	Stationary	1	1.27	0
2201211	391	Stationary	1	0.635	0
2201212	592	Stationary	1	0.635	0

2.4.2 Set 2: Imitation of classic HVOF conditions after rectification of the decarburization layer

2.4.2.1 Rectification of the decarburization layer

A in depth study on the microhardness of the substrate was led in parallel of this project by Baptiste Meynet (2022). For each substrate of the samples of set 1, a gradient of microhardness was measured on the cross section of the substrate. A microhardness gradient was also measured on a bare substrate (which has received the same initial heat treatment as the coated substrates). The microhardness values of the coated sampled were then compared to the microhardness values of the bare substrate. Figure 2.7 displays the mean values of the substrate's microhardness as a function of depth on the cross section, for the bare sample and for the coated ones (each coated sample is identifiable by the maximum temperature reached during the coating deposition process). The main observation to do here is that the hotter the sample was during the coating process, the bigger the hardness loss was near the outer surface. Under 400µm, the hardness decreases as the indent is closer to the interface.

Two hypotheses were enunciated : either the hardness loss was due to the effect of heating during the deposition process, either it was due to the initial heat treatment which induced a decarburization within the substrate. Since the bare substrate presents the same tendency of hardness loss, it was concluded that the deposition process was not responsible for the hardness loss. Therefore, an additional effort was brought onto the next sets of substrates to eliminate this artefact.

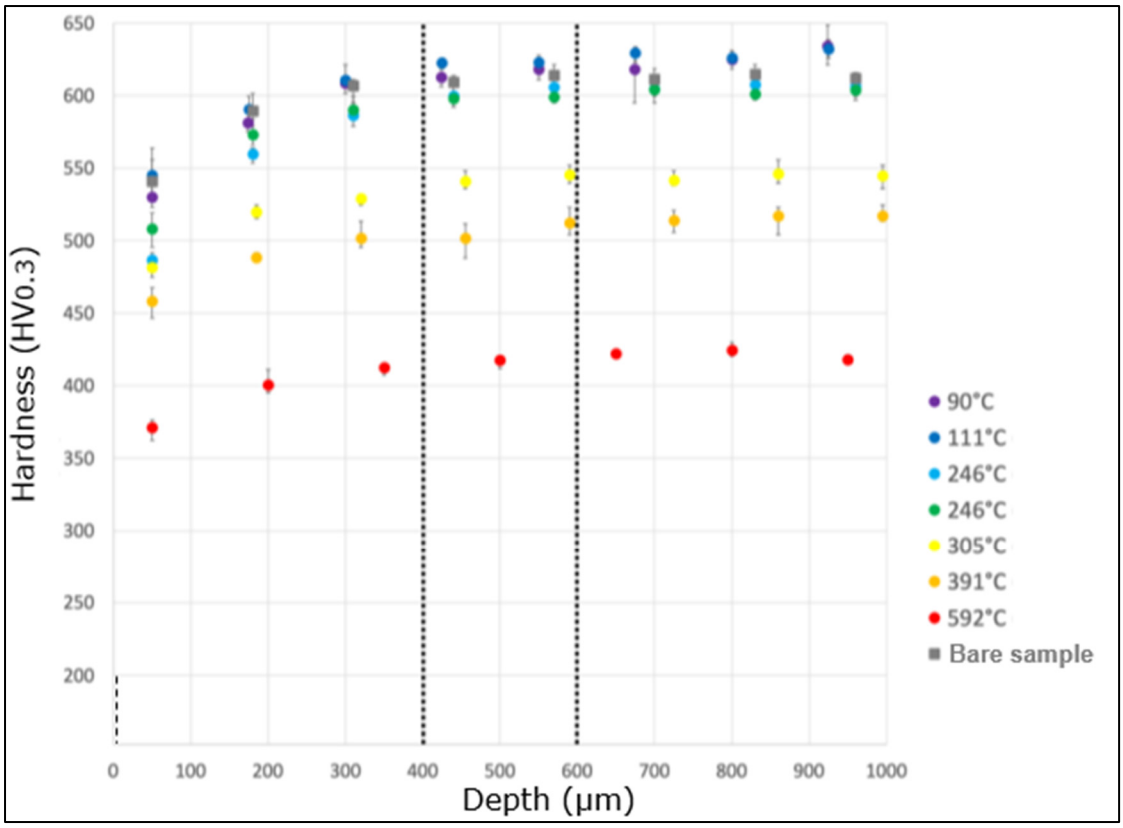

Figure 2.7 Microhardness of 4340 AISI steel substrates as a function of depth. From Meynet, (2022, p.10)

2.4.2.2 Spraying conditions

As detailed in the work of Meynet (2022), initial heat treatment had an influence on the sub-surface area of the substrate. Therefore, an additional 600 µm were rectified from the top of the substrate to eliminate the decarburization zone. On this second set of samples, the goal was once again to impose a temperature variation by adjusting the carousel diameter, the tangential surface speed and the cooling intensity.

Samples were made out of 4340 base metal coated with powder A. Each run included 4 abrasion coupons, 2 erosion coupons, a 2.54x10.16x0.625 cm (1x4x0.25 inches) plate, and 4 pull-test coupons as shown on figure 2.8.

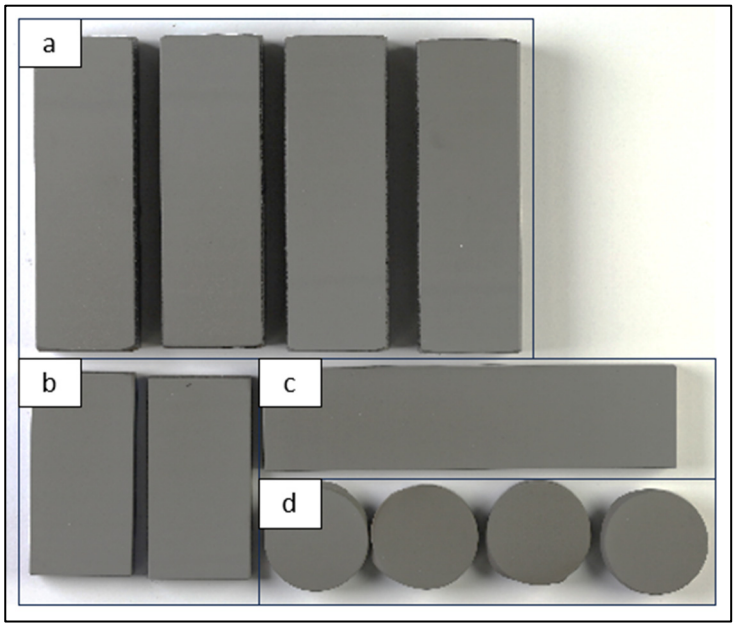

Figure 2.8 One run of samples for the second set of sample a) abrasion coupons b) erosion coupons c) basic coupon and d) pull-test coupons

The same torch (ID-Nova MK6), powder (A), and spraying distance (30mm) as in set 1 were used. Temperature variation was imposed by changing the intensity of air cooling, the size of the mounting carousels and the tangential speed of the spraying gun. Main spraying parameters are listed in table 2.5. The exhaustive list of spraying parameters is given in appendix II. Figure 2.9 shows the carousel setup used for this set.

Table 2.5 Spraying parameters for the second set of samples

Parameter	**Value**
Gas flows $H_2/O_2/N_2$	440/220/100 slpm
Spraying distance	30 mm
Feedstock WC-10Co – 4Cr	A
Surface tangential speed	1 - 1.5 - 2 m/s
Pitch	1.27 – 1.53 mm

Parameter	Value
Cooling	Air jet cooling: maximum, medium and none
Carousel diameter	18 – 38 cm (7 – 15 inches)

Figure 2.9 Setup of samples on the carousel for set 2

2.4.2.3 Temperature measurement mode

In order to measure the surface temperature, a pyrometer was focused on the surface of the samples. An example of the temperature recorded by the pyrometer is displayed on figure 2.10. The blue plot represents the raw data that the pyrometer measures. The red plot represents the corrected measurement, by considering the assigned emissivity to the sample: $\varepsilon = 0.7$.

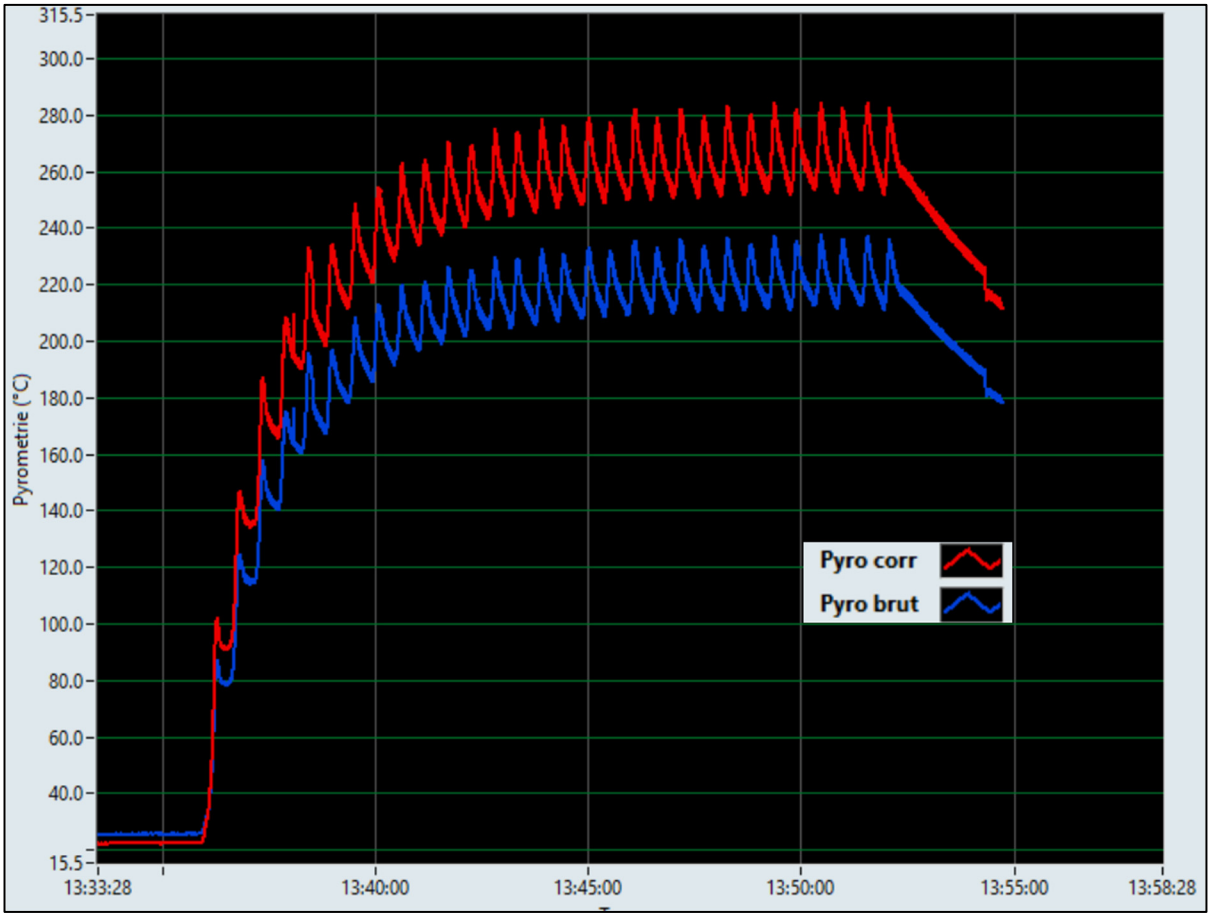

Figure 2.10 Example of pyrometer recording

2.4.2.4 Resulting samples

On the second set of samples, the maximum surface temperature ranges from 80°C to 320°C. Table 2.6 lists the resulting samples with the maximum temperature recorded by the pyrometer, the respective coating thickness and the parameters that were varied by the operator.

The samples of the second set only reached 320°C. Yet, as explained in section 3.2.1, the effect of decarburization appears for temperatures above 300°C. Therefore set 3 was manufactured: for finding the parameters to reach temperatures higher than 300°C and exhibit the effect of decarburization.

Table 2.6 Second set of samples with respective pyrometer recordings of temperature and variable parameters

Sample number	Max temperature (°C)	Carousel diameter (cm)	Tangential speed (m/s)	Cooling
2207072	80	18	2	Max
2207081	140	18	2	Max
2207071	145	38	2	None
2207111	210	38	2	Medium
2207082	280	38	2	None
2207112	290	38	1.5	None
2207121	320	38	1	None

2.4.3 Set 3: Optimizing spraying parameters to reach temperatures above 300°C

2.4.3.1 Spraying conditions

The goal for this extension of set 3 was to reach temperatures above 300°C to exhibit the effect of decarburization in the coating. The substrate used for this extended set was soft steel, and not 4340. It should not affect the properties of the coating, but this time the base metal will not be used to characterise the effects of over-tempering. Also, the powder used for this set is no longer A, but B that has finer grains.

As for set 2, each run included 4 abrasion coupons, 2 erosion coupons, a soft steel plate of 2.54x10.16x0.625 cm (1x4x0.25 inches) and 4 pull-test coupons. The components of one run are shown on figure 2.11.

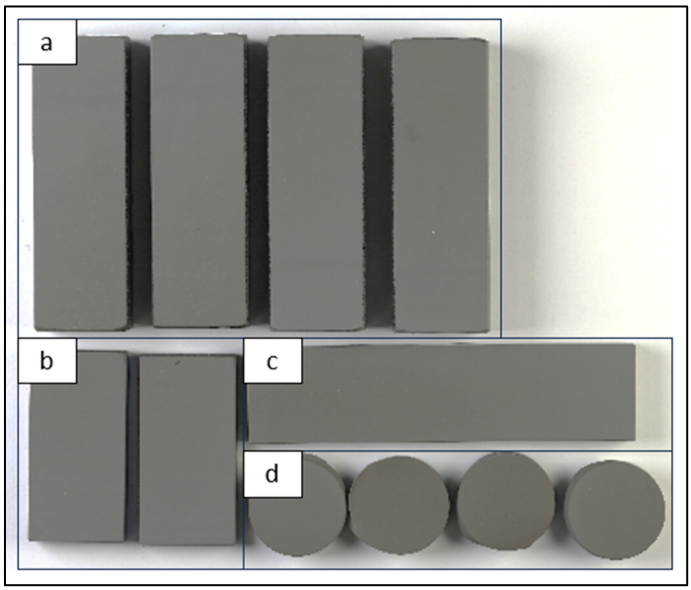

Figure 2.11 One run of samples for the third set of samples a) abrasion coupons b) erosion coupons c) basic coupon and d) pull-test coupons

A new torch was used for deposition, the Mini-Nova III torch. Spraying distance was shortened and kept constant at 25 mm. Temperature variation was imposed by changing the intensity of air cooling.. Main spraying parameters are listed in table 2.7. The exhaustive list of spraying parameters is given in appendix II The carousel setup on which the samples were mounted is shown on figure 2.12.

Table 2.7 Spraying parameters for the third set of samples

Parameter	**Value**
Gas flows $H_2/O_2/N_2$	375/190/60 slpm
Spraying distance	25 mm
Feedstock WC-10Co – 4Cr	B
Surface tangential speed	1.5 - 2 m/s
Pitch	1.27 µm
Cooling	Air jet cooling: maximum, medium and none

Figure 2.12 Setup of samples on the carousel for set 3

2.4.3.2 Temperature measurement mode and resulting samples

The temperature was measured in the same way as for set 2, with the pyrometer focused on the surface of the samples. The maximum surface temperatures range from 120°C to 500°C. Table 2.8 lists the resulting samples with the maximum temperature recorded by the pyromete and the parameters that were varied by the operator.

Table 2.8 Third set of samples with respective pyrometer recordings of temperature and variable parameters

Sample number	Max temperature (°C)	Tangential speed (m/s)	Pitch (mm)	Cooling
2303291	120	2	1.27	Max
2303301	250	2	1.27	Max
2303302	350	2	1.27	Medium
2303311	420	1.5	1.27	Medium
2303271	440	2	1.27	None
2303241	500	2	1.27	None

2.4.4 Set 4: Deposition inside a steel cylinder

2.4.4.1 Spraying conditions

The goal for the fourth set of samples was to study the effect of the surface preparation of the substrate on the properties of the coating and the over tempering of the substrate itself.

As detailed in section 2.3.1.1, initial heat treatment had an influence on the sub-surface area of the substrate. Therefore, an additional 600 µm were rectified from the top of the substrate to eliminate the decarburization zone. Half of the 4340 substrates received a surface grit blasting at 60 grit, with a 60 psi pressure (0.41 MPa) at a blasting distance of 15-20 mm and 400 % coverage. The other half received a surface shot peening following norm SAE-AMS-S-13165

and a grit blasting at 240 grit, with a 60 psi pressure, a blasting distance of 15-20 mm and 400 % coverage. Surface treatments were done by Surftec.

The dimensions of the 4340 coupons are 2.54x10.16x0.625 cm (1x4x0.25 inches). Figure 2.13 shows an example of a coupon. The coupons were coated by pairs: one only grit blasted and the second one shot peened and grit blasted. Both samples were mounted in a 4340-steel cylinder with an inner diameter of 12.2 cm (4.8 inch). The coupons will thus follow the thermal history of the cylinder. The 4340 steel cylinder is shown on figure 2.14.

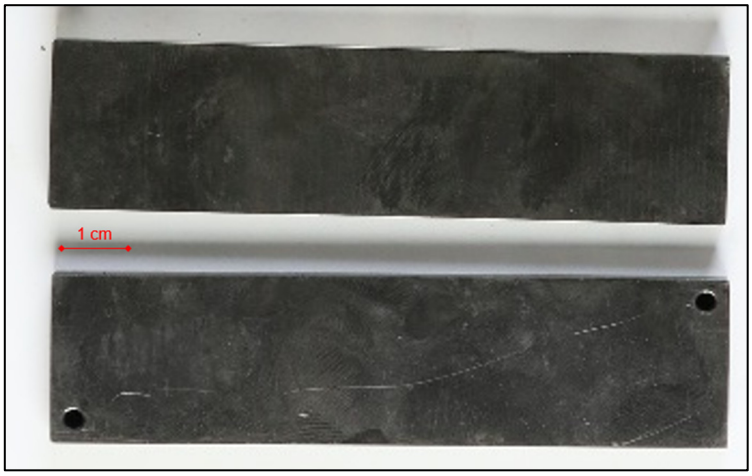

Figure 2.13 Size of 4340 coupons used for set 4

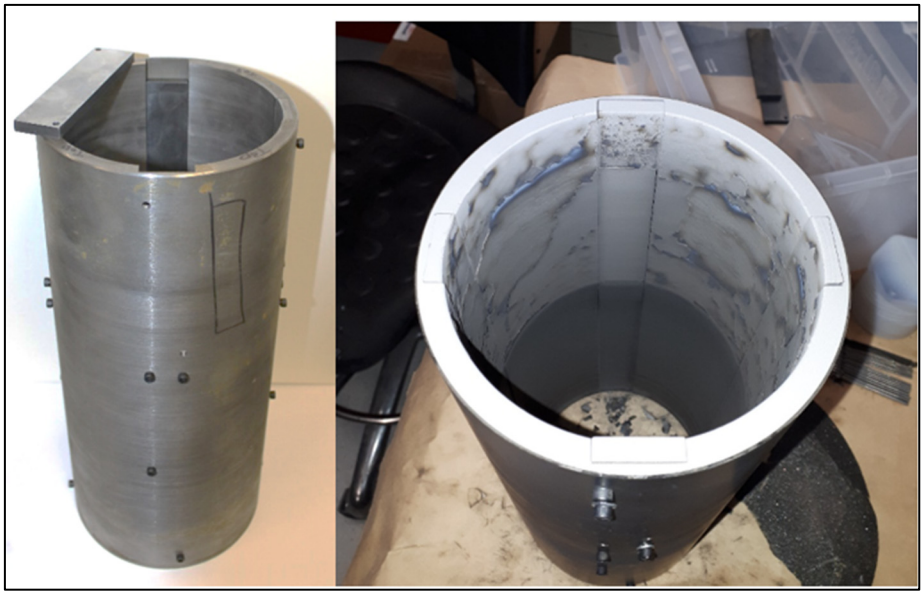

Figure 2.14 4340 cylinder used for coating set 4

The ID-Nova MK6 torch was used for deposition, as for sets 1 and 2. The powder used for this set is the finer one (B) , the same one as in set 3. Maximum surface temperature was controlled using different pauses between passes. Main spraying parameters are listed in table 2.9. The exhaustive list of spraying parameters is given in appendix II

Table 2.9 Spraying parameters for the fourth set of samples

Parameter	**Value**
Gas flows $H_2/O_2/N_2$	375/190/60 slpm
Spraying distance	25 mm
Feedstock WC-10Co – 4Cr	B
Surface tangential speed	2 – 3 m/s
Pitch	1.27 mm
Pause between passes	0 – 15 – 30 – 45 s

2.4.4.2 Temperature measurement mode and resulting samples

Temperature was measured by the same pyrometer as for set 2 and 3. For this set, the pyrometer was aiming the outside surface of the 4340 cylinder. The correlation between the temperature on the deposition surface and the measured temperature of the outside surface of samples is yet to be done. For this project, results will be referred as a function of the measured external temperature keeping in mind that the temperature inside is higher.

On the fourth set of samples, the maximum external temperature ranges from 127°C to 300°C. Table 2.10 lists the resulting samples with the maximum external temperature recorded by the pyrometer, the respective coating thickness and the parameters that were varied by the operator. The reason why a thermocouple was not mounted inside the coupons is simply because the manufacturer did not know how to install them safely enough to stay fixed during the rotation at 300 rpm.

Table 2.10 Fourth set of samples with respective pyrometer recordings of temperature and variable parameters

Sample pair number	Max temperature (°C)	Tangential speed (m/s)	Pitch (mm)	Pause between passes (s)
2301272	127	3	1.27	45
2301313	130	3	1.27	45
2301311	175	2	1.27	45
2301271	182	2	1.27	45
2301243	188	2	1.27	30
2301241	231	2	1.27	15
2301242	230	2	1.27	15
2301312	302	2	1.27	0

2.5 Overview of the characterization tests

2.5.1 Characterization of the powders

Since the coating's properties depend on the powder's properties, it was important to do some preliminary tests on the powders. These characterization tests focused on the phase composition, the morphology and the granulometry of the powders.

Phase composition analysis

In order to identify and quantify the different phases in the powders, chemical analysis was done by XRD with the XRD X'Pert^3 Panalytical software. Parameters are detailed in table 2.11. Data was analysed with HighScore XRD Data processing. The details of the analysis are presented in appendix I. Quantification of each phase proportion was calculated with a Rietveld fitting.

Table 2.11 XRD parameters for composition analysis of the powders

XRD Parameters	Value
2θ	20°-100°
Step	0.05°
Anode material	Cu-Kα
Radiation	45 kV-40mA

Morphology analysis of the powders

Morphology analysis of the powders was done with a Thermo Fisher – Apreo2 Lox Vac scanning electron microscope (SEM) at the NRC. Samples were mounted onto cold casted resin, polished with 400, 600, 800 and 1200 grit, followed by a 3 μm diamond suspension (Struers MD-Dac cloth) and colloidal silica (Struers MD-Chem).

Granulometry

Granulometry was done by laser diffraction with the LS 13 320 Laser Diffracton Particle Size Analyzer at Beckman Coulter (Montreal, Canada). Particle diameters are characterized by 3 threshold values called d_{10}, d_{50} and d_{90}. 10% of particles are smaller than d_{10}, 50% of particles are smaller than d_{50} and 90% of the particles are smaller than d_{90}.

2.5.2 Characterization of the metallic samples

Microstructure and porosity overview

In order to document the microstructure of the coatings,samples were cut (Secotom by Struers) mounted in cold casted resin and polished (Tegramin by Struers) with 220, 800, 1200 and 4000 grit paper, followed by a 3 μm diamond suspension (Struers MD-Dac cloth) and colloidal silica (Struers MD-Chem). Microstructure of the coatings was viewed with the Olympus BX-53M optical microscope. Porosity was measured at the NRC with the help of their technicians with

the Olympus Stream Motion software. Porosity is measured once with the software on each sample. The requirement for the coating's porosity is to be below 1%.

Chemical analysis by XRD

Chemical analysis was done with X-Ray Diffraction (XRD) with the XRD X'Pert^3 Panalytical under the following parameters (table 2.12).

Table 2.12 Chosen XRD parameters for chemical analysis

XRD Parameters	Value
2θ	20°-100°
Step	0.05°
Anode material	Cu-Kα
Radiation	45 kV-40mA

One analysis was done per sample and was compared to the composition of the powder composing the coating. Data analysis was led with HighScore XRD Data processing. The details of the analysis are presented in appendix I. Phase quantification was done with a Rietveld fitting.

Microhardness tests

In order to study the evolution of the hardness as function of the thermal history of the sample, hardness tests were done on the substrate and base metal. One of the HVOF evaluation criteria for goodness is to have a coating harder than 950 $HV_{0.3}$. and the hardness in the substrate was also studied to document the over-tempering effect.

During a microhardness test, the hardness of the material is measured. The most common test is the ASTM E384 standard test method for microindentation hardness of materials. The indentation is made with Knoop or Vickers indenters. The value of the hardness depends on the applied load which can be between 9.8 × 10-3 (1 gf) to 9.8 N (1000 gf). For HVOF coatings, the load is usually 300 gf.

A line of 8 indents was made across the coating as well as across the substrate. Figure 2.15 illustrates the location of the indent pattern. At least three diagonals were left between the indents and from the edges of the sample as suggested by the ASTM standards. The hardness pattern was done in a zone exempt of major defects. All microhardness indents were done with the Automated Dual Microhardness Tester from Clemex.

Samples were prepared according to the procedure detailed in section 2.7.1. Vickers microhardness indents were done under 300 gf for 10 seconds. Indents were measured by an optical microscope at 400X magnification.

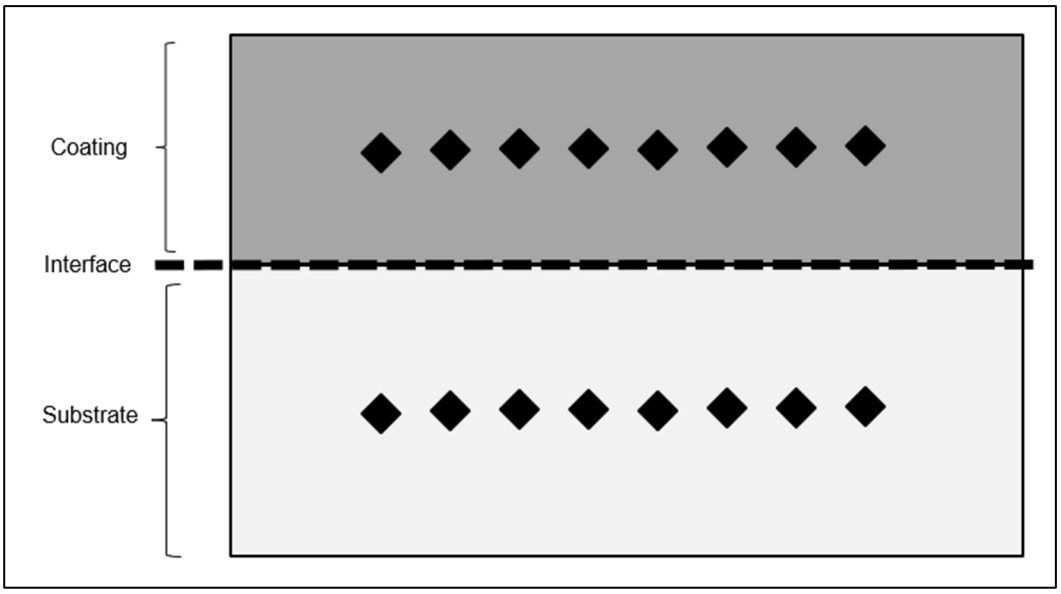

Figure 2.15 Schematization of the Vickers indents done on the coating and substrate (not to scale)

Adhesion tests

During an adhesion test, also called pull test, the operator checks if the coating adheres correctly to the substrate it was deposited. ASTM International published a standard adhesion test coating adapted for HVOF coatings. The test consists of coating one face of a substrate fixture, bonding it to the face of a loading fixture, and subjecting this assembly of coating and fixturesto a tensile load normal to the plane of the coating (ASTM C633-01). A diagram of the setup is shown on figure 2.16. The bond failure can be either adhesive, in which case the bond has failed at the coating/substrate interface, or cohesive, in which case the bond failure comes from within the coating or the substrate. The setup is illustrated on figure 2.17.

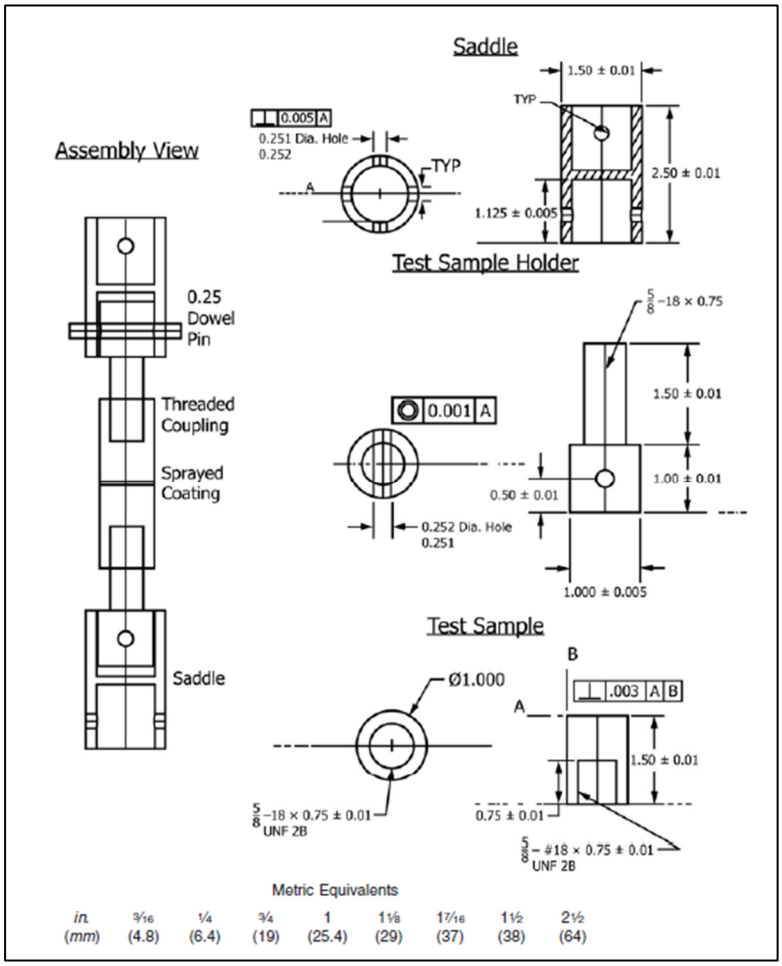

Figure 2.16 Schematized diagram illustrating the adhesion test
From ASTM(2021, p 3)

The tests were done with the INSTRON 5900R Universal testing machine. A blank reference sample was tested before testing three replicas per sample condition. Tests were performed at maximal load: 600 kN.

Figure 2.17 Pull test machine

Abrasion tests

Abrasion tests were done according to the ASTM G65-16 Standard Test Method for Measuring Abrasion Using the Dry Sand/Rubber Wheel Apparatus. More specifically, the abrasion test followed procedure A, according to the parameters in table 2.13, as the WCCoCr is expected to have medium to high abrasion resistance. At the NRC, operators use the Falex Friction and Wear Test Machine (figure 2.18). For each condition, four tests were done to assure repeatability. Ottawa AFS Testing sand 50-70 lot. is used as an abrasive. A weight of 12 lbs is added onto the lever arm to ensure an even applied force.

Table 2.13 Parameters for abrasion tests done at NRC

Specified procedure	Force against specimen	Wheel revolutions	Linear abrasion
A	130 N	6000	4309

Figure 2.18 Falex Friction and Wear Test Machine

To measure weight loss, each abrasion coupon was weighted before and after the abrasion test. Volume loss was evaluated with a NovaCam microcam 3D profilometer (figure 2.19). A step size of 0.05 μm was configured to swipe the sample's surface.

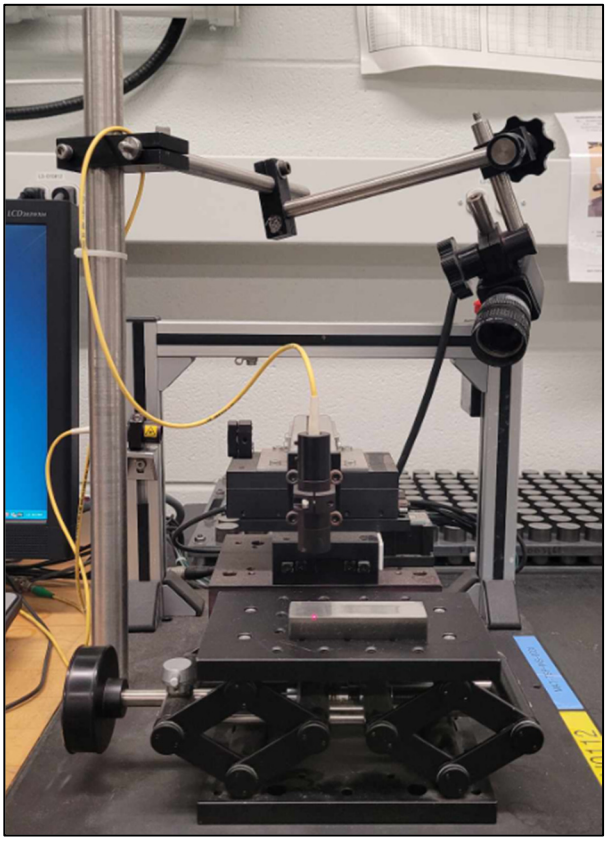

Figure 2.19 Profilometer

CHAPTER 3

RESULTS AND DISCUSSION

This chapter is divided in two parts: the first part (section 3.1) will discuss the results of the characterization tests done on the powders; the second part (section 3.2) will present the results of the conducted characterization tests on the four sets of samples that were manufactured. The goal is to establish relations between the process parameters and the coating properties.

3.1 Results of characterization tests led on WCCoCr powders

This section presents the results of the characterization tests done on the two powders used for the deposition of the coatings: phase composition, morphology analysis and granulometry. Similarities and differences between the two powders were identified.

3.1.1 Morphology analysis

The SEM images at 5000x and 25000x magnification for the A and B powders show that for both powders, particles are quite round, even spherical for some of them as illustrated in figure 3.1. For powder A, particle size presents variable grain sizes, with two that are larger than the others. For powder B, the particle size distribution is homogeneous, with no significantly larger nor smaller particles.

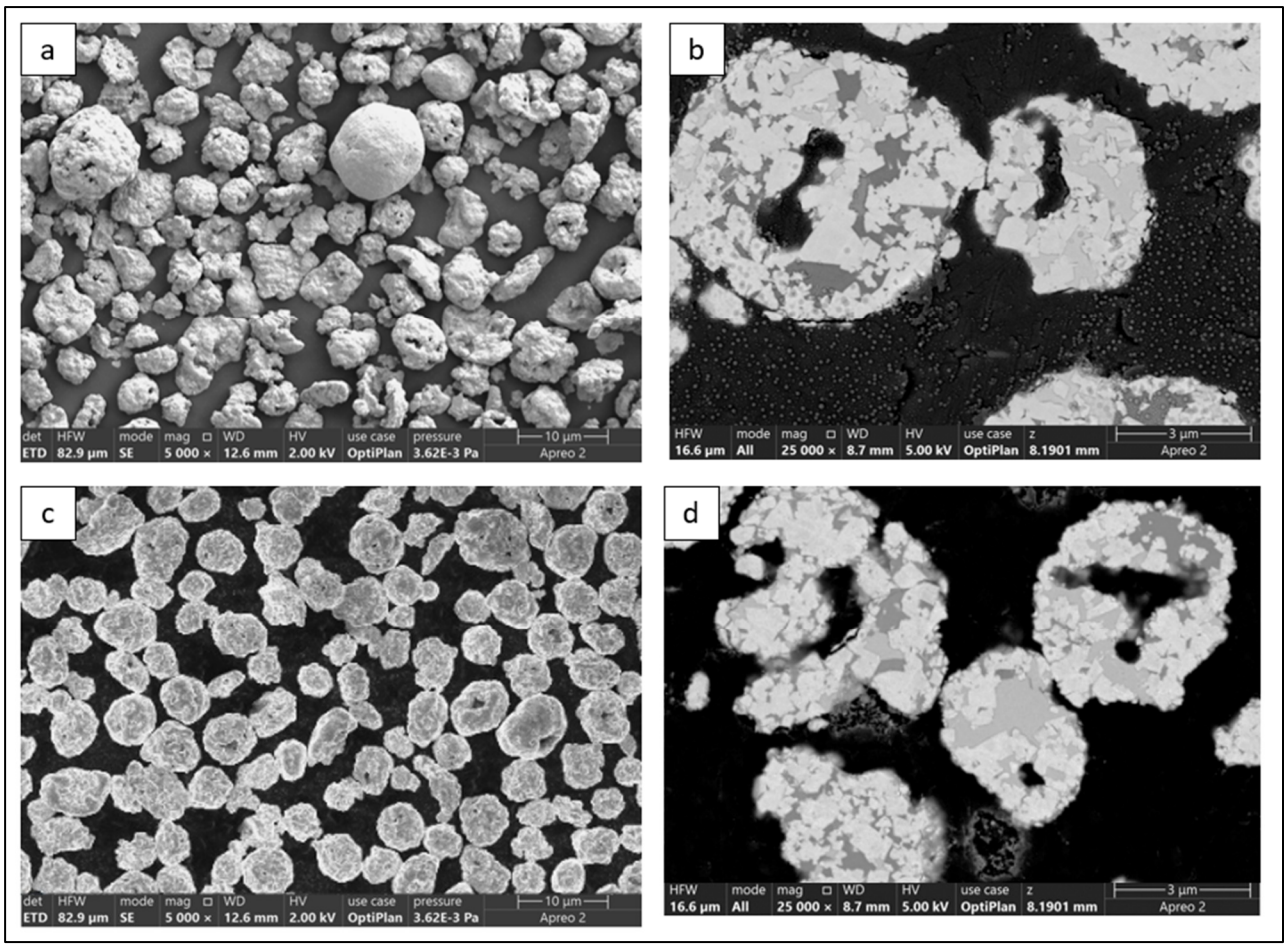

Figure 3.1 SEM images of a) powder A at 5000x magnification b) powder A at 25000x magnification c) powder B at 5000x magnification d) powder B at 25000x magnification

3.1.2 Phase composition

Diffraction patterns of the two powders used for this project as well as the phase proportions are displayed on figure 3.2. Both diffraction patterns are similar: the intensity and the position of the peaks are almost identical.

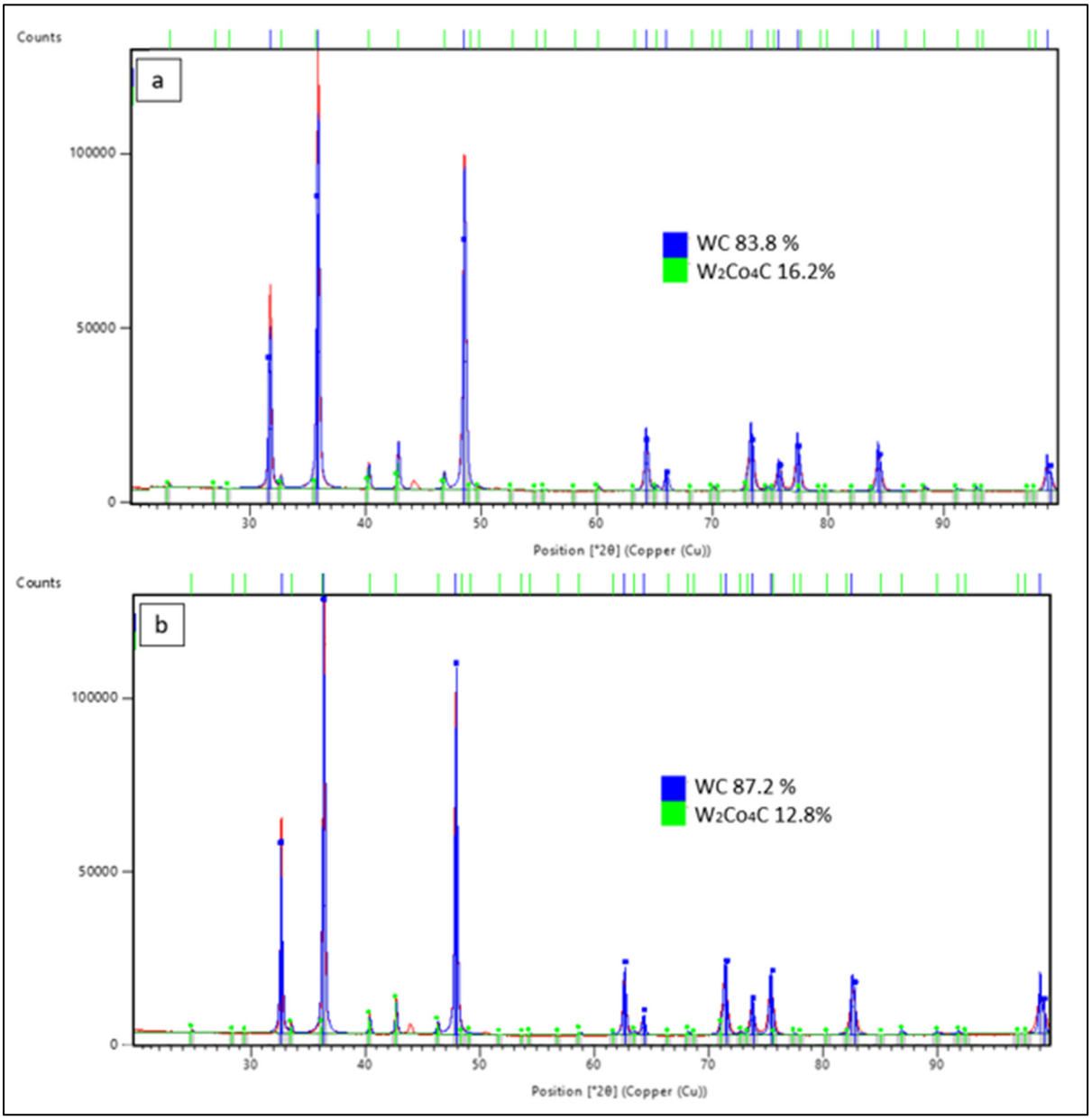

Figure 3.2 Diffraction patterns of a) powder A and b) B

For both powders, the main phase is WC. The secondary phase is W_2Co_4C. The highest peaks (in blue) correspond to the WC phase. The lowest peaks (in green) correspond to the W_2Co_4C phase.

3.1.3 Granulometry

Particle size distribution for the two studied powders is displayed on figure 3.3. The obtained curves are automatically smoothened by the used software. For powder A (highlighted in dark blue), there is an intense peak at d_{50} = 6.8 µm and a plateau for larger particle diameters. This means that the particle size distribution is multimodal (not uniform), as seen on the SEM images in section 3.1.1, figure 3.1.a. Whereas for powder B (highlighted in red), the distribution is symmetric around the intense peak at d_{50} =6.5 µm. This results in a monomodal (quite uniform) particle size distribution within the powder, as seen on the SEM images in section 3.1.1, figure 3.1.c.

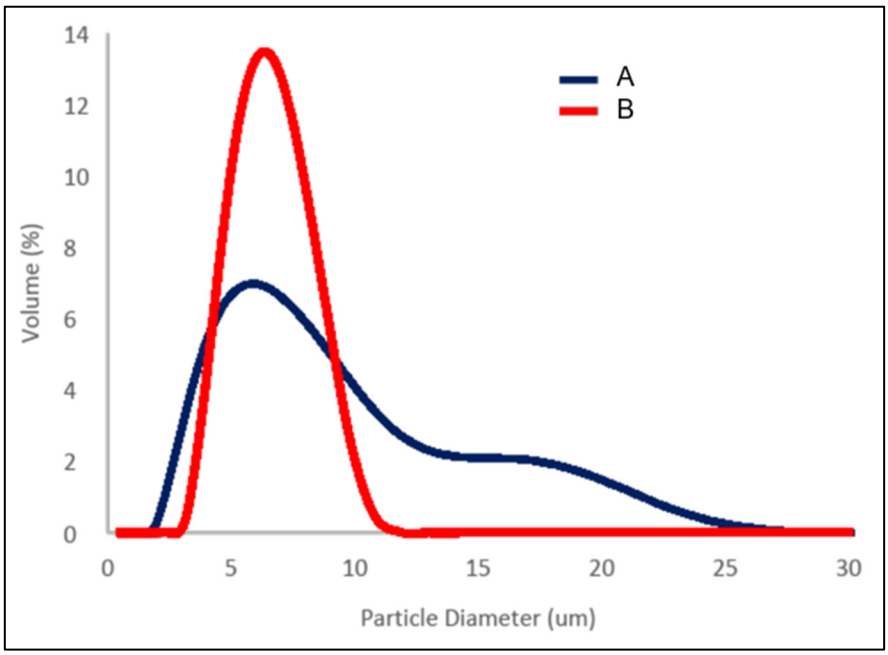

Figure 3.3 Particle size distribution for the studied powders

Granulometry also quantifies the values of d_{10} , d_{50} and d_{90}, which can provide a better idea of the particle size distribution. For example, as seen in table 3.1, 90% of powder B's particles

are smaller than 8.9 µm (d_{90}). On the other hand, 10% powder A's particles are smaller than 3.5 µm (d_{10}).

Table 3.1 d10, d50 and d90 values for the studied powders

Powder designation	d_{10} (µm)	d_{50} (µm)	d_{90} (µm)
A	3.5	6.8	14.5
B	4.5	6.5	8.9

3.2 Results of characterization tests led of WCCoCr coatings

This section presents the results of the characterization tests done on the four sets of samples that were manufactured for the project. Since there are no two sets done in the exact same conditions, sometimes it was not possible to cross the results from one set to another. Also, not all of the characterization tests listed in section 2.7 could have been done on each set by lack of samples.

3.2.1 Results of characterization tests performed on set 1

This part will present the results of the characterization tests done on the samples of set 1 which correspond to X powder of unrectified tempered 4340 samples. By lack of material, only microstructure overview, porosity measurement, chemical analysis by XRD and microhardness indents were accomplished on set 1.

Overview of the resulting coating layer

Coating thickness varied from 196 µm at 90°C and 305 µm at 592°C, with a standard deviation of 57 µm (table 3.2). For each condition, the thickness per pass was calculated. According to figure 3.4, it increases with the sample's temperature. At 592°C, the deposited thickness per pass (38 µm/pass) is almost 8 times thicker than for the lower temperatures (7µm/pass for 90°C and 5µm/pass at 111°C). If the thickness per pass seems to have a linear relation with the

temperature of the sample, it actually depends on the spraying parameters that varied for this set : the tangential speed of the nozzle, the pitch and the pause between passes.

Table 3.2 Coating characteristics of set 1

Sample number	**Number of passes**	**Max temperature (°C)**	**Coating thickness (µm)**
2201214	30	90	196
2201215	45	111	208
2201213	23	246	363
2201191	15	246	267
2201192	15	305	246
2201211	8	391	282
2201212	8	592	305

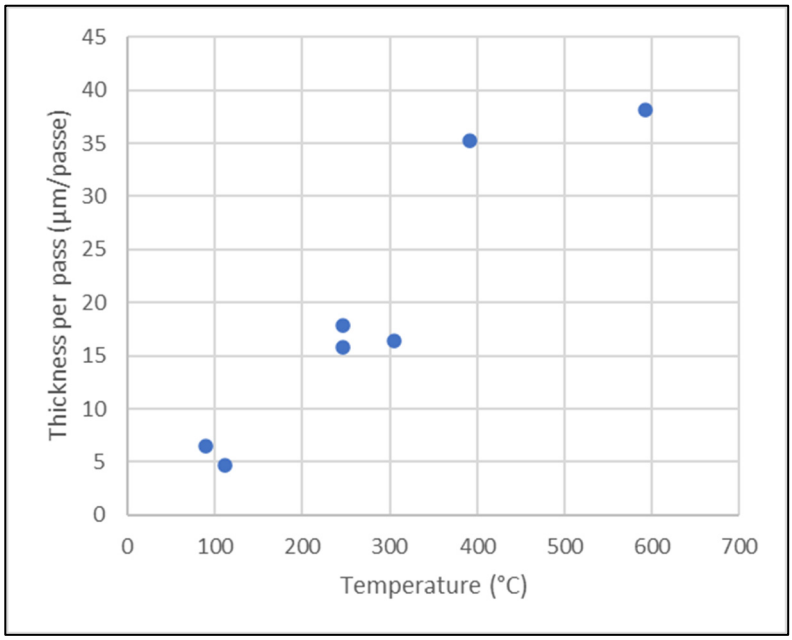

Figure 3.4 Thickness per pass for set 1

The optical microscope images of the coatings of the first set of samples are shown on figure 3.5. For the colder samples, coatings seem to be exempt of defects. Delamination is visible on the two hottest samples, 2201211 and 2201212. Even though some coatings presented microcracks, the rest of the study will focus on zones who contain less defects whilst the improvement of the deposition process is in progress.

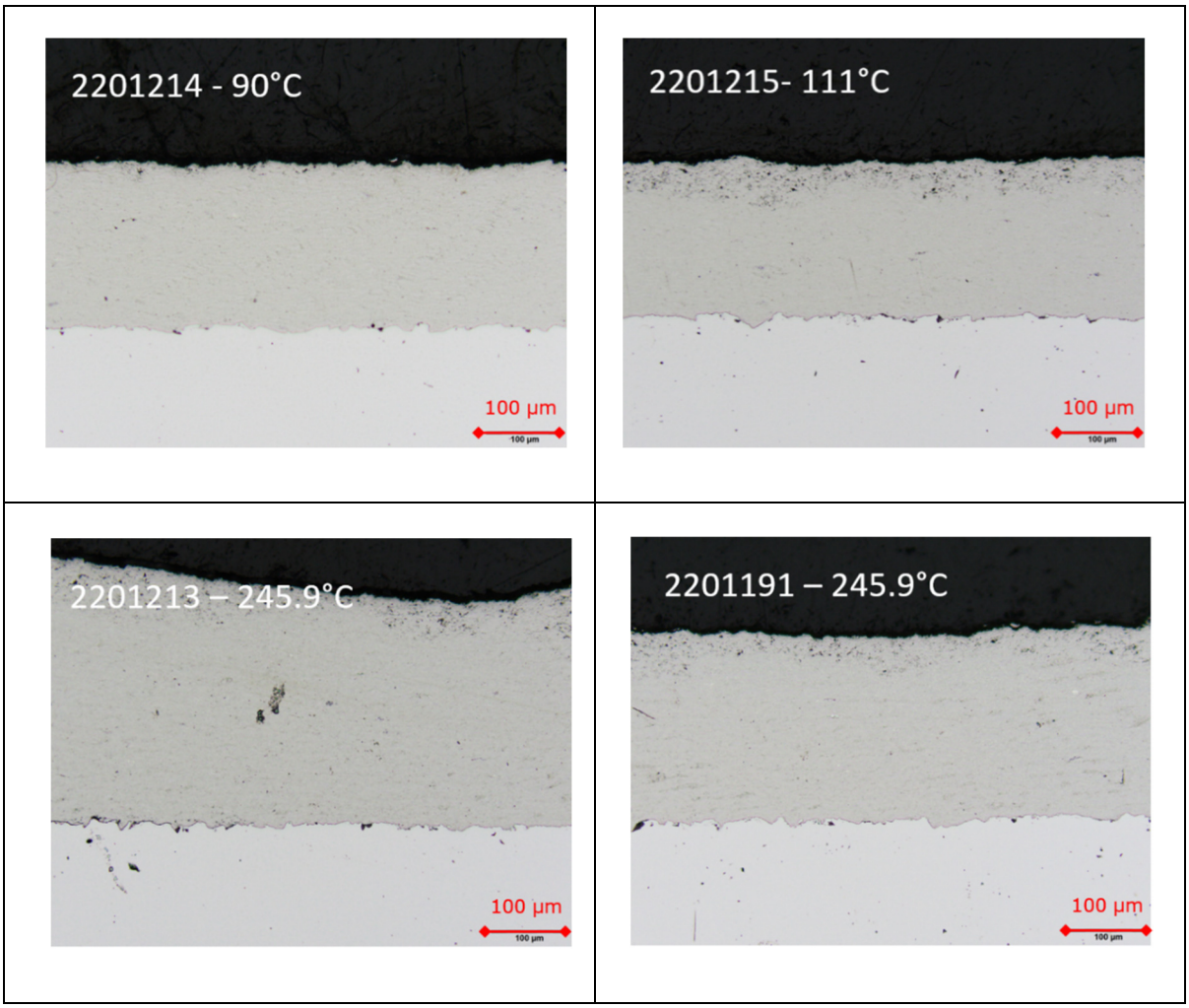

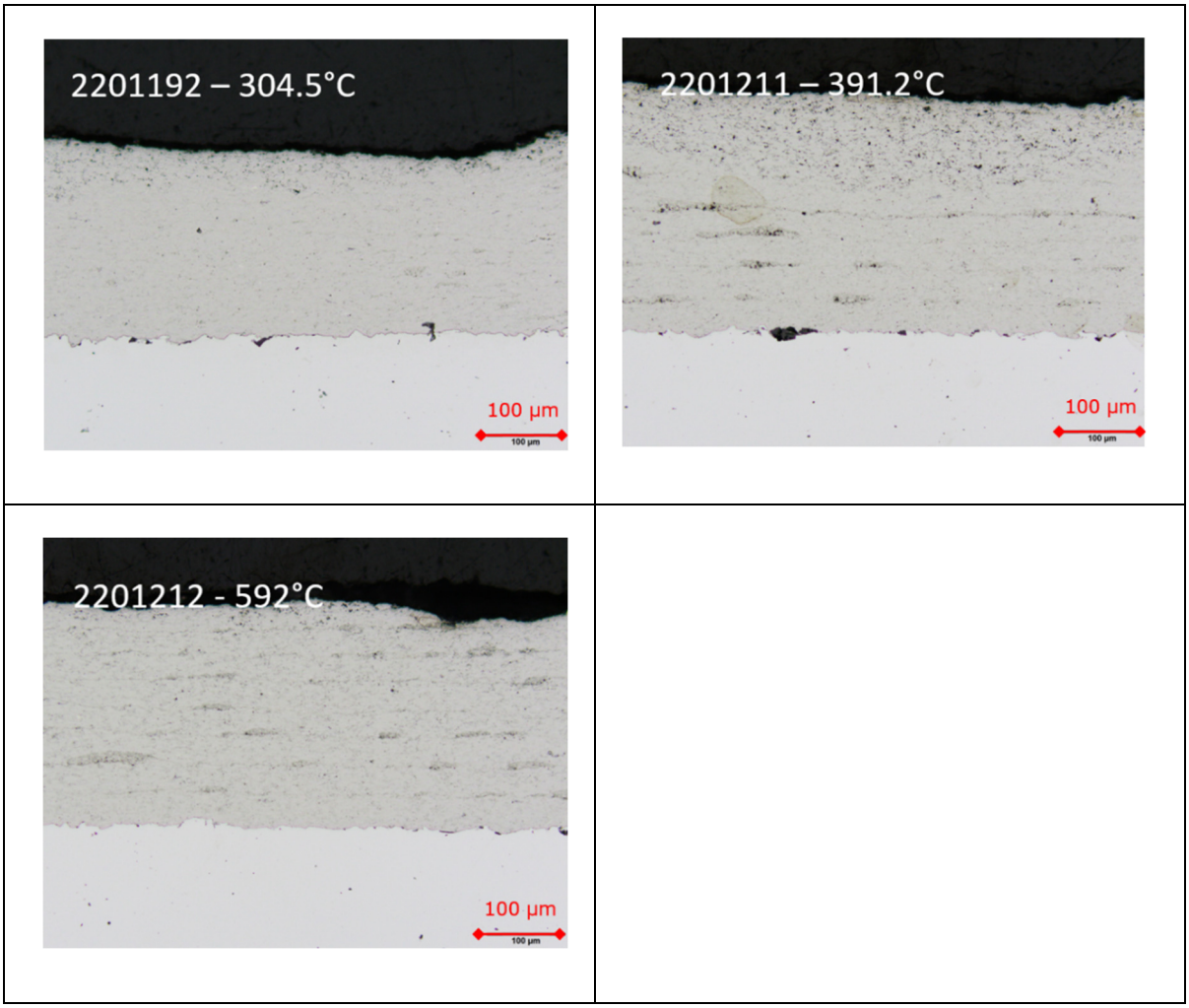

Figure 3.5 Optical microscope images of set 1 HVOF coatings presented by increasing deposition temperature

For all seven samples, the interfaces between coating and substrate look similar to one another and no visible defects are present. Temperature does not seem to affect the quality of the interface. Figure 3.6 shows the optical microscope images of the coating/substrate interfaces of set 1. Martensite is visible on etched samples.

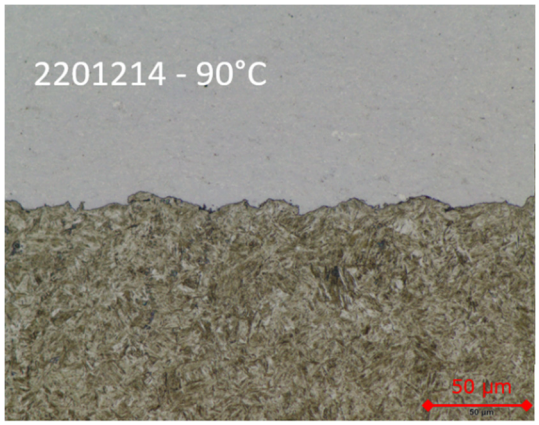
2201214 - 90°C
50 µm

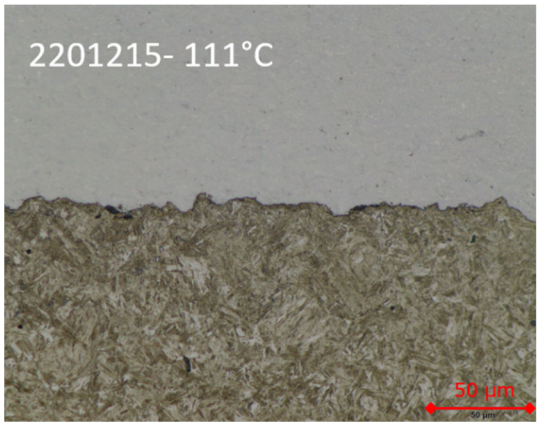
2201215- 111°C
50 µm

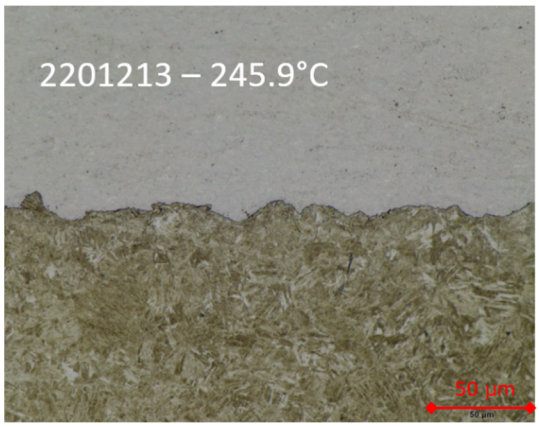
2201213 – 245.9°C
50 µm

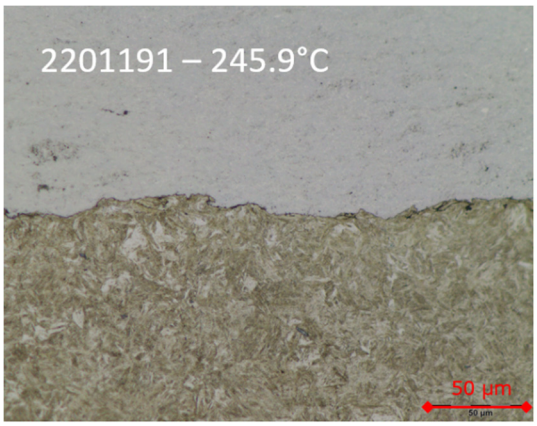
2201191 – 245.9°C
50 µm

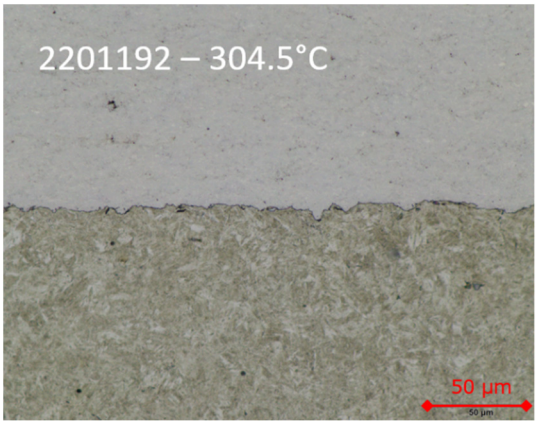
2201192 – 304.5°C
50 µm

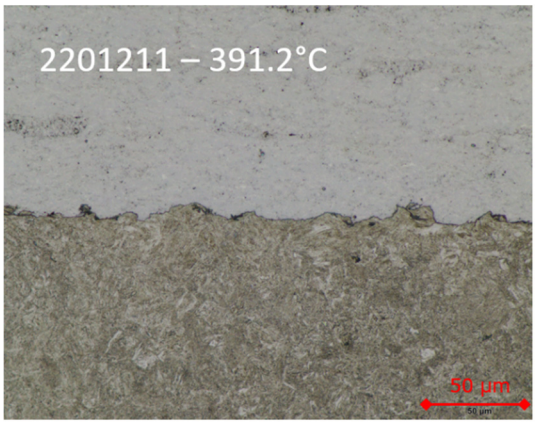
2201211 – 391.2°C
50 µm

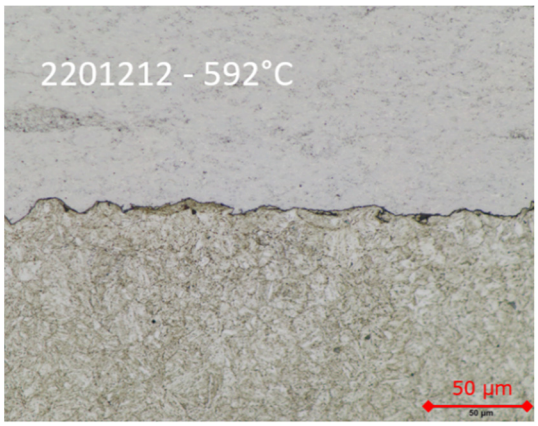

Figure 3.6 Optical microscope images of set 1 coating/substrate interfaces ordered by temperature

Porosity

The coating's porosity must remain below 1% as mentioned in the project's evaluation criteria (based on the performance of the torch). Figure 3.7 displays the porosity measures as a function of temperature. Most of the coatings from this set have an acceptable porosity. Two of the samples have respective porosities of 1.1% and 1.2%, which is not excessive but still above the evaluation criteria. It could be that the delamination visible on figure 3.5 has affected the porosity results. Also, porosity was measured in only one region of the coating so it only gives a rough idea of the overall value. Therefore, the porosity evaluation criteria is not critical.

Since, the variation of the porosity is not linear, temperature is not considered as an influencing parameter on the evolution of the coatings' porosity.

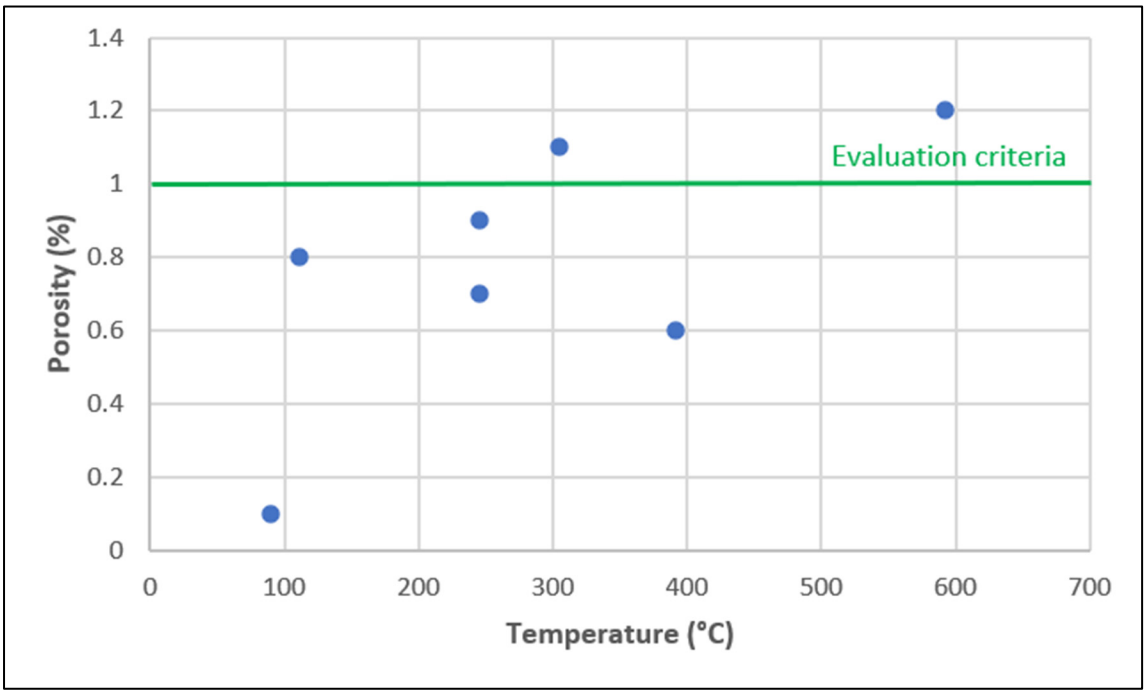

Figure 3.7 Porosity results for set 1

Chemical analysis by XRD

The XRD spectrums of each specimen are displayed on figure 3.8. The intensities and positions of the peaks are coherent regarding the reference diffraction pattern for WCCoCr coatings (see section 1.4.1, figure 1.10). At a first glance, they are similar to one another, with some slight variations on the position and the intensity of the peaks. The main phase composing the coating is WC. The decarburized phase, W_2C, represents between a tenth and a quarter of the coating's composition. Lastly, a minor amorphous phase (Co_3O_4) is identifiable.

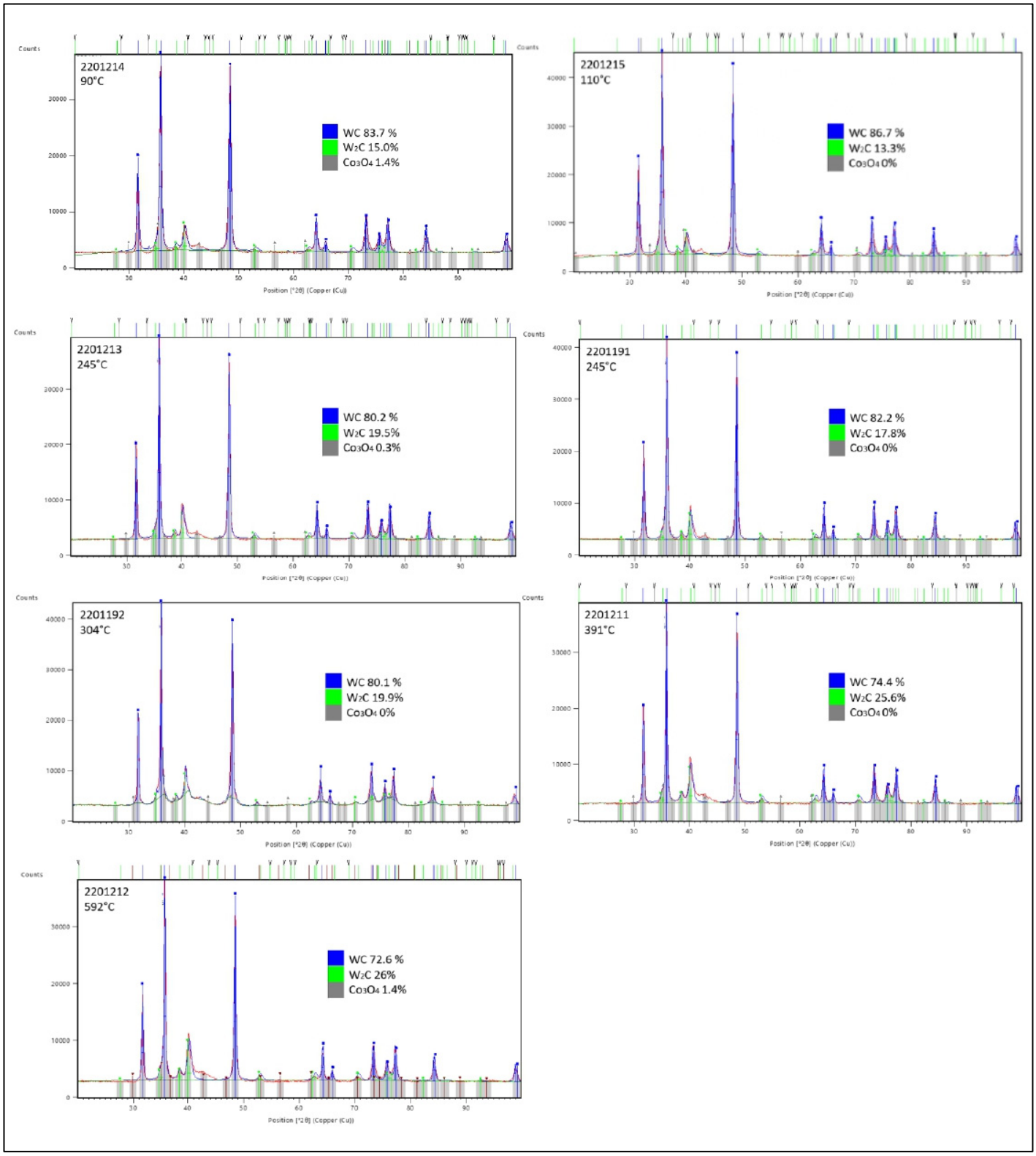

Figure 3.8 Diffraction patterns and phase proportions of set 1 ordered by temperature

Figure 3.9 displays the weight percentage of each phase depending on the temperature measured by the thermocouple inside of each sample. 83.8 wt % is the percentage of WC found in the A powder. The difference between this value and the value found in each sample corresponds to the degree of decarburization. As the temperature increases, the proportion of WC drops, thus increasing the degree of decarburization.

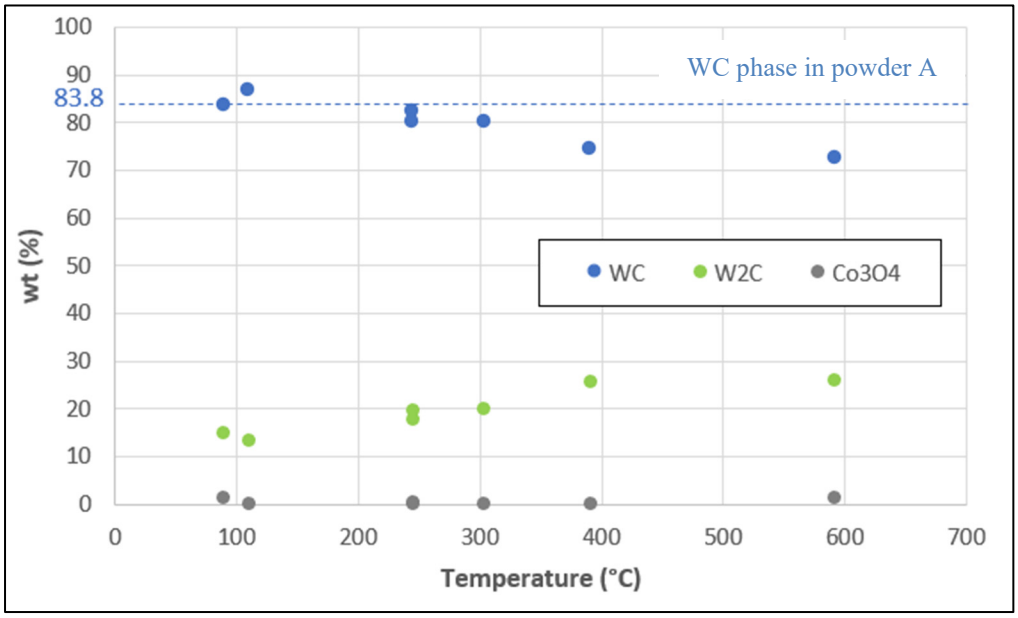

Figure 3.9 Phase proportion of set 1 as a function of temperature

Microhardness

The mean hardness of the coating and the substrate for each temperature condition of set 1 is displayed on figure 3.10. The nominal hardness of the coating is 950 $HV_{0.3}$ – it is indicated as a red line. Under 300°C, there is no specific behavior in the coating's hardness. Whereas above 300°C, the hardness steadily increases. The nominal hardness of the substrate is 600 $HV_{0.3}$ – it is indicated as a green line. Under 300°C, there is no specific behavior in the substrate's hardness. Above 300°C, the substrate's hardness drops.

These hardness results can be correlated to the XRD phase analysis results. As shown on figure 3.9, the decarburization degree in the coating starts to significantly drop after 300°C. During decarburization, the proportion of WC decreases and the proportion of W_2C increases. Since there is more carbon in the coating, its hardness increases.

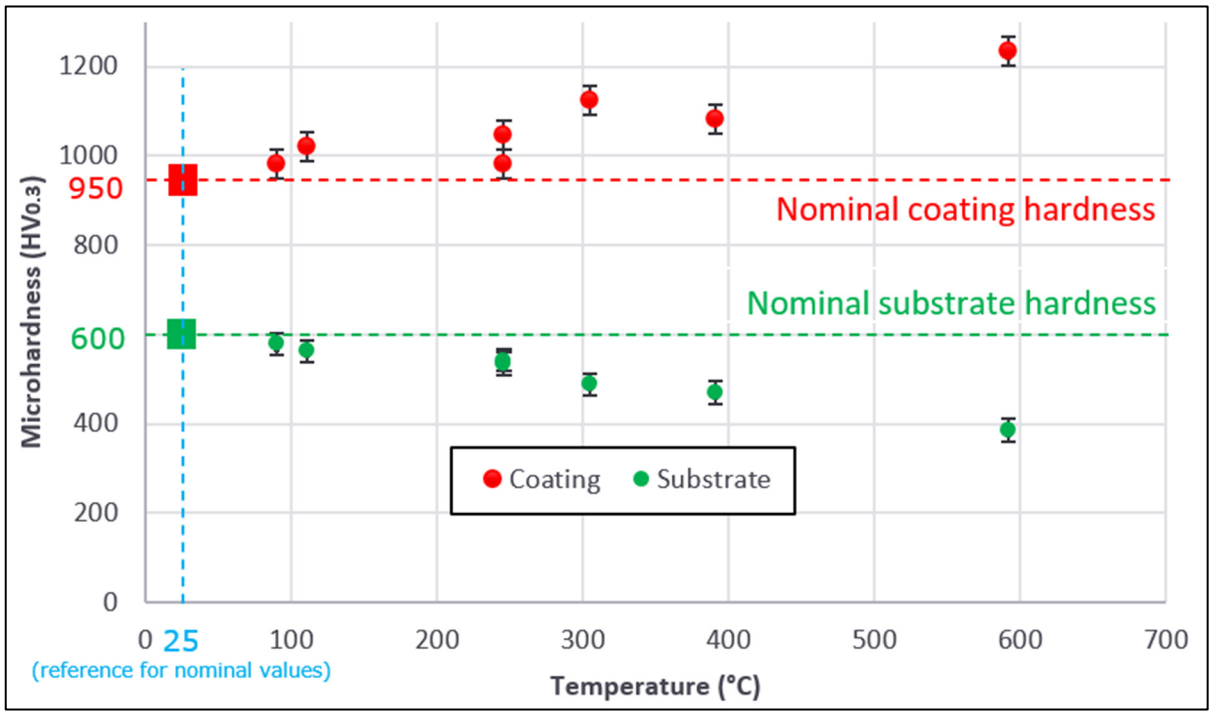

Figure 3.10 Microhardness results for set 1

3.2.2 Results of characterization tests performed on set 2

This part presents the results of the characterization tests done on set 2 corresponding to 4340 AISI steel coupons coated with powder A (the coarse powder). With the available material, it was possible to do a microstructure overview, porosity measurements, chemical analysis by XRD, microhardness measurements and abrasion tests.

Overview of the resulting coating layer

Coating thickness varied from 99 µm at 80°C and 226 µm at 320°C, with a standard deviation of 31 µm (table 3.3). For each condition, the thickness per pass was calculated. According to figure 3.11, the thickness per pass is stable (approximately 5µm/pass) except for the hottest sample, where it tripled (14µm/pass). Contrary to set 1, the thickness per pass for set 2 does not seem to have a linear relation with the temperature of the sample. For set 2, the diameter of the sample holder, the tangential speed and the cooling intensity varied. Since the variable parameters differ from those for set 1 (tangential speed, pitch and pause between passes), it may have affected the thickness per pass.

Table 3.3 Coating characteristics of set 2

Sample number	**Number of passes**	**Max temperature (°C)**	**Coating thickness (µm)**
2207072	30	80	145
2207081	30	140	135
2207071	30	145	160
2207111	30	210	163
2207082	30	280	163
2207112	22	290	135
2207121	16	320	226

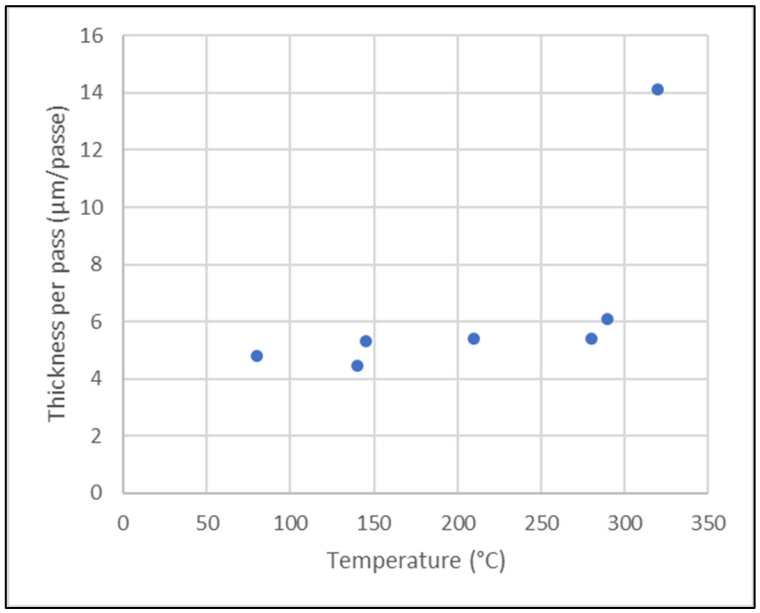

Figure 3.11 Thickness per pass for set 2

Optical microscope images of the coatings of set 2 are presented on figure 3.12. The coatings look all similar to one another but seem more porous compared to set 1. Coatings are exempt of cracks or delamination.

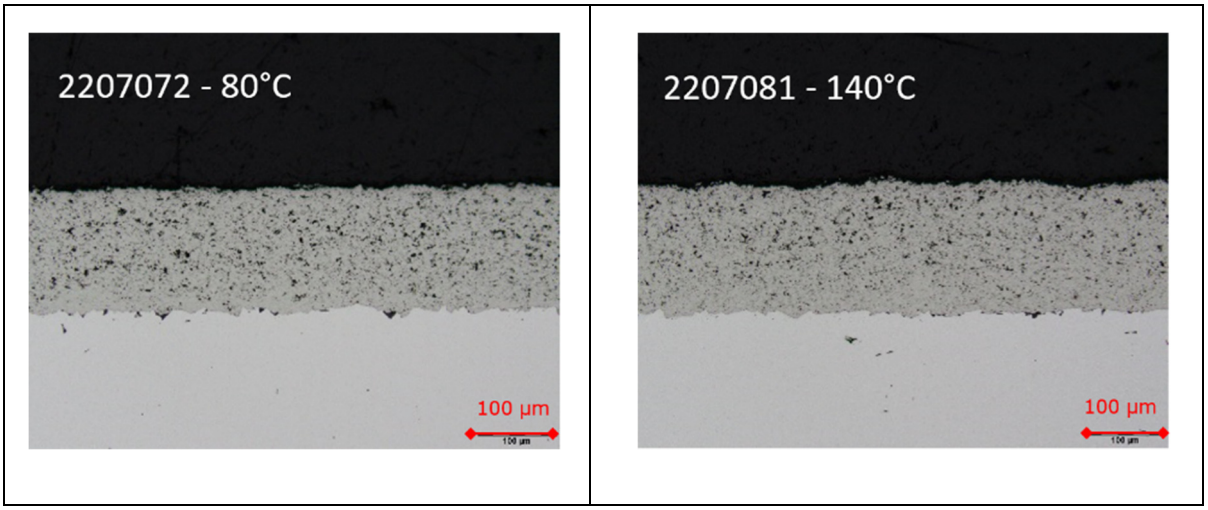

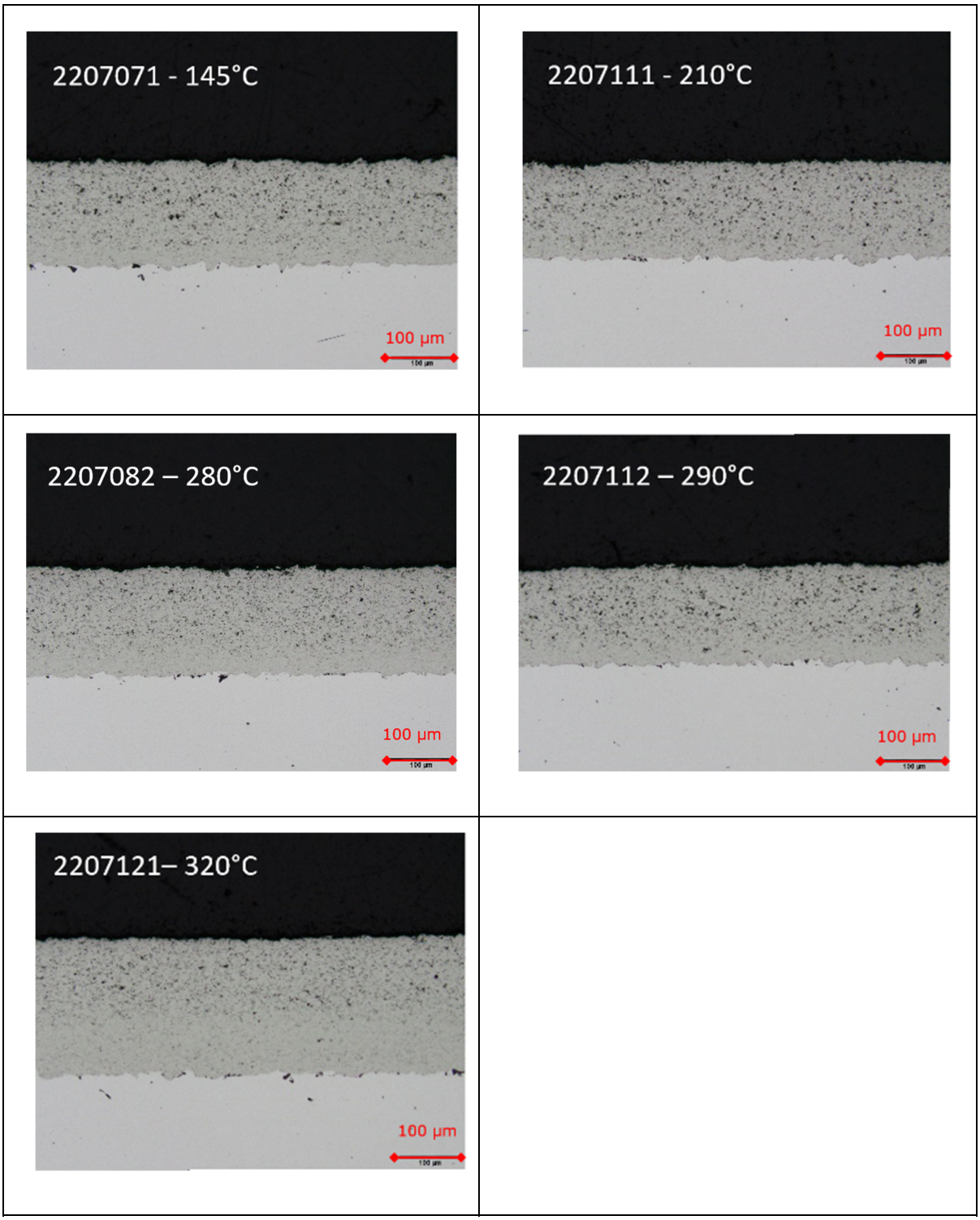

Figure 3.12 Optical microscope images of set 2 HVOF coatings presented by increasing deposition temperature

Porosity

Figure 3.13 displays the porosity values for the coating of set 2. The coatings of set 2 are more porous than the ones from set 1 with values reaching 2.5% for the lower temperatures. For this set, the more porous samples are the coldest ones, whereas for set 1, the hottest ones were more porous. Even if the spraying gun and the powder remained unchanged from set 1, the diameter of the rotating sample holder used for set 2 was larger and the cooling levels of set 2 were higher. The evaluation criteria demanded porosities below 1% and this set does not meet the criteria unfortunately.

For set 1, samples below 500°C have met the porosity requirement. Whereas for set 2, the evaluation criteria has been met for samples hotter than 300°C. Therefore, temperature does not affect the porosity of the coating. It seems more likely that the deposition setup is more of an influencing factor : perhaps the cooling method or the size of the carousel influences the porosity of the coatings.

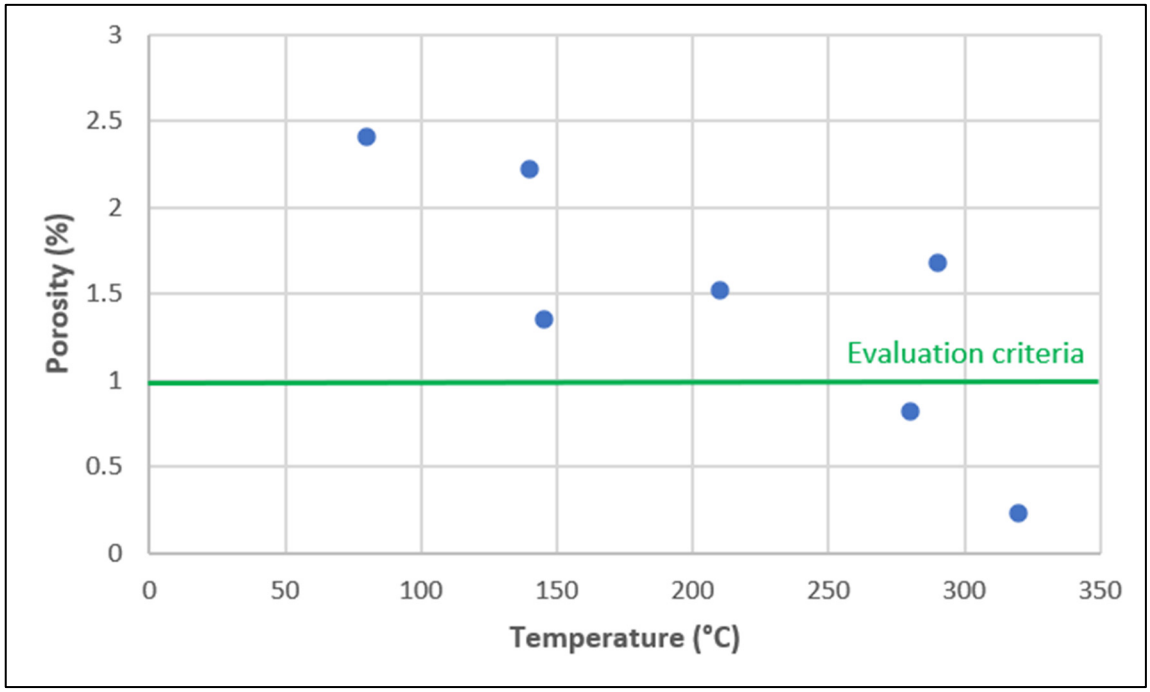

Figure 3.13 Porosity results for set 2

Chemical analysis by XRD

Figure 3.14 displays the XRD spectrums of each specimen. The diffraction patterns match the reference pattern for WCCoCr coatings (see section 1.4.1, figure 1.10). WC is the main phase as expected. The decarburized phase, W_2C, is close to a quarter of the total composition. On this set, the proportion of the amorphous phase could not be detected.

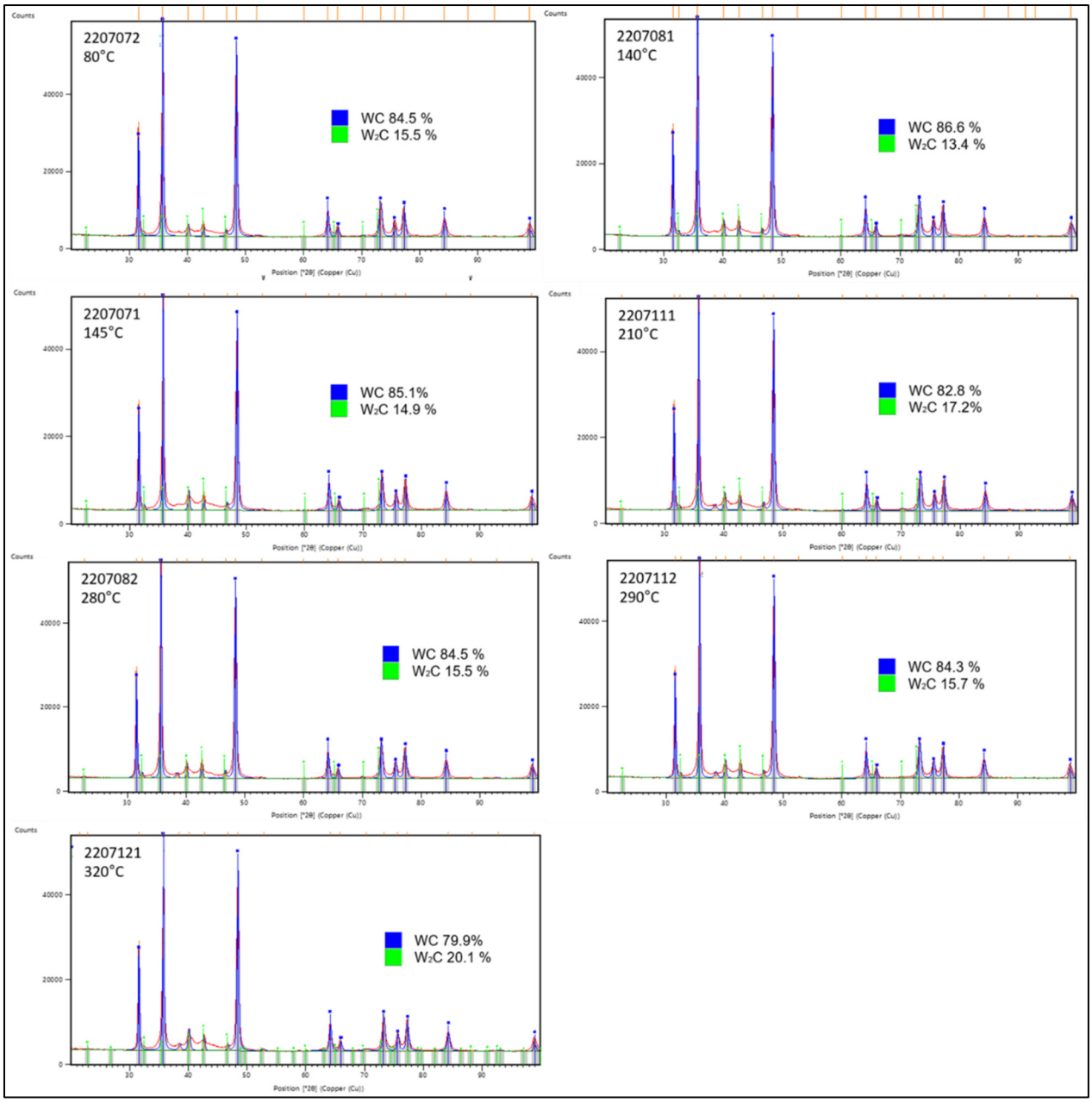

Figure 3.14 Diffraction patterns and phase proportions of set 2 ordered by temperature

Figure 3.15 displays the weight percentage of each phase depending on the temperature measured by the pyrometer. 83.8 w t% is the percentage of WC found in the A powder. The difference between this value and the value found in each sample corresponds to the degree of decarburization. For this set, there is no major variation of the degree of decarburization. As written in section 3.2.1.2, the degree of decarburization started to increase after 300°C. Yet, the temperatures for set 2 do not go far above 300°C. Thus, they are not hot enough to observe a major effect on the WC phase percentage.

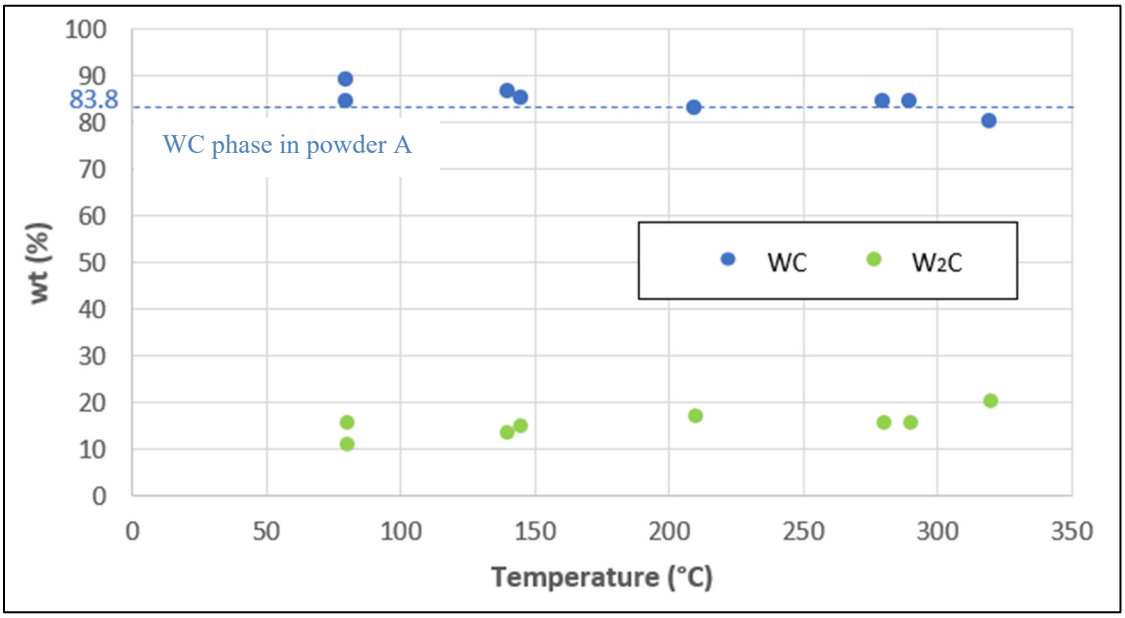

Figure 3.15 Phase proportion of set 2 as a function of temperature

Microhardness

Figure 3.16 displays the mean hardness of the coating and the substrate for each temperature condition of set 2. The standard deviations for the coating measurements are significant. This is probably due to the defects present within the coating which can affect the reading during the measurement. all samples reach the nominal hardness of the coating (950 $HV_{0.3}$ – indicated as a red line). There is no particular tendency visible for the coating's hardness.

The standard deviations for the measures done within the substrate are almost negligeable. The nominal hardness of the substrate is 600 $HV_{0.3}$ – it is indicated as a green line. There is no particular tendency visible for the coating's hardness nor for the substrate's hardness. In section 3.2.1, a correlation between the degree of decarburization and the sample's hardness was established. It was also established that these two parameters started to change for temperatures above 300°C. Since for set 2, temperatures mainly stayed below 300°C, it is not expected to see any increase or decrease in hardness values.

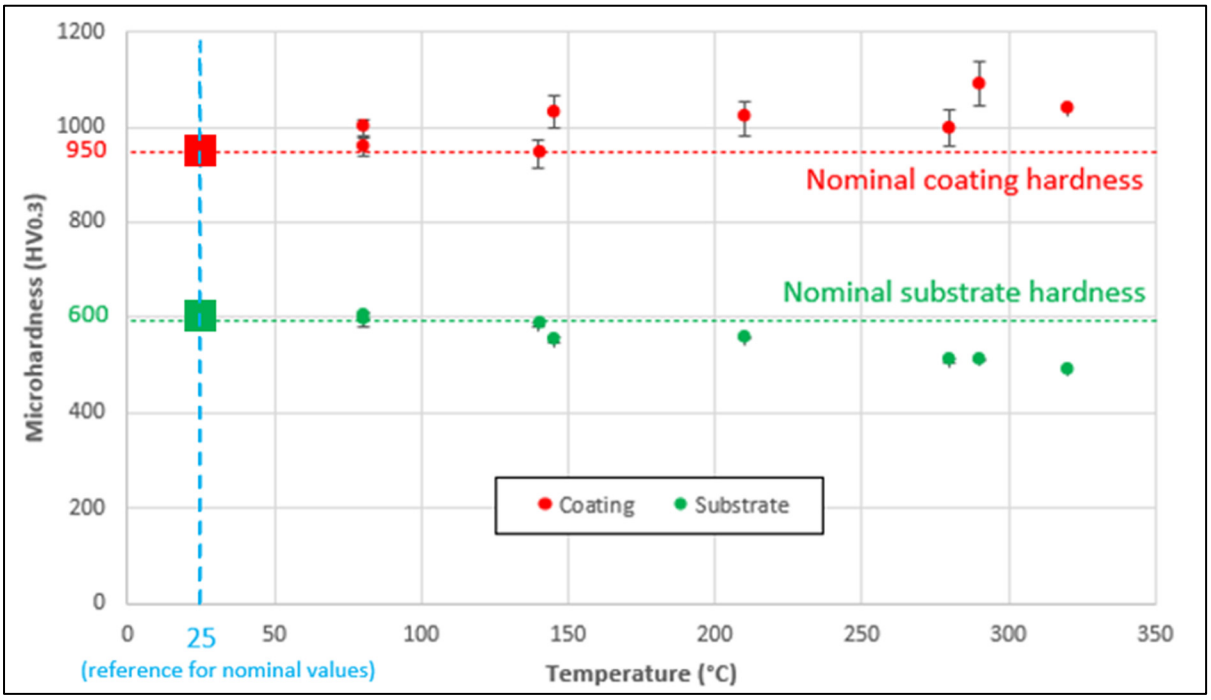

Figure 3.16 Microhardness results for set 2

Abrasion tests

Abrasion results are displayed on figure 3.17. More precisely, it shows the mean lost weight as a function of the temperature measured by the pyrometer for each spraying condition. Values seem to be randomly spread around 0.04 g, regardless of the spraying conditions. Standard deviations do not differ much between different conditions. The highest standard deviation is 0.0089 g at 210°C and the lowest one is 0.0042 g for 140°C.

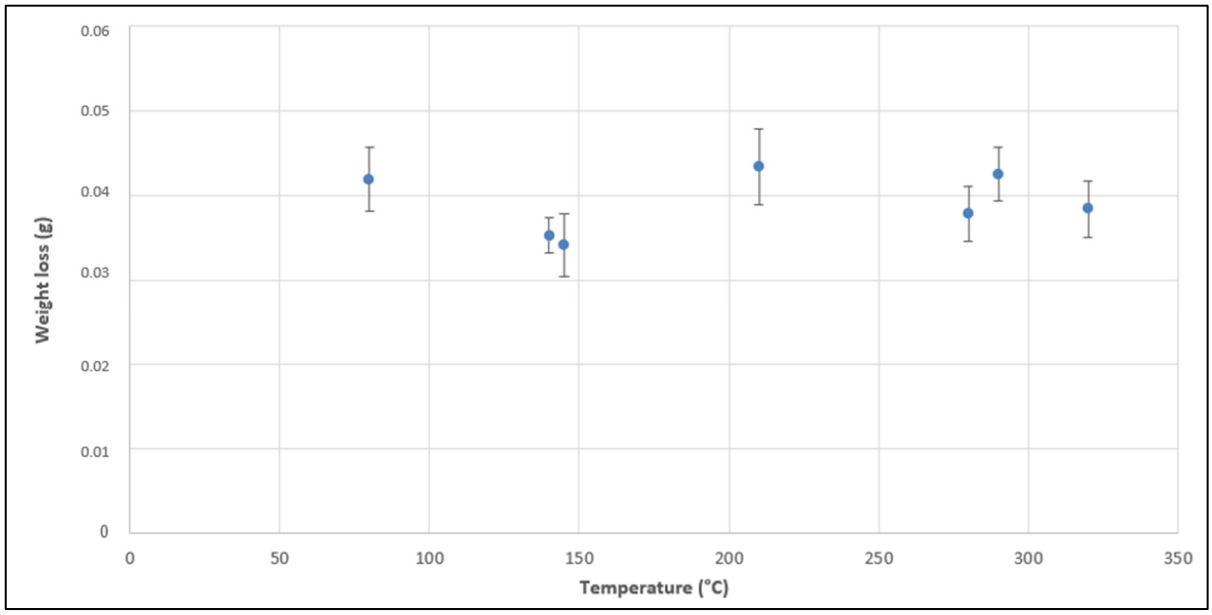

Figure 3.17 Abrasion results for set 2

3.2.3 Results of characterization tests performed on set 3

This part presents the results of the characterization tests done on set 3 corresponding to the soft steel coupons coated with powder B (with finer grains) . With the available material, it was possible to do a microstructure overview, porosity measurements, chemical analysis by XRD, microhardness measurements and abrasion tests.

Overview of the resulting coating layer

Coating thickness varied from 185 µm at 500°C and 236 µm at 120°C, with a standard deviation of 19 µm (table 3.4). For each condition, the thickness per pass was calculated. According to figure 3.18, the thickness per pass does not vary depending on the temperature of the sample (values between 3 and 2.5 µm/pass), contrary to set 1 where it increased with the temperature. For set 3, the operator only varied the cooling intensity. In this case, a linear relation seems to exist between the thickness per pass and one spraying parameter.

Table 3.4 Coating characteristics of set 3

Sample number	Number of passes	Max temperature (°C)	Coating thickness (µm)
2303291	80	120	236
2303301	80	250	211
2303302	112	350	229
2303311	100	420	218
2303271	80	440	198
2303241	120	500	185

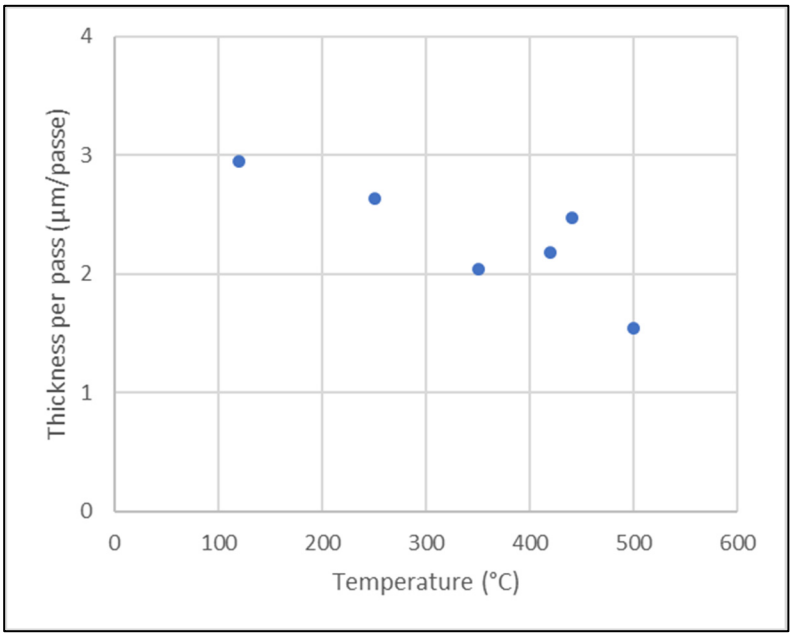

Figure 3.18 Thickness per pass for set 3

Optical microscope images of the coatings of set 3 are displayed on figure 3.19. No major defects are visible although coatings seem more porous compared to set 1.

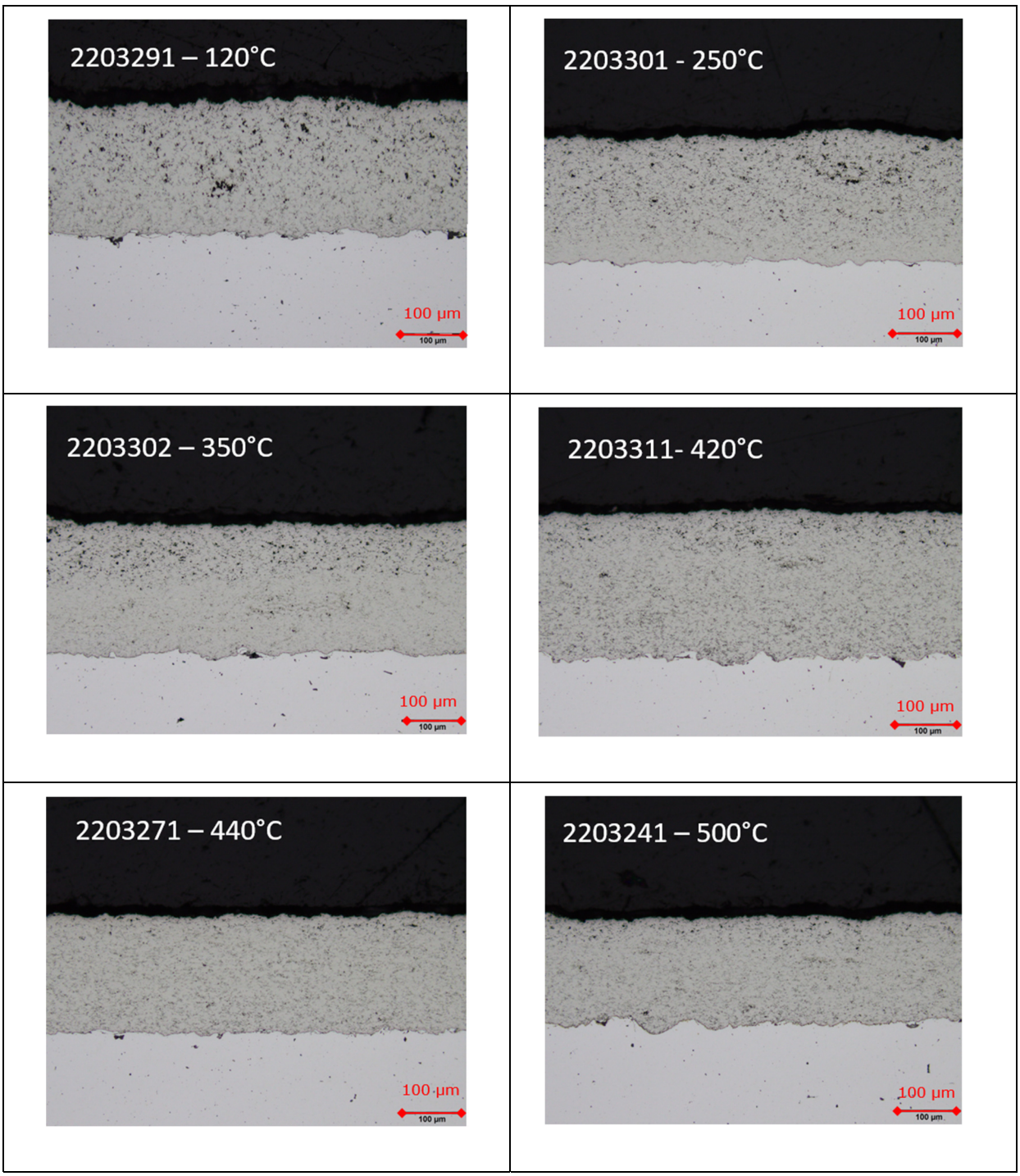

Figure 3.19 Optical microscope images of set 3 HVOF coatings presented by increasing deposition temperature

Porosity

Figure 3.20 displays the porosity results for set 3. Porosity drops as the sample's temperature increases. Acceptable samples are the hottest ones, more specifically those whose temperature is above 300°C. The evaluation criteria is not met for the two lowest temperatures since their porosities are above 1%.

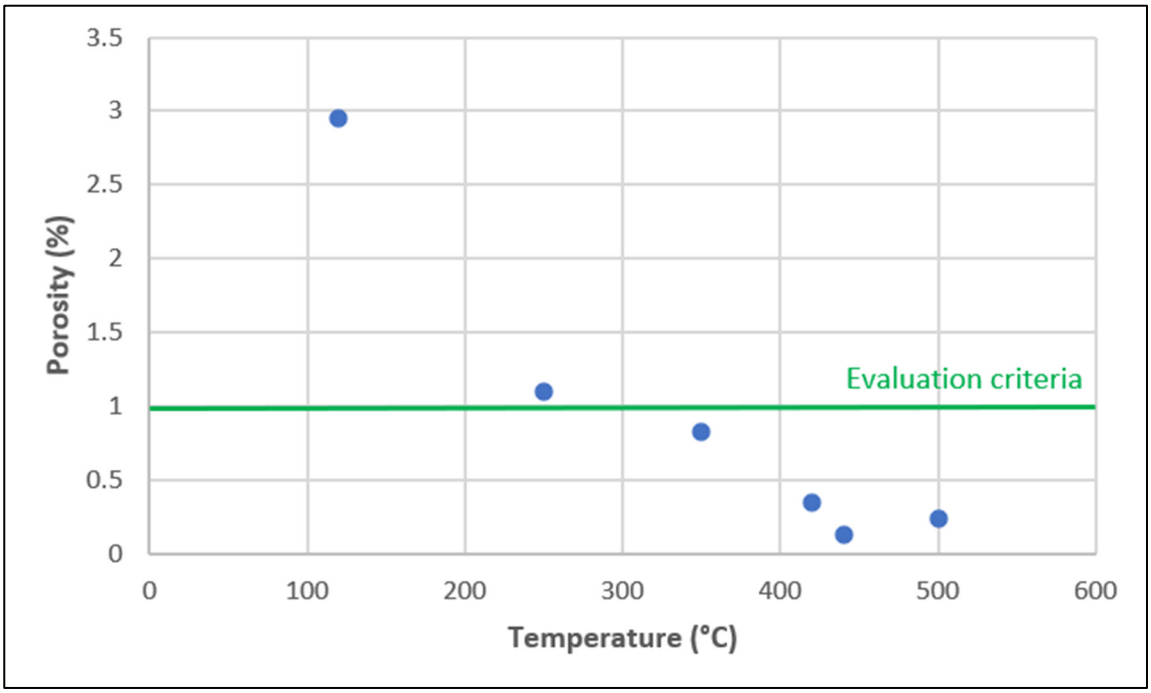

Figure 3.20 Porosity results for set 3

Chemical analysis by XRD

Figure 3.21 displays the XRD spectrums of each specimen of set 3. The diffraction patterns match the reference pattern for WCCoCr coatings (see section 1.4.1, figure 1.10). WC is the main phase as expected. The proportion of the decarburized phase, W_2C, randomly varies between 2.9% and 20.9%. On this set, the proportion of the amorphous phase is negligeable.

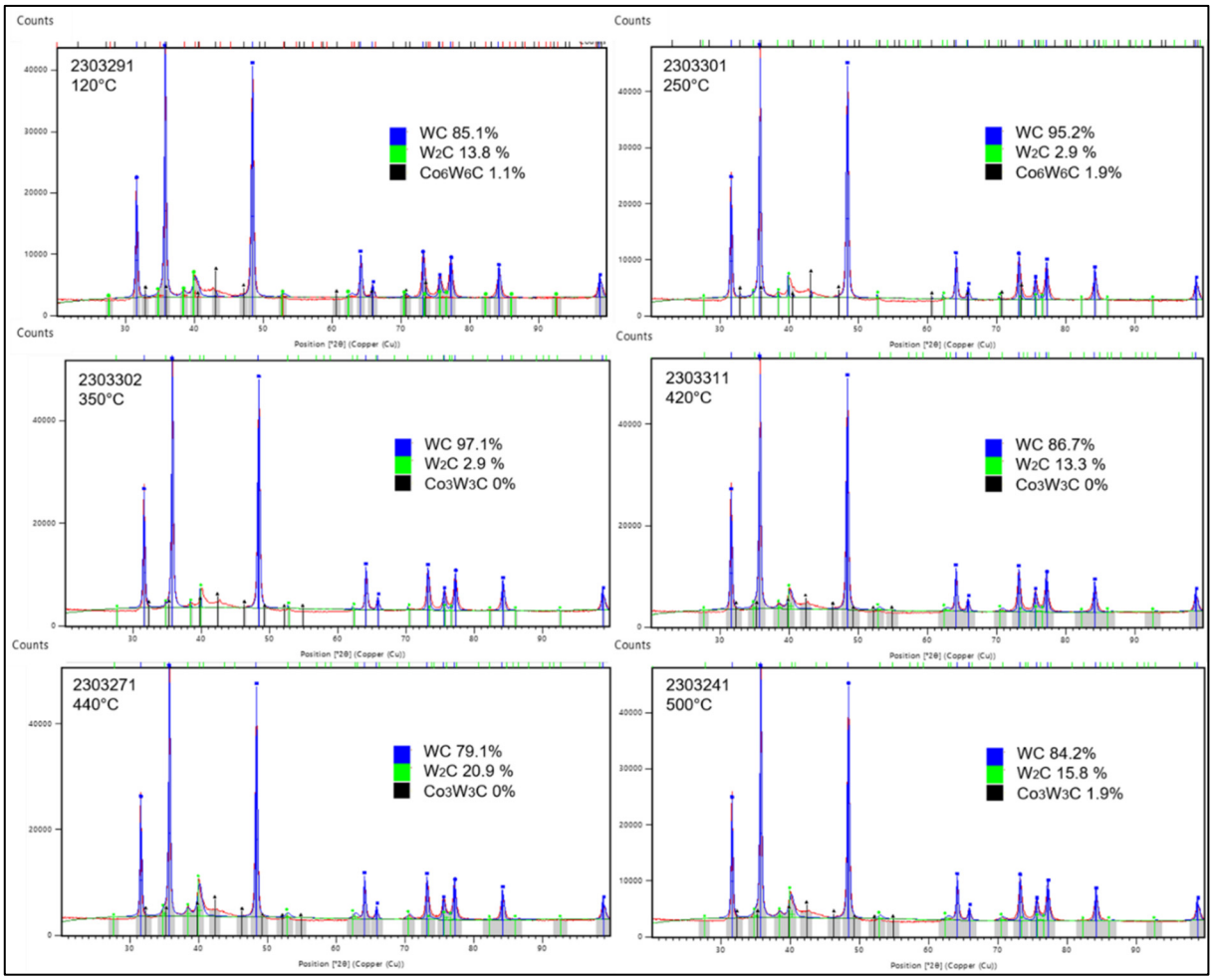

Figure 3.21 Diffraction patterns for set 3

Figure 3.22 displays the weight percentage of each phase depending on the temperature measured by the pyrometer. 87.2 wt % is the percentage of WC found in the B powder. Contrary to what was expected, there is no major decarburization happening above 300°C. This may be linked to the particle distribution of the powder B. As explained in section 3.1, B is much finer than A, which was used for sets 1 and 2. Therefore, there may be a correlation between the particle distribution of the powders and the decarburization within the coating. When using a coarser powder, such as A, decarburization begins at approximately 300°C. For finer powders, such as B, it seems that decarburization is either completely absent or it would

begin at temperatures even higher than those reached during the manufacturing of samples for this project.

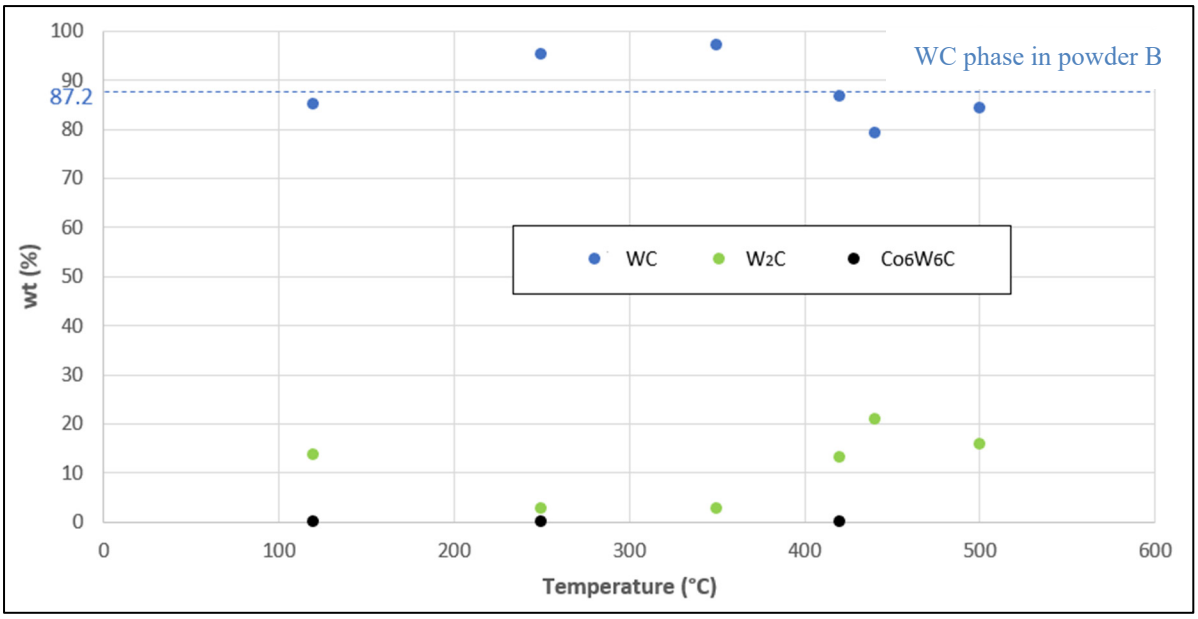

Figure 3.22 Phase proportion of set 3 as a function of temperature

Microhardness

Figure 3.23 displays the mean hardness of the coating and the substrate for each temperature condition of set 3. Since the substrate used for set 3 is not 4340 AISI steel, there was no interest in measuring the hardness of the substrate. The nominal hardness of the coating is 950 $HV_{0.3}$ – it is indicated as a red line. There is no particular tendency visible for the coating's hardness. In section 3.2.1, a correlation between the degree of decarburization and the coating's hardness

was established. Since for set 3, there is no major decarburization happening within the coating, it is not expected to see any increase or decrease in hardness values.

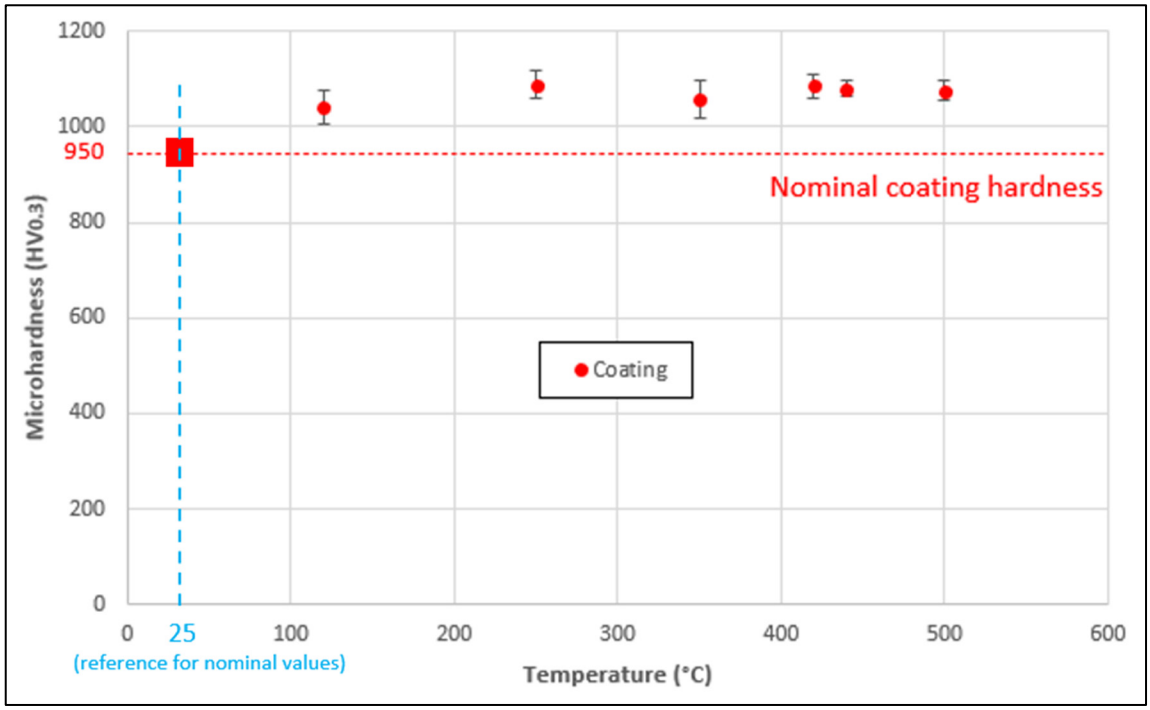

Figure 3.23 Microhardness results for set 3

Abrasion tests

Abrasion tests on set 3 followed the exact same procedure that for set 2 but with a newer version of the apparatus. The resulting mean lost weight as a function of the temperature measured by the pyrometer for each spraying condition is displayed in figure 3.24. Weight loss values do not seem to have a specific behavior depending on the temperature, as they are randomly spread around 0.034g (for set 2, values were randomly spread around 0.04g). Even if a finer powder (B) was used for set 3 (powder A was used for set 2), the coarseness of the powder does not affect the magnitude of the lost weight. Contrary to set 2, standard deviation

are different depending on the spraying conditions. The lowest is 0.0005 g at 250°C and the highest is 0.009 g at 500°C.

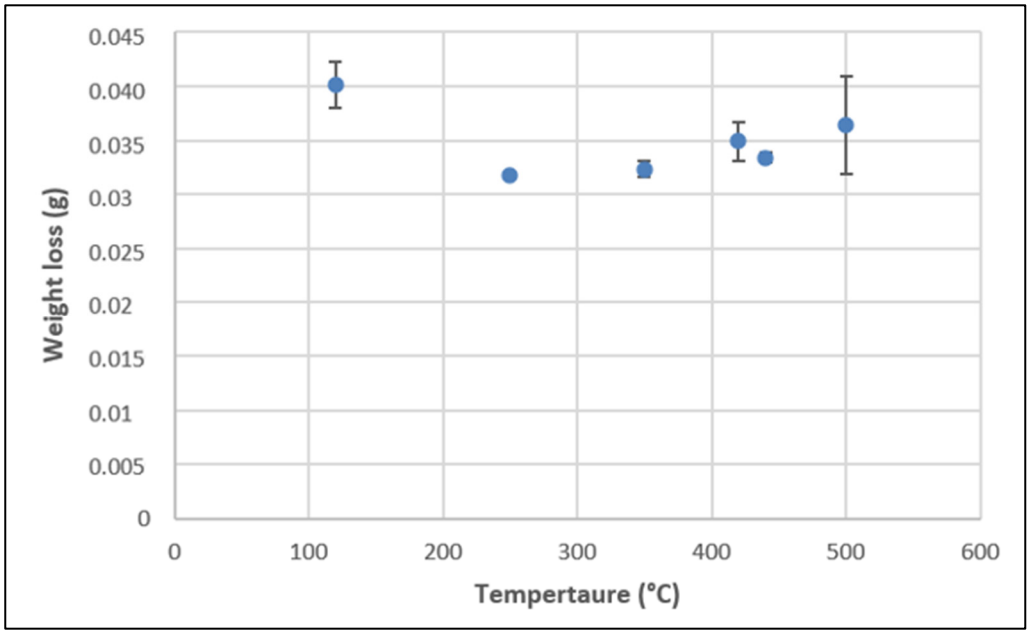

Figure 3.24 Abrasion results for set 3

3.2.4 Results of characterization tests performed on set 4

This part presents the results of the characterization tests done on set 4 which correspond to the samples mounted inside a cylinder made of 4340 AISI steel. With the available material, it was possible to do a microstructure overview, porosity and microhardness measurements. In the captions, “GB” refers to the samples that were only grit blasted prior to the coating deposition, “SP+GB” refers to the samples that were shot peened and grit blasted before the coating deposition.

Overview of the resulting coating layer

Coating thickness varied from 106 µm at 182°C and 172 µm at 300°C, with a standard deviation of 19 µm (table 3.5). Some of the coatings were too thin compared to the others, such as the ones produced at 180°C or 230°C. When observing figure 3.25, the thickness per pass randomly varies between 4 and 7 µm/pass. For this set, only the pause between passes varied.

Table 3.5 Coating characteristics of set 4

Sample pair number	Number of passes	Max temperature (°C)	Coating thickness (µm)
2301272	24	127	160
2301313	36	130	158
2301311	24	175	147
2301271	24	182	107
2301243	24	188	142
2301241	24	230	142
2301242	24	230	150
2301312	24	300	173

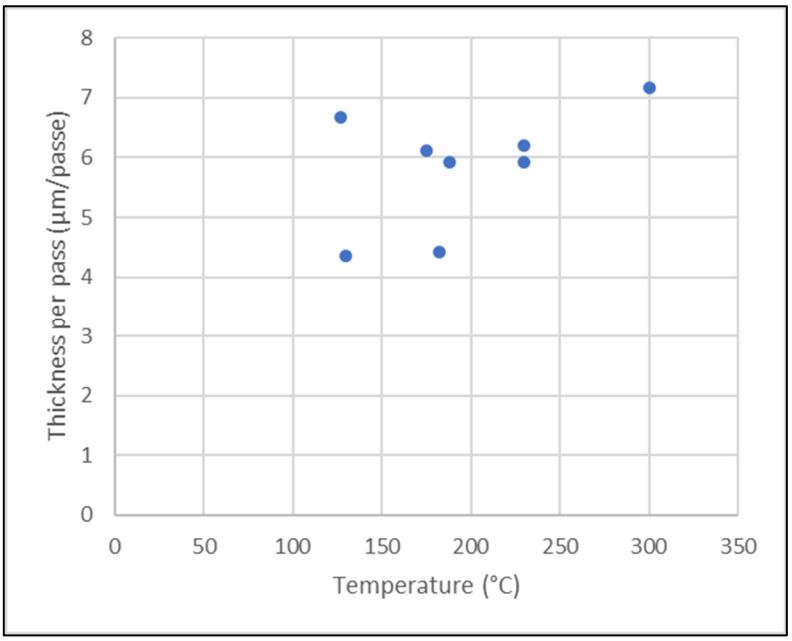

Figure 3.25 Thickness per pass for set 4

Optical microscope images of the samples obtained for set 4 with the corresponding temperature measured outside of the rotating cylinder are shown on figure 3.26. Unfortunately, many shot peened and grit blasted (SP+GB) sampled were cracked at the interface, such as 2301272SP+GB, 2301313SP+GB and 2301313SP+GB. The reason why some samples contain

major defects is the thermal shock that was induced during the deposition. In these cases, the torch was introduced too quickly into the 4340 AISI steel cylinder and the samples heated too fast, hence the cracks. A way of preventing the thermal shock is by preheating the samples or by reducing the speed at which the torch enters the 4340 AISI steel cylinder. Since there was no way of preheating the samples at the NRC, the second method was employed by the operator to decrease the thermal choc.

Overall, the shot peened set is not exploitable in its entirety due to the presence of these cracks and a limited number of tests that was possible. The samples that were exempt of cracks were used to for fatigue tests, which are a part of an ulterior project.

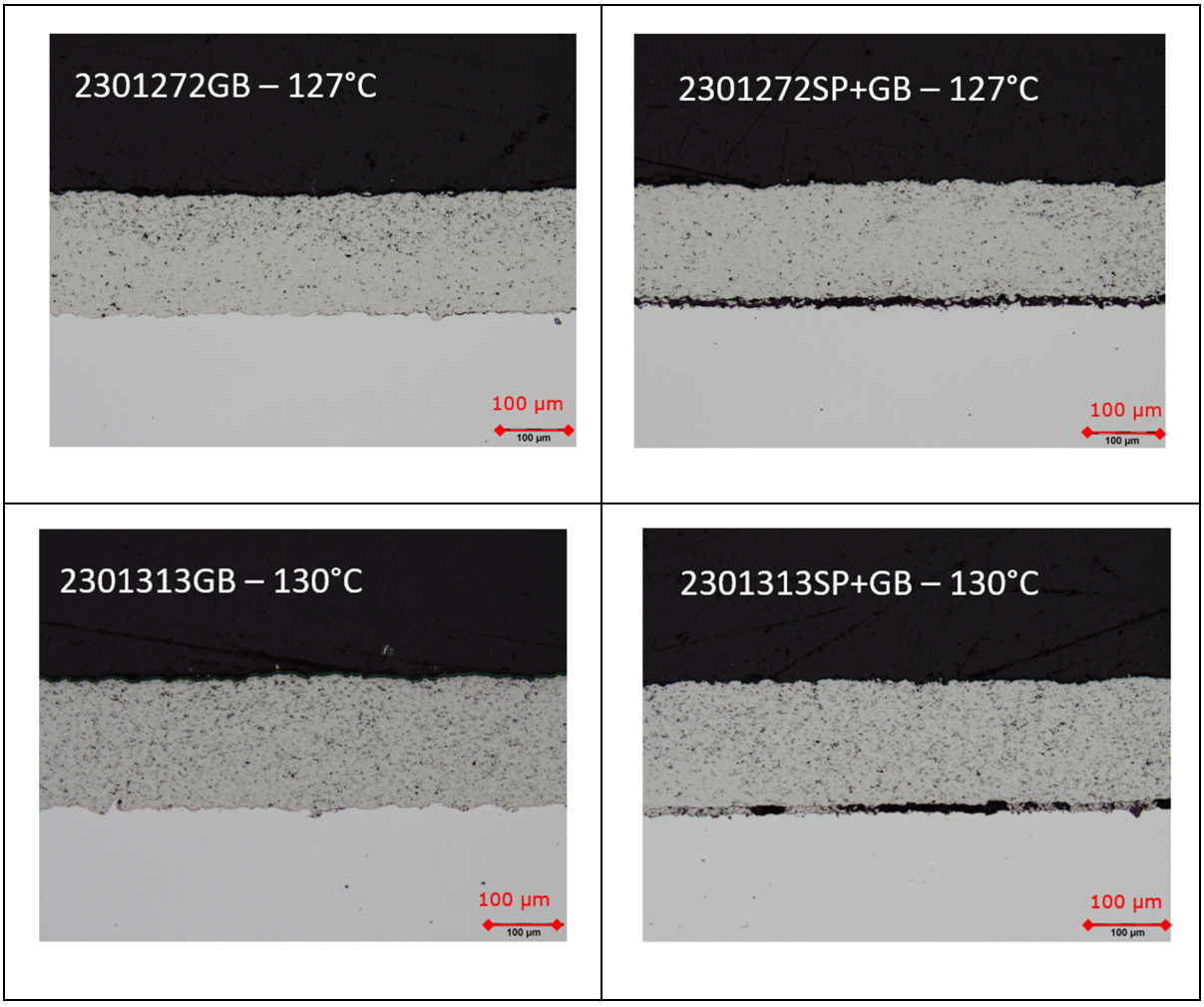

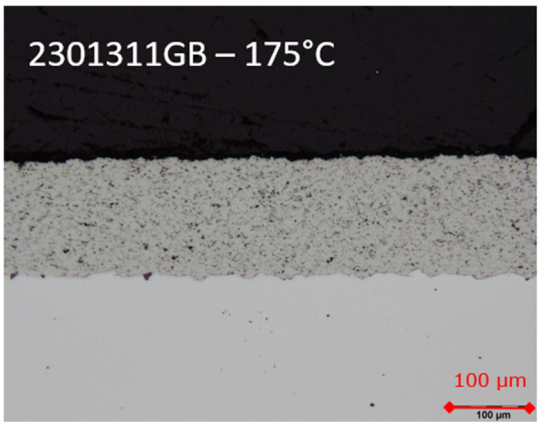
2301311GB – 175°C
100 µm
100 µm

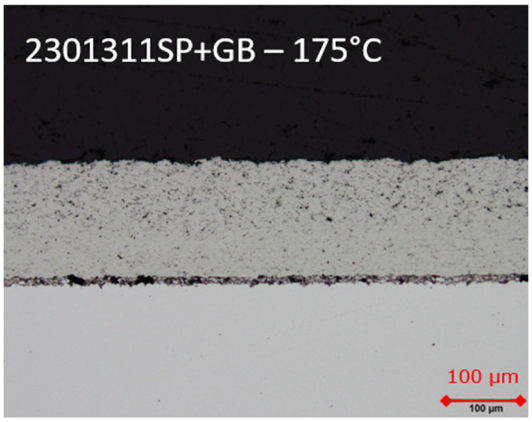
2301311SP+GB – 175°C
100 µm
100 µm

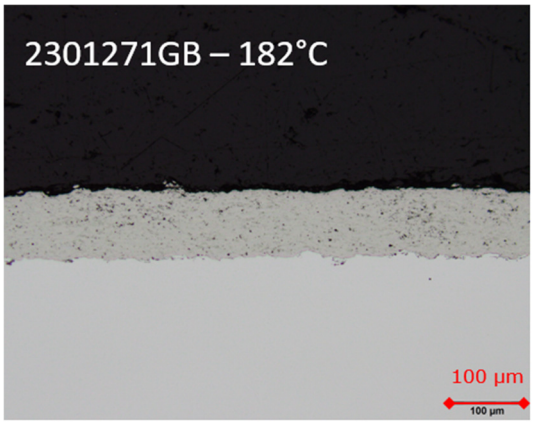
2301271GB – 182°C
100 µm
100 µm

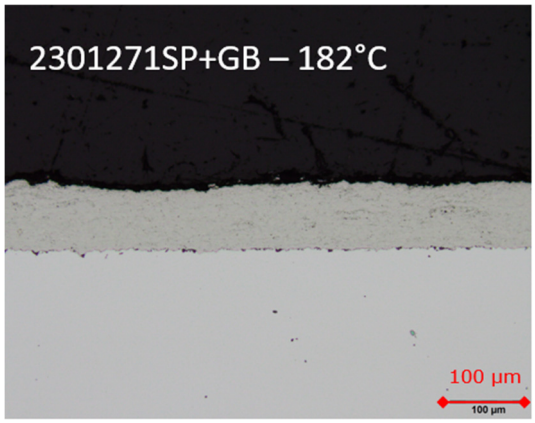
2301271SP+GB – 182°C
100 µm
100 µm

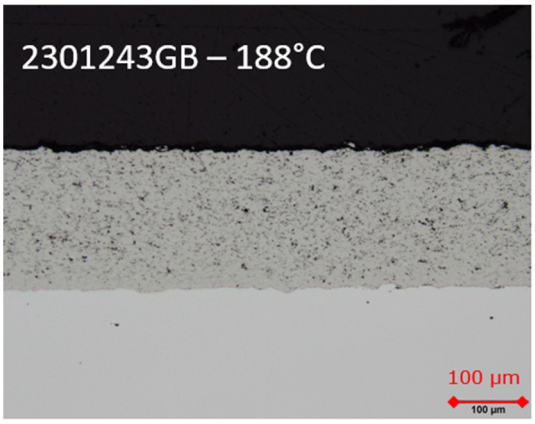
2301243GB – 188°C
100 µm
100 µm

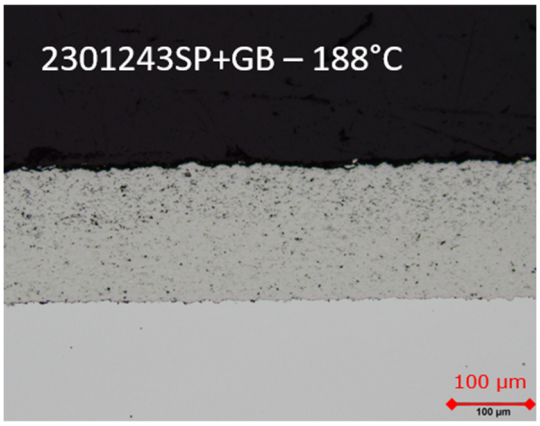
2301243SP+GB – 188°C
100 µm
100 µm

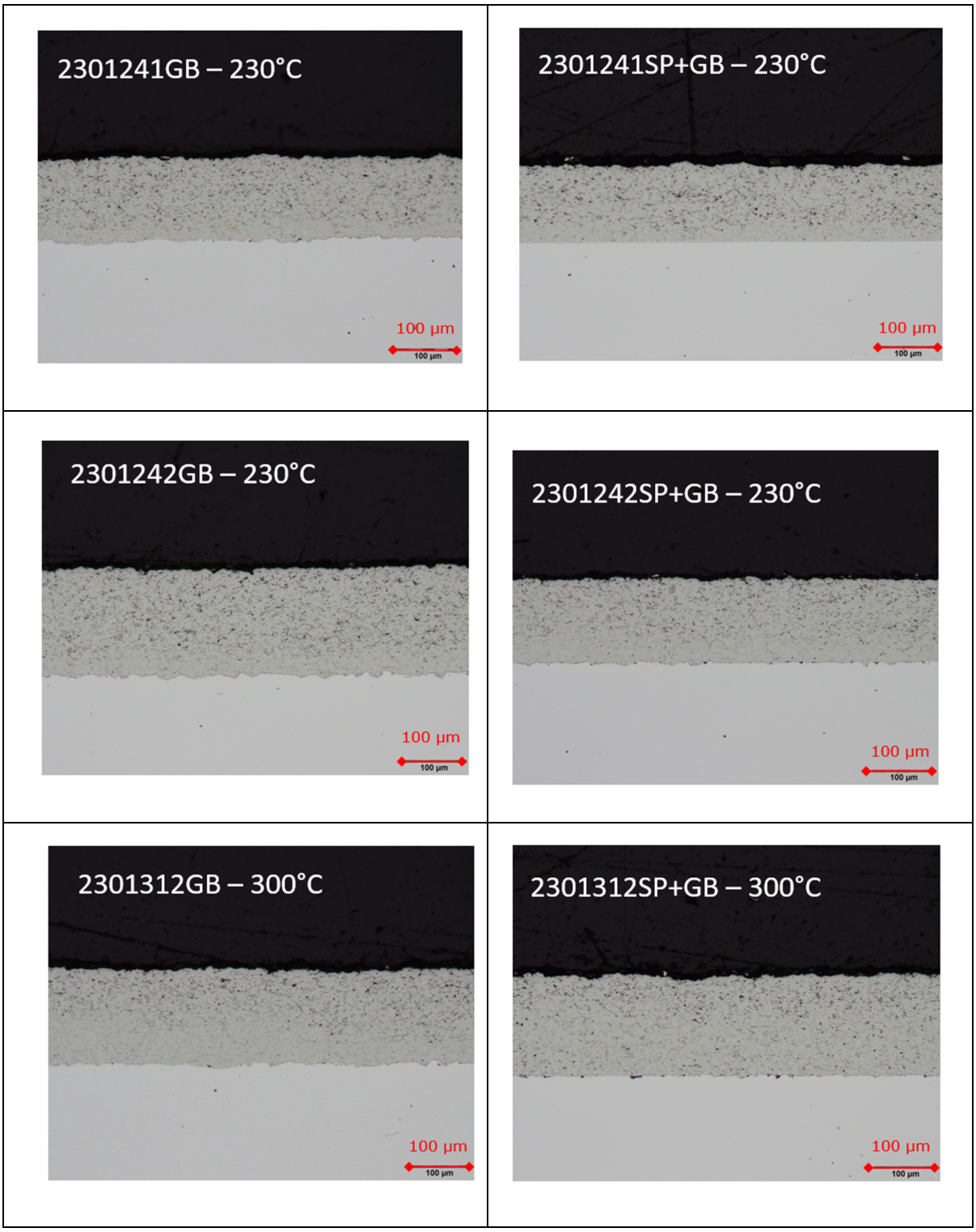

Figure 3.26 Optical microscope images of set 4 HVOF coatings presented by increasing deposition temperature

Porosity

Despite the presence of cracks and defects, this set of samples meets the porosity requirement (figure 3.27) showing that the projection condition is now acceptable for the powder. Porosity does not seem to be affected by the surface treatment received by the substrate since its distribution is quite random, showing that it depends on where the sample was cut.

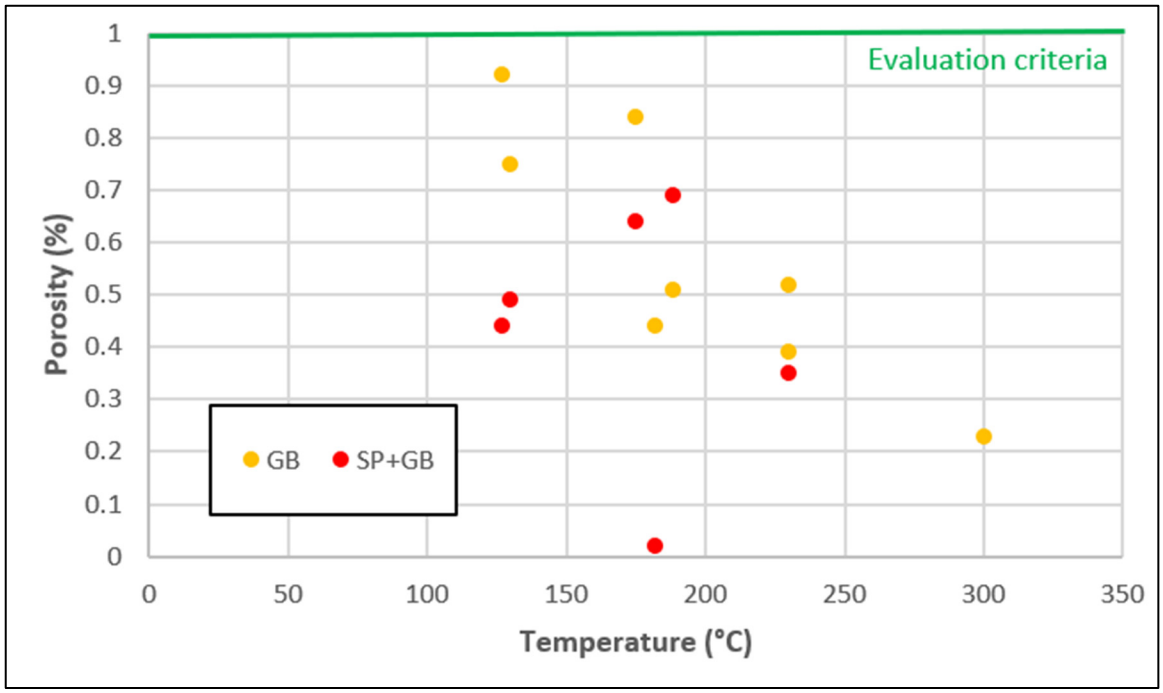

Figure 3.27 Porosity results for set 4

Microhardness

Microhardness results for the coatings and the substrates of the samples of set 4 as a function of the temperature measured outside of the 4340 AISI steel cylinder by the pyrometer are displayed on figure 3.28.

When comparing the values of the hardness values of the coating or the substrate for one temperature, the difference between the two surface treatment conditions does not exceed the standard deviation. Therefore, the surface treatment received by the substrate prior to the

deposition process does not affect the hardness of the coating nor of the substrate itself. In the coatings, the hardness increases with the temperature. Since the temperature has been measured for this set corresponds to the outside temperature and not the temperature of the coupon itself, the values cannot be compared directly. For better correlations, a thermocouple inside of the rotating cylinder will be installed for the next set of tests. This will also enable to correlate the outside and the inside temperature.

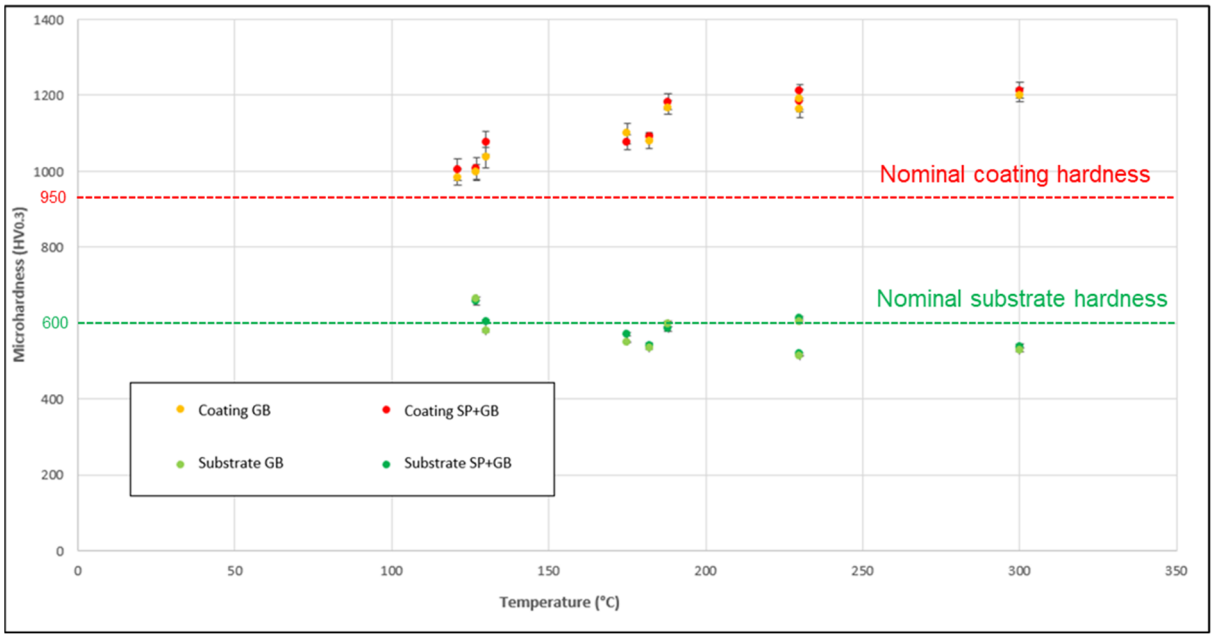

Figure 3.28 Microhardness results for set 4

When depositing a coating, it is important to know how thick the resulting coating be. Yet, for each set, a different relation linking the thickness per pass and the spraying parameters was established. It is therefore complicated for the operator to estimate the required number of passes for each spraying condition.

When comparing porosity of the four sets of samples, only set 4 completely meets the evaluation criteria of being under 1%, even if set 3 used the same powder as set 4. However, an acceptable porosity does not result in an acceptable coating : for set 4, some samples did not adhere to the substrate even if their porosity was under 1%. In the same way, a porosity above 1% is not critical, since its value depend on the threshold set during the image analysis

and on the presence of defects in the region of interest. Overall, porosity is not affected by the temperature of the sample during deposition.

When looking at the chemical analysis of the coatings of sets 1 and 2, who used a coarser powder (A), decarburization increases drastically after 300°C. But for set 3, where a finer powder (B) was used, decarburization seems to be absent (or perhaps delayed) even above 300°C.

For sets 1 through 3, the coating's hardness is correlated with the degree of decarburization. Indeed, for set 1, while the proportion of the WC phase drops, the coating hardens. For set 2 and 3, since there is no observable decarburization, the coating's hardness stays quite constant. For set 4, the coating hardens when increasing the temperature. Yet, since the measured temperature is not the real temperature of the samples, a correlation between the measured outside temperature and the sample's temperature should be done eventually for more accurate results.

Abrasion tests have only been done on sets 2 and 3, but the results are not affected by the spraying conditions. Even if different powders were used for set 2 (powder A - coarser) and set 3 (powder B - finer), the coarseness of the powder did not affect the lost weight during the abrasion tests.

CHAPTER 4

PERSPECTIVES

This chapter will present the project's following steps and perspectives. A first section will be dedicated to the characterization tests that are yet to be done on the samples: adhesion tests, erosion tests, residual stress measurements and fatigue tests. A second section will present a parallel project led on the substrates of set 4. The goal of this parallel project was to assess the effect of the surface treatment (shot peening and/or grit blasting) on the properties of the substrate.

4.1 Characterization tests to be done

This section presents the characterization tests that still have to be done to have a complete overview of the results. Some of the tests could not have been done by lack of means, others are a part of a further study that is not included in this project.

4.1.1 Pull tests

To quantify the adhesion performance of the samples, pull tests will be performed at the NRC on the specimens. These tests will be performed when the NRC's schedule will allow it. The complete procedure is detailed in sections 1.5.4 and 2.7.4.

4.1.2 Erosion

Erosion tests have been initiated at the NRC for some of the produced samples. During this test, sand is blasted through a narrow nozzle on the sample. Erosion tests are performed with a projection angle of 90° and 30° between the nozzle and the surface of the sample. The goal is to assess the erosion behavior of the coatings depending on the projection angle. The detailed procedure and results remain confidential for the moment.

4.1.3 Residual stress

Residual stress measurements are done by XRD. WCCoCr coatings require a copper anode, as used for phase composition analysis. Neither ÉTS nor the NRC currently have yet a residual stress measurement machine with this kind of anode. Therefore, it was not possible to do this characterization test. ÉTS will have an equipment able to perform such measurement by April 2024.

The goal is to establish a residual stress profile and document how it varies with experimental conditions. To do so, the first measure point is located on the surface of the coating. Then, thin layers (a few microns) of material are removed by electropolishing and at each depth, the residual stress is measured. This way, it is possible to visualize the evolution of the residual stress value as a function of the depth under the surface within the coating.

4.1.4 Fatigue

The next axis consists in a study of the mechanical behavior and fatigue properties of coated samples since the ultimate goal of this project is to replace hard chrome plating by ID-HVOF for complex geometries of landing gears. A comprehensive study will be led on the mechanical response of the material system to loading, including coating delamination and substrate fatigue behavior. Fatigue sample will be manufactured with standard finishing conditions and an extensive number of fatigue tests will be run in order to capture the dispersion of the data for several loading conditions. Since the goal is to assess fatigue beahvior in ID-HVOF conditions, coupons would be coated at a short spraying distance of 25 mm, using the ID-Nova gun (like for set 4).

Using a microtensile machine and high precision digital imaging correlations, the interactions between the coating defects, over-tempered regions and substrate inclusions could be documented. The goal would be to be able to predict the reason of failure.

It was possible to manufacture some fatigue specimens with the samples of set 4 that were exempt of cracks at the coating/substrate interface. Of course, the number of fatigue specimens

is not enough to do a complete and standardised fatigue study. Therefore, it will be necessary to produce another set of samples specifically for the second axis of the project.

4.2 Effect of surface preparation on the properties of 4340 steel

The substrates used for set 4 received two different surface treatment before the coating deposition process (the same substrates as the ones used for set 4). Half of the 4340 substrates received a surface grit blasting at 60 grit, with a 60 psi pressure, a blasting distance of 15-20 mm and 400 % coverage. The other half received a surface shot peening following norm SAE-AMS-S-13165 and grit blasting at 240 grit, with a 60 psi pressure, a blasting distance of 15-20 mm and 400 % coverage. Surface treatments were done by Surftec.

The first goal for this sub-project is to assess the effect of the surface treatment received by the substrate on the hardness et residual stress of the substrate itself. Another aspect tackled by this sub-project was the prediction of hardness loss from tempering parameters. The second goal is to assess the effect of tempering time and temperature on the hardness et residual stress of the substrate.

Prior to any surface treatment, samples of 4340 AISI steel received the following treatment:

- Annealement at 845°C followed by an oil quench
- Tempering at 200°C for 1 hour
- Recitifcation of one side of the sample of 600µm to remove any carbon depleted surface

Experiments will done on 4 types of substrates:

- A rectified sample (R): this sample has not received any surface treatment after rectification
- A shot peened sample (SP): this sample has been shot peened according to SAE-AMS-S-13165 (0.008A;S170 steel shot; 120% coverage)
- A shot peened and grit blasted sample (SP+GB): this sample has been shot peened according to SAE-AMS-S-13165 and grit blasted at 240 grit
- A grit blasted sample (GB): this sample has only been grit blasted at 60 grit (60 psi;15-20mm distance; 400% coverage)

Tempering conditions were similar to the procedure followed in the work of B. Meynet (2022). According to his work, a major loss of hardness was observed for temperatures above 200°C and for heating times longer than 4 minutes. Therefore, experiments will be done for temperatures of 200°C and 250°C, and for times ranging from 4 minutes to 128 minutes.

Experiments include the measurement of roughness, a gradient of hardness on the cross section of the samples and a residual stress profile on the cross section of the samples.

CONCLUSION

The principal objective of this study was to define coating characteristics within the experimental domain imposed by ID-HVOF for WCCoCr coatings deposition. More specifically, the goal was to establish relations between the HVOF process parameters and the obtained coating properties.

A first study consisted of exhibiting differences between two WCCoCr powders which differed by the grain sizes and distribution. Characterization tests performed on the used powders included morphology analysis; phase composition analysis and granulometry.

A second study focused on the characterization of WCCoCr coatings deposited in different conditions. Four sets of samples were manufactured :

- A first set of samples included WCCoCr coatings deposited on 4340 AISI steel in classic HVOF conditions for temperature ranging from 90°C to 592°C
- A second set of samples included WCCoCr coatings deposited on 4340 AISI steel in classic HVOF condition for temperature ranging from 80°C to 320°C
- A third set of samples included WCCoCr coatings deposited of soft steel in the same conditions as for set 2, for temperatures ranging from 120°C to 500°C
- A fourth set of sampled included WCCoCr coatings deposited on 4340 AISI steel while being placed inside a cylinder made of the same material as the substrate, in order to mimic ID-HVOF geometrical conditions, for temperatures ranging from 127°C to 300°C

Characterization tests performed on the different sets of samples included microstructure and porosity overview, chemical analysis by XRD, microhardness tests and abrasion tests. Since not all tests could have been performed on all sets, not all results can be correlated to the spraying conditions. With the available results, the following conclusions were formulated made :

- Coating thickness : If coating thickness increased with the temperature for sets 1 and 2, it was not affected by temperature variation for sets 3 and 4.

- Porosity : Porosity is not related to the maximum temperature reached by a sample during the deposition process nor to the coarseness of the powder composing the coating.
- Chemical analysis : When using a coarser powder (A), coatings will decarburize drastically above 300°C. Using a finer powder (B) may help delay the phenomenon of decarburization.
- Coating microhardness : Hardness loss within the coating is correlated to the degree od decarburization. For set 1, the degree of decarburization dropped above 300°C and the coating's hardness increases. For sets 2 and 3, since there was no observable decarburization, the coating's hardness stayed constant. Since there was no chemical analysis done for set 4, it is not possible to bring any relevant conclusions.
- Abrasion : Regardless of the powder that was used for the coating, abrasion results were acceptable and were not affected by the spraying conditions.

Throughout this study, its was possible to exhibit the relation between the HVOF process parameters, such as the temperature reached by the samples, with the different properties of the coatings.

RECOMMANDATIONS

As mentioned in Chapter 4.1, it would be necessary to extend the series of characterization tests on the coatings by doing pull tests, erosion tests, residual stress measurements and fatigue tests. This way, a complete set of data will be available to establish any possible correlations between the results.

Moreover, it would be helpful to manufacture larger sets of samples to be sure that every characterization test can be done. The lack of coupons was a recurring obstacle during this project since it was then impossible to compare test results for different spraying conditions.

Since trying out every possible spraying condition combination is expensive and time consuming, using an experiment design or another statistical tool could be helpful to establish spraying parameters for the following sets of samples.

APPENDIX I

EFFECT OF BACKGROUND FITTING ON XRD SPECTRUMS ANALYSIS

By performing a chemical analysis of a sample by X-Ray Diffraction (XRD), it is possible to identify and quantify the different phases composing the studied sample. The first step of the analysis is to collect the raw data. For this project, the raw data was analyzed with XRD X'Pert^3 Panalytical software. Parameters are in listed in table AI.1. The raw data was then analysed with HighScore XRD Data processing.

Table AI.1 XRD parameters for composition analysis

XRD Parameters	**Value**
2θ	20°-100°
Step	0.05°
Anode material	Cu-Kα
Radiation	45 kV-40mA

An example of an analysed spectrum is shown on figure AI.1. The raw spectrum is traced in red. The fitted spectrum is traced in blue on top of the raw spectrum. The different identified phases are marked with vertical lines with a colored shape on top. After collecting the raw data, it is important to do a correct profile fitting of the raw spectrum before analyzing the data. Profile fitting consists of 5 steps (Speakman, 2021):

- Background fitting
- Peak search
- Profile fitting
- Quality evaluation of the profile fitting
- Calculations

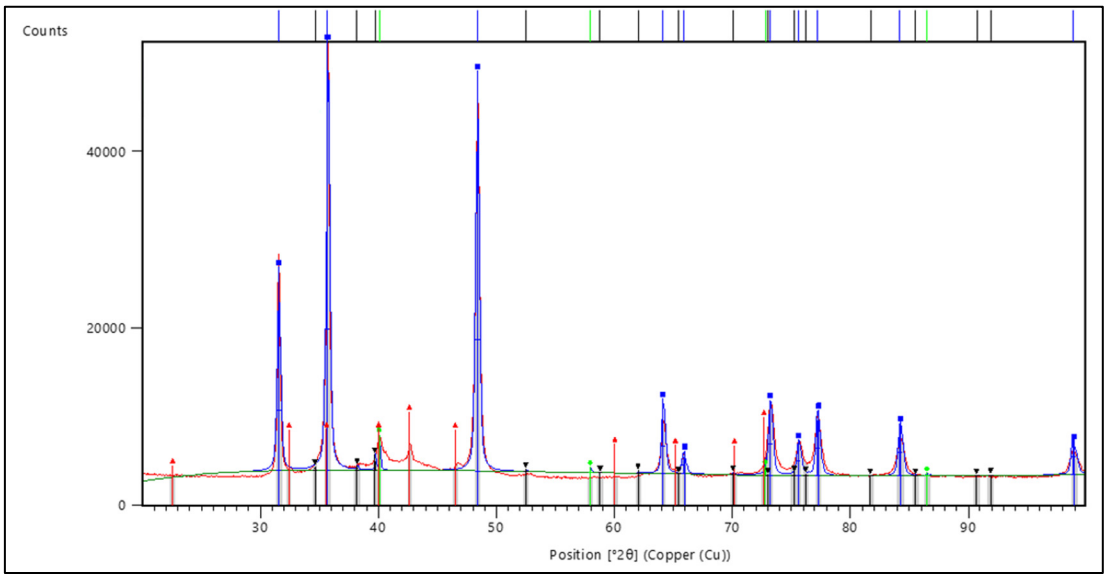

Figure AI.1 Example of an XRD spectrum

Background fitting must be done correctly or else the analysis results can be altered. When performing a background fitting of a spectrum, two parameters are modified : the granularity and the bending factor. Granularity affects the sampling step of the background fitting and usually ranges from 10 to 30 (Speakman, 2021). The bending factor allows to adjust to the nonlinearity and curvature of the raw profile and usually ranges between 0 and 2 (Speakman, 2021).

In the case of an overfit (figure AI.2.a), the bending factor is too high or granularity is too small. In the case of an underfit (figure AI.2.b), the bending factor is too low or the granularity is too large. Figure AI.2.c displays an example of a good background fit.

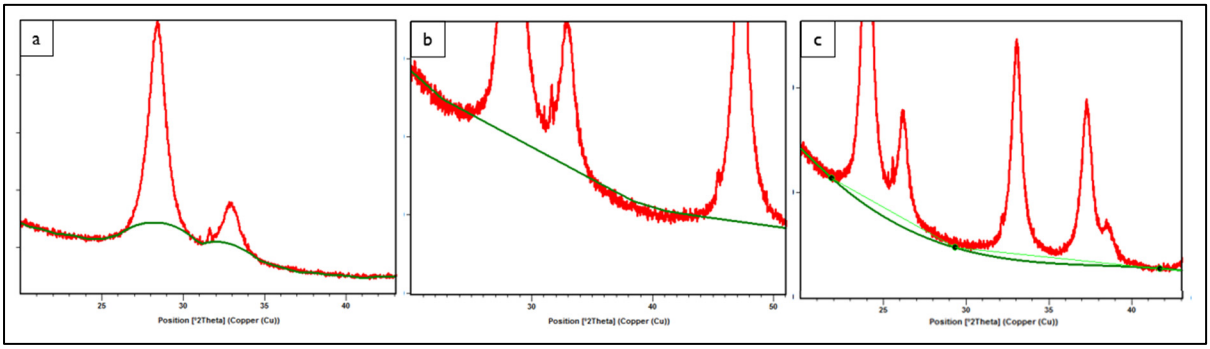

Figure AI.2 Examples of background fitting a) overfit b) underfit and c) good fit

Four pairs of values of granularity and bending factors were used to study the effect of background fitting on phase quantification (table AI.2). BFX-GY corresponds to a bending factor equal to X and a granularity set to Y.

Table AI.2 Selected pairs of background fitting parameters

	Pair 1	**Pair 2**	**Pair 3**	**Pair 4**
Bending Factor	0	0	1	2
Granularity	15	30	22	15

The study was performed on the sample coatings of set 2. The sample characteristics are listed in table AI.3. The coating of each sample is composed of three phases : WC, W and W_2C. Figure A1.3 displays the weight percentage of each phase for all of the samples set 2 for different pairs of background fitting parameters. For each one of the three phases found in the coatings of set 2, pairs BF0-G15 and BF1-G22 exhibit a value of weight percentage that does not coincide with the other pairs of background fitting parameters. Otherwise, pairs BF2-G15 and BF0-G30 match perfectly and could both be used for the background fitting of the other spectrums. For the rest of the project, pair BF0-G30 was selected for background fitting.

Table AI.3 Second set of samples with respective pyrometer recordings of temperature and variable parameters

Sample number	**Max temperature (°C)**	**Carousel diameter (cm)**	**Tangential speed (m/s)**	**Cooling**
2207072	80	18	2	Max
2207081	140	18	2	Max
2207071	145	38	2	None
2207111	210	38	2	Medium
2207082	280	38	2	None
2207112	290	38	1.5	None
2207121	320	38	1	None

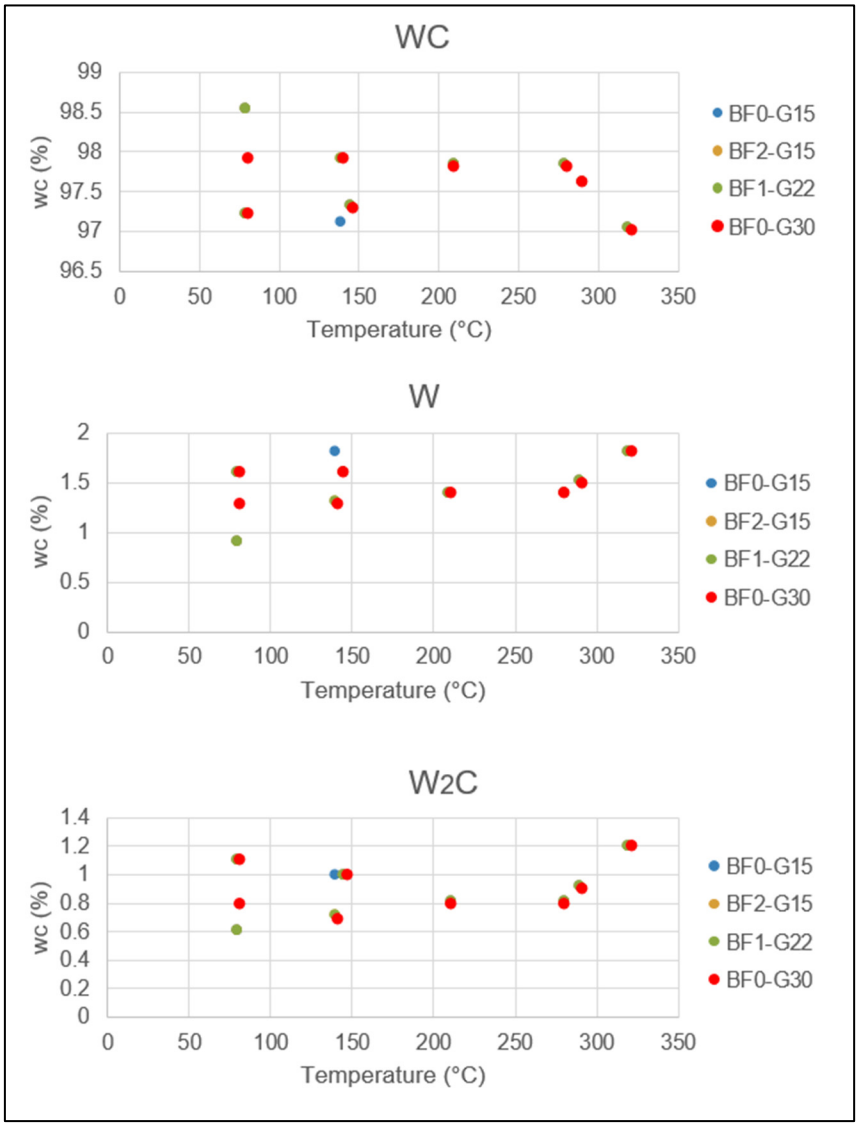

Figure AI.3 Phase quantification of coatings of set 2 depending on the background fitting parameters

APPENDIX II

EXHAUSTIVE LIST OF SPRAYING PARAMETERS

Only the main spraying parameters were given in chapters 2 and 3 of this thesis. This appendix lists the exhaustive list of the spraying parameters used for each set of samples.

Table AII.1 Complete list of spraying parameters for set 1

Gun	Sample number	Powder	H2 flow	O2 flow	N2 flow	Spraying distance	Fixture type	Fixture speed
	#		slpm	slpm	slpm	mm		rpm
ID-Nova	2201191	A	440	220	100	30	Stationnary	-
ID-Nova	2201192	A	440	220	100	30	Stationnary	-
ID-Nova	2201211	A	440	220	100	30	Stationnary	-
ID-Nova	2201212	A	440	220	100	30	Stationnary	-
ID-Nova	2201213	A	440	220	100	30	Stationnary	-
ID-Nova	2201214	A	440	220	100	30	Rotating	210
ID-Nova	2201215	A	440	220	100	30	Rotating	317

Tangential speed	Robot speed	Pitch	Pause between passes	Max Temperature	Number of passes	Thickness/pass	Coat thickness
m/s	mm/s	µm	s	°C	#	µm	µm
1	1000	1270	15	246	15	18	267
1	1000	1270	0	305	15	16	246
1	1000	635	0	391	8	35	282
1	1000	635	0	592	8	38	305
1.5	1500	1270	15	246	23	16	363
2	4.5	1270	15	90	30	7	196
3	6.7	1270	15	111	45	5	208

Table AII.2 Complete list of spraying parameters for set 2

Gun	Sample number	Powder	H2 flow	O2 flow	N2 flow	Spraying distance	Fixture type	Fixture speed
	#		slpm	slpm	slpm	mm		rpm
ID-Nova	2207061	A	440	220	100	30	15	101
ID-Nova	2207071	A	440	220	100	30	15	101
ID-Nova	2207072	A	440	220	100	30	15	101
ID-Nova	2207081	A	440	220	100	30	7.125	210
ID-Nova	2207082	A	440	220	100	30	7.125	210
ID-Nova	2207111	A	440	220	100	30	7.125	210
ID-Nova	2207112	A	440	220	100	30	7.125	158
ID-Nova	2207121	A	440	220	100	30	7.125	105

Tangential speed	Robot speed	Pitch	Pause between passes	Max Temperature	Number of passes	Thickness/pass	Coating thickness
m/s	mm/s	µm	s	°C	#	µm	µm
2	2.5	1524	0	80	24	4	99
2	2.5	1524	0	145	30	5	160
2	2.5	1524	0	80	30	5	145
2	4.5	1270	0	140	30	4	135
2	4.5	1270	0	280	30	5	163
2	4.5	1270	0	210	30	5	163
1.5	3.4	1270	0	290	22	6	135
1	2.2	1270	0	320	16	14	226

Table AII.3 Complete list of spraying parameters for set 3

Gun	Sample number	Powder	H2 flow	O2 flow	N2 flow	Spraying distance	Fixture type	Fixture speed
	#		slpm	slpm	slpm	mm		rpm
MN III -3	2303241	B	375	190	60	25	4.8	101
MN III -3	2303271	B	375	190	60	25	4.8	101
MN III -3	2303291	B	375	190	60	25	4.8	101
MN III -3	2303301	B	375	190	60	25	4.8	210
MN III -3	2303302	B	375	190	60	25	4.8	210
MN III -3	2303311	B	375	190	60	25	4.8	210

Tangential speed	Robot speed	Pitch	Pause between passes	Max Temperature	Number of passes	Thickness/pass	Coating thickness
m/s	mm/s	µm	s	°C	#	µm	µm
2	5.8	1270	0	500	120	2	185
2	5.8	1270	0	440	80	2	198
2	5.8	1270	0	120	80	3	236
2	5.8	1270	0	250	80	3	211
2	5.8	1270	0	350	112	2	229
1.5	4.3	1270	0	420	100	2	218

Table AII.4 Complete list of spraying parameters for set 4

Gun	Sample number	Powder	H2 flow	O2 flow	N2 flow	Spraying distance	Fixture type	Fixture speed
	#		slpm	slpm	slpm	mm		rpm
ID-Nova	2301241	B	375	190	60	25	4.8	313
ID-Nova	2301242	B	375	190	60	25	4.8	313
ID-Nova	2301243	B	375	190	60	25	4.8	313
ID-Nova	2301271	B	375	190	60	25	4.8	313
ID-Nova	2301272	B	375	190	60	25	4.8	470
ID-Nova	2310311	B	375	190	60	25	4.8	313
ID-Nova	2310312	B	375	190	60	25	4.8	313
ID-Nova	2310313	B	375	190	60	25	4.8	470

Tangential speed	Robot speed	Pitch	Pause between passes	Max Temperature	Number of passes	Thickness/pass	Coating thickness
m/s	mm/s	µm	s	°C	#	µm	µm
2	6.6	1270	15	230	24	6	142
2	6.6	1270	15	230	24	6	150
2	6.6	1270	30	188	24	6	142
2	6.6	1270	45	182	24	4	107
3	10	1270	45	127	24	7	160
2	6.6	1270	45	175	24	6	147
2	6.6	1270	0	300	24	7	173
3	10	1270	45	130	36	4	158

LIST OF BIBLIOGRAPHICAL REFERENCES

Aguero A., Camon F., Garcia De Blas J., Del Hoyo J.C., Muelas R., Santaballa A., Ulargui S., Vallés P. (2011). HVOF-Deposited WCCoCr as Replacement for Hard Cr in Landing Gear Actuators. Journal of Thermal Spray Technology, Vol. 20(6), 1292-1309 https://doi.org/10.1007/s11666-011-9686-1

AISI 4340 Steel, normalized, 25 mm round, (s.d.). MatWeb. Consulted on the 8th June 2023 at https://www.matweb.com/search/DataSheet.aspx?MatGUID=fd2df45bffa54018b54989bc14092d9f&ckck=1

AMS 2447-D, Aerospace Material Specification. (2012). Coating, Thermal Spray High Velocity Oxygen/Fuel Process.

AMS 2448, Aerospace Material Specification. (2004). Application of Tungsten Carbide Coatings on Ultra High Strength Steels High Velocity Oxygen/Fuel Process.

ASTM B117. (2019). Standard Practice for Operating Salt Spray (Fog) Apparatus. United States: ASTM International.

ASTM C633-01. (2010). Standard Test Method for Adhesion or Cohesion Strength of Thermal Spray Coatings. United States: ASTM International.

ASTM E384. (2021). Standard Test Method for Microindentation Hardness of Materials. United States: ASTM International.

ASTM E466-15. (2021). Standard Practice for Conducting Force Controlled Constant Amplitude Axial Fatigue Tests of Metallic Materials. United States: ASTM International

ASTM G65-16. (2017). Standard Test Method for Measuring Abrasion Using the Dry Sand/Rubber Wheel Apparatus. United States: ASTM International.

ASTM G99. (2010). Standard Test Method for Wear Testing with a Pin-on-Disk Apparatus. United States: ASTM International.

Barényi I., Lipták P., Vojtovič S. (2014). Effect of over tempering at UHSLA Steel ARMPW500. Advanced materials research,Vol.875-877, 1324-1328. https://doi.org/10.4028/www.scientific.net/AMR.875-877.1324

Bertula K. (2022, 29 November) Particle distribution analysis – guide to method selection. Measurlabs. Consulted on the 16 of May 2023 at https://measurlabs.com/blog/particle-size-distribution-analysis-method-selection/#:~:text=Its%20principle%20is%20based%20on,intensity%20than%20from%20smaller%20ones

Bulut B., Unal F., Baydogan M., Kayali E. S. (2021). Effect of particle morphology on physical, mechanical and wear properties of cobalt metal powders. Transactions of the Indian Institute of Metals, Vol.74, 2345-2355. https://doi.org/10.1007/s12666-021-02331-5

Colpan C.O., Nalbant Y., Ercelik M. (2018). Energy dispersive X-ray spectroscopy [image online]. Science Direct. https://www.sciencedirect.com/topics/engineering/energy-dispersive-x-ray-spectroscopy

Davis, J.R. (2004). Handbook of Thermal Spray Technology - 6.3 High-Velocity Oxyfuel Spray (HVOF). ASM International. Retrieved from https://app.knovel.com/hotlink/pdf/id:kt008JAKJ4/handbook-thermal-spray/high-velocity-oxyfuel

Fang, D. (2010). Diagnostic et adaptation des trajectoires robotiques en projection thermique [thèse de doctorat, Université de Technologie de Belfort-Montbéliard]. Archives ouvertes. https://tel.archives-ouvertes.fr/tel-00598778

García-Rodríguez S., Torres B., López A.J., Otero E., Rams J. (2019). Characterization and mechanical properties of stainless-steel coatings deposited by HVOF on ZE41 magnesium alloy. Surface and Coatings Technology, Vol.359, 73-84. https://doi.org/10.1016/j.surfcoat.2018.12.056

Hong S., WU Y.P., Gao W.W., Wang B., Guo W.M., Lin J.R. (2014). Microstructural chracterisation and microhardness of HVOF sprayed WC-10Co-4Cr coating. Surface Engineering, Vol.30(1), 53-58. https://doi.org/10.1179/1743294413Y.0000000184

Houdková, Š., Kašparová M., Zahálka F. (2010). The influence of spraying angle on properties of HVOF sprayed hardmetal coatings. Journal of Thermal Spray Technology, Vol.19(5), 893- 901. https://doi.org/10.1007/s11666-010-9514-z

Kawakita J., Kuroda S. (2004). Oxidation restriction of in-flight particles upon GS-HVOF spraying by nitrogen addition to combustion gas. Material transactions, Vol.45(2), 346-349. https://doi.org/10.2320/matertrans.45.346

Marple B.R. Lima R.S., (2005). Process temperature/velocity-hardness-wear relationships for high-velocity oxyfuel sprayed nanostructured and conventional cermet coatings. Journal of Thermal Spray Technology, Vol.14(1), 67-76. https://doi.org/10.1361/10599630522729

Meynet B. (2022). Quantification et prediction de la taille de la zone de sur-revenu générée par le proceed HVOF dans les pieces en aciers martensitiques. [Internship report, SeaTech – Ecole d'Ingénieurs de l'Université de Toulon]

Nazemi F., Hamel-Akré J., Bocher P. (2018). Modeling of cementite coarsening during tempering of low-alloyed-medium carbon steel, Journal of Materials Science, Vol.53(8), 6198– 6218. https://doi.org/10.1007/s10853-017-1943-3

Picas J. A., Punset M., Baile M.T., Martin E., Forn A. (2011). Effect of oxygen/fuel ratio on the in-flight particle parameters and properties of HVOF WC-CoCr coatings. Surface and Coatings Technology, Vol. 205(2), S364-S368. https://doi.org/10.1016/j.surfcoat.2011.03.129

Rachel Ross. (December 2018). What is X-Ray Spectroscopy ? Livescience. https://www.livescience.com/64241-x-ray-spectroscopy.html

Salehi Doolabi, M., Ghasemi, B., Sadrnezhaad, S.K., Habibolahzadeh A., Jafarzadeh K. (2018). Evaluation and Selection of Optimal Oxygen/Fuel Ratio for Best Mechanical Properties. Oxidation Resistance and Microstructure of HVOF NiCoCrAlY Coatings Using AHP–VIKOR Method. Oxid Met, Vol.89, 429-451. https://doi.org/10.1007/s11085-017-9797-2

Song B., Bai M., Voisey K.T., Hussain T. (2017). Role of oxides and porosity on high-temperature oxidation of liquid-fueled HVOF thermal-sprayed Ni50Cr coatings. Journal of Thermal Spray Technology, Vol.26, 554-568. https://doi.org/10.1007/s11666-017-0531-z

Speakman S.A. (2021). Profile Fitting for Analysis of XRPD Data using Highscore Plus v3. Consulted on the 6th of December 2022 at http://prism.mit.edu/xray/oldsite/4%20Profile%20Fitting%20for%20Quantitative%20Analysis.pdf.

Spraywerx Technologies. (2021). ID-Nova HVOF: Internal Diameter High Velocity Oxygen Fuel Torch Brochure. Spraywerx Technologies. https://spraywerx.com/wp-content/uploads/2021/04/SprayWerx-ID-NOVA-27Apr21.pdf

Spraywerx Technologies. (2021). Mini-Nova HVOF: Internal Diameter High Velocity Oxygen Fuel Torch Brochure. Spraywerx Technologies. https://spraywerx.com/wp-content/uploads/2021/04/SprayWerx-Mini-Nova-27Apr21.pdf

Tejero-Martin D., Rezvani Rad, M., McDonald, A., Hussain T. (2019). Beyond Traditional Coatings: A Review on Thermal-Sprayed Functional and Smart Coatings. Journal of Thermal Spray Technology, Vol. 28, 598–644. https://doi.org/10.1007/s11666-019-00857-1

Tucker Jr., R. C. (2013). ASM Handbook, Volume 05A - Thermal Spray Technology 26.1.1.2 Topcoat. ASM International. Retrieved from https://app.knovel.com/hotlink/pdf/id:kt00C1ZJN2/asm-handbook-volume-5a/topcoat

Vanat K.J., Sucharksi G.B., Paredes R.S.C., Pukasiewiez A.G.M. (2021). Deposition of aluminum coatings by HVOF process on complex geometries. Journal of Thermal Spray Technology, Vol.30, 1905-1926. https://doi.org/10.1007/s11666-021-01249-0

Vasudev H., Thakur L., Bansal A., Singh H., Zafar S. (2019). High temperature oxidation and erosion behaviour of HVOF sprayed bi-layer Alloy-718/NiCrAlY coating. Surface & coatings technology, Vol. 362, 366-380. https://doi.org/10.1016/j.surfcoat.2019.02.012

Vats A., Patnaik A., Meena M.L., Shringi D. (2020). Role of micro-factors on microstructure and on the tribological performance of HVOF coatings: A review. [Conference] IOP Conference Series: Materials Science and Engineering, Jaipur (India), https://iopscience.iop.org/article/10.1088/1757-899X/1017/1/012010

Vieira L.F.S, Voorwald H.J.C., Cioffi M.O.H. (2015). Fatigue performance of AISI 4340 steel Ni-Cr-B-Si-Fe HVOF thermal spray coated. Procedia Engineering, Vol. 114, 606 – 612. https://doi.org/10.1016/j.proeng.2015.08.111

Yari M. (January 2017). Corrosion assessment: 8 corrosion tests that help engineers mitigate corrosion. Corrosionpedia. https://www.corrosionpedia.com/corrosion-assessment-8-corrosion-tests-that-help-engineers-mitigate-corrosion/2/1389

Yuan J., Zhan Q., Huang J., Ding S., Li H. (2013). Decarburization mechanisms of WC-Co during thermal spraying: Insights from controlled carbon loss and microstructure characterization. Materials chemistry and physics, Vol. 142, 165-171. http://dx.doi.org/10.1016/j.matchemphys.2013.06.052

Xu L., Song J., Zhang X., Deng C., Liu M., Zhou K. (2018). Microstructure and Corrosion Resistance of WC-Based Cermet/Fe-Based Amorphous Alloy Composite Coatings. Coatings, Vol. 8(11), 393. https://doi.org/10.3390/coatings8110393

Zhao L., Maurer M., Fischer F., Dicks R., Lugscheider E. (2004). Influence of spray parameters on the particle in-flight properties and the properties of HVOF coating of WC CoCr. Wear, Vol. 257(1-2), 41-46. https://doi.org/10.1016/j.wear.2003.07.002